Vibration Performance of a CLT Floor System:
Comparison of onsite measurements with and without architectural finishing to numerical and analytical calculations

L.L. Klappe

Delft University of Technology

TU Delft

LŪNING
Ingenieurs in houtconstructies

Vibration performance of a CLT floor system

Comparison of onsite measurements with and without architectural finishing to numerical and analytical calculations

by Lilly Klappe

Master of Science Thesis
Building Engineering Track // Structures Design Specialisation
Delft University of Technology // Faculty of Civil Enigneering (CiTG)

Student number:	4539192	
Project duration:	November 2022 – Oktober 2023	
Thesis committee:	Dr. Ir. G.J.P. Ravenshorst,	TU Delft, Chair
	Ir. R. Verhaegh,	Lüning, Supervisor
	Ir. M. Felicita,	TU Delft, Supervisor
	Ir. C. Noteboom,	TU Delft, Supervisor
	Dr. Ir. J.W.G. van de Kuilen,	TU Delft, Supervisor

LŪNING
Ingenieurs in houtconstructies

Preface

This thesis was written for my Master of Civil Engineering graduation at the Faculty of Civil Engineering and Geosciences, Delft University of Technology. During the program, I chose to specialize in Building Engineering, with a focus of Structures. It was during this period that my fascination for Timber structures grew. Engaging in discussions with knowledgeable professors within the field ultimately led me to the topic of this paper.

I would like to thank my research committee for their support, invaluable knowledge, expert guidance and for giving me a constant source of motivation. I want to thank Geert Ravenshorst for his profound expertise in timber structures, which resulted in numerous insightful ideas. Maria Felicita's stimulating discussions were instrumental in fostering insightful concepts, and her support throughout the research process is deeply appreciated. I want to thank Chris Noteboom for introducing me to Luning and helping me find structure in my study and paper, which ensured the academic quality of my work. I want to thank Rob Verhaegh for his extensive knowledge of timber building construction, which not only enriched my understanding of the subject but also provided valuable insights into problem-solving approaches.

This thesis was made in collaboration with Luning, and I want to express my gratitude to all my colleagues at Luning. I could always ask questions and they created an inspirational working environment. I am also thankful for including me in research discussions within lining on the topic of this thesis, which has taught me insights into real-world applications.

Lastly, I extend my deepest thanks to my fellow students at the TU Delft, friends and family for their continuous support and care. Your willingness to lend an empathetic ear during moments is very valuable to me.

With sincere gratitude,
Lilly Klappe

Abstract

Currently, the building industry contributes to up to 50% of climate change. A way to reduce the impact is by replacing current building materials with more environmentally friendly materials, such as timber. Engineered wood products, such as cross-laminated timber (CLT) panels, have increased strength, stiffness, and stability which enables building higher buildings and floors with bigger spans. However, due to the low weight of timber, CLT floors are susceptible to unwanted high floor vibrations and therefore need to be verified on their footfall-induced vibration performance. Predicting the vibration performance is a complex problem as the load-bearing structure and architectural finishing have distinct structural behavior under small vibrations. Due to the novelty of the problem, the distinct behavior is not captured well in the current design codes. As a result, the Eurocode 5 guidelines on vibrations are currently being updated and extended. In support, this thesis addresses the critical issue of predicting the vibration performance of CLT floors, with a specific focus on the impact of architectural finishing.

To achieve this goal, a literature review was conducted to identify structural components that are often overlooked, but may lead to inaccuracies in vibration predictions. These factors include the connections between CLT panels and different types of floor finishing. A case study was then carried out using the building HOUTlab, which features CLT floors with a concrete floating screed. On-site measurements were performed at key locations, including at the inter-panel connection line and in the middle of the panel. This was done before and after architectural finishing was placed. Subsequently, analytical and numerical calculations were used to gain insight into the structural behavior of the system subject to footfall-loading by investigating the accuracy of common engineering practices and other assumptions regarding their structural behavior.

Onsite measurements, where the floor was loaded and the response was measured at the same location, showed that the root mean square velocity (v_{rms}) values were much higher at the inter-panel connection line compared to in the middle of the panel. The v_{rms} is a measure of the amplitude of the vibration. The initial finite element analysis (FEA), assuming a rigid inter-panel connection, inaccurately located the highest v_{rms} values. When assuming a hinge, the FEA correctly allocated the critical v_{rms} values but compromised the accuracy of frequency estimates. The experimental results revealed that adding architectural finishing increased the damping, reduced the v_{rms}, and maintained a similar frequency, ultimately improving the vibration performance from level 3 to level 1 according to the preliminary Eurocode 5 (prEC5) standards. The prEC5 and FEA following common engineering practices accurately estimated the frequency before architectural finishing was placed but underestimated it by 39% after it was placed, indicating a higher increase in the bending stiffness of the floor than initially assumed. While prior calculations assumed slip between the floor layers due to the presence of the insulation layer, assuming full cooperation between the layers resulted in an overestimation of the frequency by 9%, suggesting that there is some cooperation, but the floors are not fully bonded.

This research implies that for CLT floors subject to footfall loading, inter-panel connections have a low rotational stiffness, which reduces the vibration performance of one-way and two-way span floors. More research is recommended to establish an amplification factor for the v_{rms} calculation in the prEC5 that accounts for the decreased transversal bending stiffness due to the presence of inter-panel connections. Moreover, inter-panel connections influence the modal mass, this should be incorporated into the modal mass formula prescribed by the prEC5 for CLT floors. In addition, this research revealed that for this Case study, adding a floating screed to a CLT floor increases the bending stiffness much more compared to common engineering beliefs. The increase is attributed to the increased bending stiffness of the standalone CLT and screed layers, in conjunction with cooperation between the layers when subjected to small vibrations. Therefore the next step is to do more experimental research of CLT floors with different floor finishing to establish appropriate bending stiffness values for the prediction of the vibration performance.

Contents

List of Abbreviations

$CCIP$	Cement and Concrete Industry Publication
CEP	Common Engineering Practices
CFA	CADS Footfall Analysis
CLT	Cross Laminated Timber
DAF	Dynamic amplification factor
FEM	Finite Element Method
GL	Glued laminated
$MDOF$	Multi degree of freedom
$prEC5$	preliminary Eurocode 5
SCI	Steel Construction Institute
$SDOF$	Single degree of freedom
SLS	Serviceability limit state

Nomenclature

α	Angle [-]
ρ	Density [kg/m3]
ρ_k	Characteristic Density [kg/m^3]
ρ_{mean}	Mean Density [kg/m^3]
ζ	Damping ratio [-]
B	Floor width [m]
d	Diameter of fastener
$E_{m,0,k}$	5 percentile modulus of elasticity parallel bending [kg/m2]
$E_{m,0,mean}$	Mean modulus of elasticity parallel bending [kg/m2]
$E_{m,90,mean}$	Mean modulus of elasticity perpendicular bending [kg/m2]
f	frequency [Hz]
f_w	Walking frequency [Hz]
$f_{c,0,k}$	Characteristic compressive strength parallel to the grain [N/mm2]

$f_{c,90,k}$	Characteristic compressive strength perpendicular to the grain [N/mm2]
$f_{m,k}$	Characteristic bending strength[N/mm^2]
$f_{t,0,k}$	Characteristic tension strength parallel to the grain [N/mm2]
$f_{t,90,k}$	Characteristic tension strength perpendicular to the grain [N/mm2]
G	Shear modulus [kg/m2]
k_{mod}	Modification factor [-]
K_R	Rotational stiffness of the connection [kN/mm]
K_{ser}	Slip modulus [KN/mm]
K_T	Translation stiffness of the connection [kN/mm]
L	Floor span [m]
n	number of fasteners
t	Thickness [mm]
v	Poisson's ratio [-]
v_{rms}	Root mean square velocity [mm/s2]

List of Figures

List of Tables

1 Introduction

This section provides an overview of the research topic, starting with the relevance of the study in Section 1.1, followed by the problem definition is Section 1.2. Next, the objectives and main research question are presented in Section 1.3. Finally, Section 1.4 outlines the methodology and Section 1.5 presents the scope adopted for this MSc thesis.

1.1 Relevance of research

The construction industry is under increasing pressure to reduce its environmental impact, prompting advancements in timber structures. Timber possesses distinct advantages, including high carbon storage, low production energy requirements, renewability, and a favorable strength-to-weight ratio, thereby reducing transportation energy needs [11]. In addition, engineered wood products, such as cross-laminated timber (CLT) panels offer enhanced strength, structural stability, and streamlined construction procedure compared to solid wood alternatives [12]. As floors account for approximately 20% of a building's environmental impact, replacing regular concrete floors with CLT floors bid a lot of potential for carbon and energy savings.

However, due to timbers' low density, CLT floors risk unwanted high floor vibrations induced by footfall loading. Subsequently, the vibration performance becomes one of the governing design requirements. The vibration performance is quantified using the modal properties; fundamental frequency, modal mass and damping, which are inherent to the floor system. The preliminary Eurocode 5 (prEC5) provides an analytical method for simple floor systems, while for more complex systems using FEA is recommended. CLT floors generally have a relatively low fundamental frequency and modal mass, consequently resulting in a low vibration performance.

Due to the novelty of the problem, there is a limited understanding of the structural behavior of CLT floors subject to footfall loading, especially the effect architectural finishing has on the overall dynamic behavior lacks awareness. As a result, existing methods result in under or overestimation of the vibration performance. Recent numerical investigations have underscored the substantial impact of the low stiffness of inter-panel CLT connections on vibration performance, suggesting that neglecting these connections can lead to an overestimation of the vibration performance [6]. However, these findings warrant substantiation of experimental data. Moreover, a recent empirical study involving onsite measurements during various construction phases, has unveiled a significant underestimation of the frequency subsequent to the installation of a floating cement screed. Ultimately resulting in an underestimation of the vibration performance of CLT floors [7]. Both of these studies highlight the distinctive behavior of floor systems subjected to footfall loading.

To enable an accurate forecast of vibration performance, it is imperative to develop a profound understanding of the response of CLT floor characteristics and architectural finishing to footfall-induced vibrations. Specifically, the influence of inter-panel connections and floor finishing has emerged as pivotal factors that have not been adequately considered in vibration performance predictions. This research seeks to bridge these knowledge gaps and provide valuable insights into the complex dynamics of CLT floor systems under footfall-induced vibrations, thereby advancing sustainable construction practices.

1.2 Problem Statement

Due to the low density of timber, CLT floors become susceptible to high floor vibrations induced by footfall loading. Thereby the vibration performance often becomes the governing design requirement of CLT floors. However, due to the distinct dynamic behavior of CLT floors and architectural finishing subject to footfall-induced vibrations, predicting the vibration performance is a complex and novel task. As a result existing methods still struggle to accurately predict the vibration properties, which may lead to costly mitigation measurements applied to CLT floors or on the other end, it might result in uncomfortable floor vibrations. To avoid this of happening, design rules and codes need to be improved and extended to accurately model the structural behavior of CLT floor systems including capturing the complex interplay between structural and non-structural components.

1.3 Objective and Research question

From the problem definition, the objective follows. The objective of this thesis is to detect and understand the behavior of CLT floor characteristics and architectural finishing when subject to footfall-induced vibration so that CLT floor systems can appropriately be modeled in various vibration performance prediction methods. By expanding the knowledge base, engineers will gain a more comprehensive understanding of vibration performance analysis, enabling them to make more precise predictions and designs. In addition, increasing the accuracy and reliability of these methods will contribute to the competitiveness of CLT floors to other less environmentally friendly floor systems and thereby advance the sustainability of the construction industry.

To achieve the main goal, some specific objectives related to this research are set out:

1. Identify and quantify from onsite measurements the effect of CLT floor characteristics and architectural finishing on the vibration performance
2. Investigate design codes and common engineering practices in the field of vibration performance analysis of CLT floors and architectural finishing
3. Investigate other possible assumptions on the structural behavior of CLT floors and architectural finishing subject to footfall-induced vibrations.

As a result of the objective the main research question of this research is as follows:

How can CLT floor systems be modeled in order to accurately predict the vibration performance when taking into account architectural finishing?

1.4 Methodology

The following is a breakdown of the report structure, outlining the subjects addressed in each chapter. Within this framework, a methodology is presented to fulfill the objectives. In alignment with each section, corresponding sub-questions will be addressed and resolved.

Chapter 2 - Footfall Induced Vibrations
This chapter provides an in-depth understanding of footfall-induced vibrations and methods for their quantification. It begins by explaining the fundamental principles of footfall-induced vibrations and then examines existing guidelines to quantify the vibration performance. Crucial parameters for footfall analysis and potential sources of inaccuracies are presented. The chapter also explores Modal analysis, discussing a wide range of experimental and numerical methods to obtain reliable modal property values. The chapter will address the following sub-questions:

- Which parameters govern the vibration performance of floors subjected to footfall loading?
- Which parameters used in the prEC5 vibration calculations might lead to inaccuracies in the vibration performance of Cross-Laminated Timber (CLT) floors?

Chapter 3 - Dynamics of CLT Floors
This chapter assesses the dynamic behavior of CLT floors within timber structures, considering both structural and non-structural components. Special attention is given to elements like partitions, screed, and inter-CLT panel connections, as prior research indicates their impact on the overall dynamic behavior of timber structures. This chapter serves as the foundation for establishing initial parameter values and assumptions building behavior for the case study. Additionally, it aids in interpreting and validating results from experimental, analytical, and numerical analyses. The following sub-questions are addressed within this chapter:

- What is the current state of the art research concerning the dynamic response of CLT floors subject to footfall loading?
- How does architectural finishing influence the dynamic response of lightweight floors subject to footfall loading according to existing research?

Chapter 4 - Case Study
This chapter employs a case study to identify and quantify the effects of CLT floor characteristics and architectural finishing on the dynamic behavior of CLT floor systems. This chapter entails a description of the case study and different construction phases in which onsite measurements are conducted. In addition, this chapter presents the experimental, analytical and numerical methods used and analysis procedures to investigate the behavior of the case study floor system. Finally, this chapter displays several verification methods used in this thesis.

Chapter 5 - Results
In this chapter, the results of the onsite measurements with and without architectural finishing are presented and discussed. After, it presents the results of the comparative study of onsite measurements to the predicted modal properties according to common engineering practices. Subsequently, the results of the sensitivity study are presented and the significant parameters affecting the vibration performance are deduced. Finally, the results of the numerical comparative study on the stiffness behavior of connections and the results of the analytical comparative study on the effective bending stiffness are presented and analyzed.

Chapter 6 - Discussion
This section first delves into the assumptions and decisions made in this thesis, discussing their potential impact on the accuracy and reliability of results. Which, this chapter discusses on the results and observations obtained in this research.

Chapter 7 - Conclusion and Recommendations
The results and insights obtained from various stages of the research are summarized to address the main research question. In addition, this section offers recommendations for future research.

1.5 Scope

Given the extensive scope of vibration performance in timber floors and architectural finishing, this research is limited to the following:

1. Investigation of CLT floors, as they offer advantages such as pre-fabrication, rapid on-site erection, and construction efficiency, aligning with the goal of flexible and quick construction in dense urban areas.

2. Focus on the analytical method provided by the preliminary Eurocode 5 on vibrations, as it is expected to be widely used in the future and represents the most up-to-date method available.

2 Footfall induced vibrations

2.1 Introduction

This chapter provides a comprehensive understanding on footfall-induced vibrations and outlines methods for their quantification. The initial focus is on explaining the fundamental principles underlying footfall-induced vibrations. Subsequently, existing guidelines that quantify vibration performance are examined in-depth, enhancing comprehension of parameters essential for footfall analysis, along with potential factors that might introduce inaccuracies. Furthermore, the chapter delves into Modal analysis, where methods for assessing the vibration characteristics through both experimental and numerical approaches are given so that reliable knowledge can be obtained. At the end of the chapter, the following questions will be answered:

- Which parameters govern the vibration performance of floors subjected to footfall loading?
- Which parameters used in the prEC5 vibration calculations might lead to inaccuracies in the vibration performance of Cross-Laminated Timber (CLT) floors?

2.2 Basic principles of footfall-induced vibrations

This chapter explains the basic principles of Footfall-induced vibrations in three components; the footfall loading, the vibrating structure, and the sensitivity of humans to the vibration. Herein it is defined what determines the overall dynamic response and how it can be described using the vibration properties.

2.2.1 Footfall loading

Human-induced loads on floors are in principle walking, running, or jumping. The most common load within buildings is walking. The dynamic load of humans walking is dependent on their step frequency and weight [1]. Figure 1 depicts a velocity-time response of a floor to a walking load. Here you can see that the force of a single step generates a regular response. An interval containing one velocity peak depicts one single-step response.

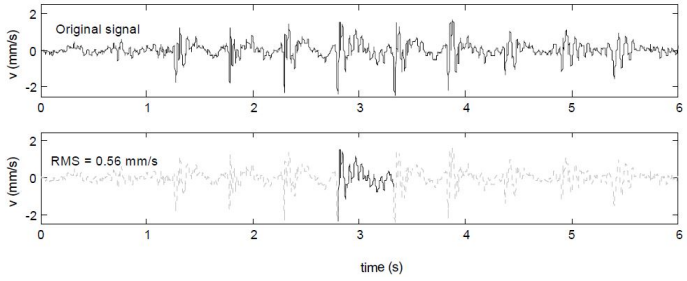

Figure 1: Floor response [1]

The dynamic loading of a single step can be normalized into a normalized step load that can be used in dynamic analysis to model the footfall loading. The normalized step load can be used in dynamic analysis to model the footfall loading. A widely used method to determine the normalized step load is given by the 'Human-induced vibration of steel structures' (HIVOSS) in 2010, where every footfall load is described by a polynomial, see formula 1 for the normalized step load [1]:

$$\frac{F(T)}{G} = K_1 t + K_2 t^2 + K_3 t^3 + K_4 t^4 + K_5 t^5 + K_6 t^6 + K_7 t^7 + k_8 t^8 \tag{1}$$

G is the mass of the person. K_1 to K_8 are coefficients dependent on the step frequency (f_s) given in figure 2 and t is the time in seconds. t_s is the load duration and given by equation 2 [1]:

$$t_s = 2.6606 - 1.757 * f_s + 0.3844 * f_s^2 \tag{2}$$

	$f_s \leq 1.75$	$1.75 < f_s < 2$	$f_s \geq 2$
K_1	$-8 \times f_s + 38$	$24 \times f_s - 18$	$75 \times f_s - 120.4$
K_2	$376 \times f_s - 844$	$-404 \times f_s + 521$	$-1720 \times f_s + 3153$
K_3	$-2804 \times f_s + 6025$	$4224 \times f_s - 6274$	$17055 \times f_s - 31936$
K_4	$6308 \times f_s - 16573$	$-29144 \times f_s + 45468$	$-94265 \times f_s + 175710$
K_5	$1732 \times f_s + 13619$	$109976 \times f_s - 175808$	$298940 \times f_s - 553736$
K_6	$-24648 \times f_s + 16045$	$-217424 \times f_s + 353403$	$-529390 \times f_s + 977335$
K_7	$31836 \times f_s - 33614$	$212776 \times f_s - 350259$	$481665 \times f_s - 888037$
K_8	$-12948 \times f_s + 15532$	$-81572 \times f_s + 135624$	$-174265 \times f_s + 321008$

Figure 2: K1 to K8 coefficients [1]

If $t > t_s$, $F(t) = 0$
otherwise table 2 must be used.
The walking load function is made by repeating the normalized step load. Figure 3 depicts the step load of four distinct step frequencies and an example of a normalized walking load function.

2.2.2 Vibrating Structure

The vibrating structure consists of all the components in the structure that dissipate the energy induced by the source. Every component has its own stiffness, modal mass and damping, which determines the amount and at what time energy is dissipated. These properties can be altered to increase the vibration performance of floors. To understand the dynamic behavior this chapter explains the two different types of response to footfall loading and the basic vibration theory that can be described using a single-degree-of-freedom (SDOF) system and a multi-degree-of-freedom (MDOF) system for analysis.

A system's response to repetitive force can take the form of either the plot of figure 4 or 5 [1]. Respectively these depict a resonant response (or steady-state response) and a transient response. A resonant response generally only occurs when the natural frequency of the floor is close to the excitation frequency or a multiple of the excitation frequency. After a multiple of four times the excitation frequency, the added energy is so little there is no risk of a resonant response anymore. The excitation

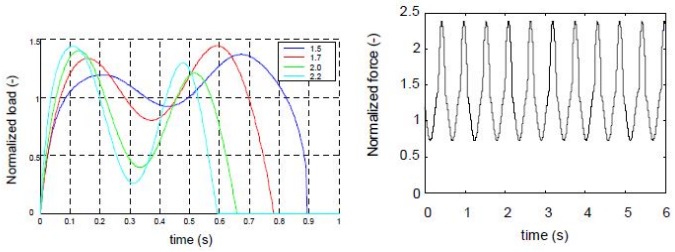

Figure 3: graph left: step load; graph right: normalized walking load [1]

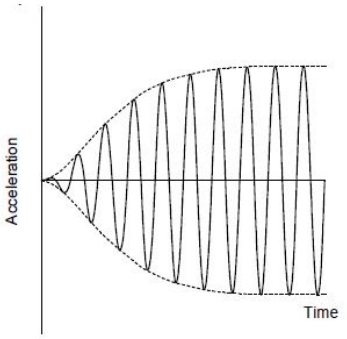

Figure 4: resonant response [1]

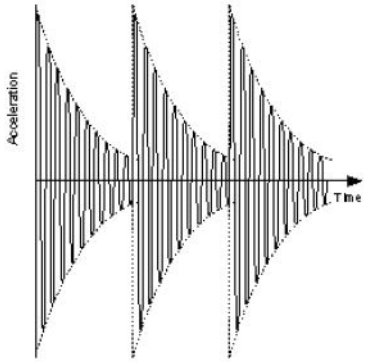

Figure 5: transient response [1]

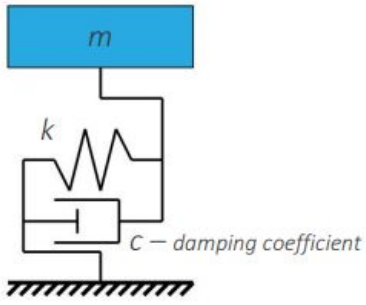

Figure 6: SDOF with damping

force of walking is between 1,5 and 2,5 Hz, therefore the risk of a resonant response only applies to floors with a fundamental natural frequency up to 10 Hz.

One vibrating component can be described with a single-degree-of-freedom system (SDOF), which is a system that can either translate along a line or rotate around a pivot, figure 6 depicts a schematized structure. M is the participating mass, k is the stiffness of the structure and c depicts the damping coefficient of the structure. There are two different kinds of vibration possible, a free vibration and a forced vibration. A free vibration moves in the 'natural frequency' (f_0) of the floor as a result of a single force. The frequency depicts how fast the mass completes one period of its motion. The natural frequency of an SDOF is inherent to the system and is determined by the mass and stiffness. In general light and stiff SDOF systems vibrate fast and, heavy and soft SDOf systems vibrate slow[2].

$$natural frequency = f_0 = \sqrt{\frac{k}{m}} \tag{3}$$

Forced vibrations are subjected to a continuous force. The base moves with a sinusoidal movement. The response of the SDOF is now also dependent on the frequency of the base. When the frequency of the base is smaller than the natural frequency, the structure moves in phase. Otherwise, it moves in anti-phase so that the base and structure vibrate counter-directed. The corresponding equation to a forced vibration is the Equation of motion:

$$mu_{structure} + ku_{structure} = ku_{base} \tag{4}$$

In structural analysis the equation of motion is often rewritten into another form[2]:

$$ku_{relative} + ku_{relative} = -mu_{base} \tag{5}$$

and

$$u_{relative} = u_{structure} - u_{base} \tag{6}$$

$$u_{base}t = u_0 sin(\omega * t) \tag{7}$$

$$if \frac{\omega}{\omega_0} < 1 : inphase$$

$$if \frac{\omega}{\omega_0} > 1 : inantiphase$$

Figure 7 depicts the dynamic amplification factor, it shows how much larger the maximum deflection of the structure will be than the static deflection under the force of the same magnitude. The DAF is dependent on the ratio of the frequency of the base to the natural frequency [2]. The dynamic

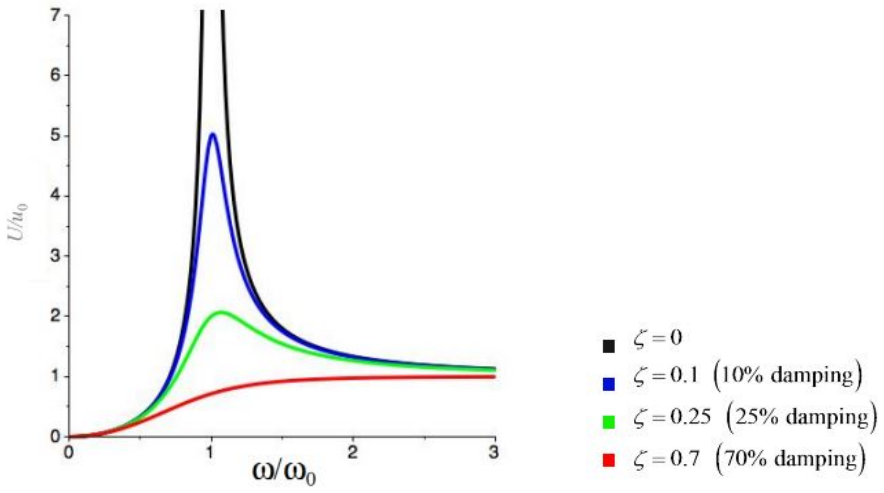

Figure 7: Dynamic amplification factor with different damping [2]

amplification factor can be very large when the frequency of the base is close to the natural frequency of the structure. This leads to significant amplification of the response, resulting in the resonant response depicted in figure 6 on the left. Dissipation of energy always takes place in the course of structural vibrations such as in floors, walls, joints and additional damping devices. Damping is energy dissipation and is given in percentage[13]. The vibration of the structure with damping decays with time and becomes smaller. Figure 7 shows how an increased damping reduces the amplification factor, the larger the damping the quicker the decay of the vibration[13]. The equation of motion and amplification factor with damping is determined with equation 5 . Equation 6 shows that the dynamic response of a forced vibration is dependent on the natural frequency of the floor, the walking frequency, and the damping. If these frequencies are close to each other resonance occurs, which can lead to uncomfortable floor vibrations. Damping reduces the dynamic response, especially at the point of resonance.

Multi-degree-of-freedom system

Often, a SDOF is not enough to describe the vibrations of a structure. A two storey house can for example be simply modeled by a two degree of freedom modal, shown in figure 8. However, if a more complex structure is modeled a MDOF system is needed[14]. A MDOF system contains multiple natural frequencies and therefore multiple base motions can cause resonance. Distinct shapes of vibrations correspond to distinct natural frequencies.

Every free body has its own separate equation, these equations can be merged into a matrix form. For a 2DOF system as shown in figure 8 the corresponding equations of motion are equation 8 and 9. The equations can be written in matrix form.

$$m_1\ddot{u}_1 + c_1\dot{u}_1 + (k_1 + k_2)u_1 = F_1(t) \tag{8}$$

$$m_2\ddot{u}_2 + c_2\dot{u}_2 + k_2u_2 = F_2(t) \tag{9}$$

$$\begin{bmatrix} m_1 & 0 \\ 0 & m_2 \end{bmatrix} \begin{bmatrix} \ddot{u}_1 \\ \ddot{u}_2 \end{bmatrix} + \begin{bmatrix} c_1 + c_1 & -c_2 \\ -c_2 & c_2 \end{bmatrix} \begin{bmatrix} \dot{u}_1 \\ \dot{u}_2 \end{bmatrix} + \begin{bmatrix} k_1 + k_1 & -k_2 \\ -k_2 & k_2 \end{bmatrix} \begin{bmatrix} u_1 \\ u_2 \end{bmatrix} = \begin{bmatrix} f_1 \\ f_2 \end{bmatrix}$$

In general, a MDOF system can be described in the following form [15]:

$$\bar{M}\ddot{u}(t) + \bar{C}\dot{u}(t) + \bar{K}u(t) = \bar{f}(t) \tag{10}$$

where $\bar{M}$ is the mass matrix, $\bar{C}$ is the damping matrix, $\bar{K}$ the stiffness matrix, $\bar{f}$ is the force vector. The natural frequency of a MDOF system without damping can be found by setting the matrix to zero, called the equation of motion:

$$M\ddot{u}(t) + Ku(t) = 0 \tag{11}$$

The initial conditions of the displacement $u(0) = u_0$ and the acceleration $\dot{u(0)} = \dot{u_0}$ are defined to find the movements of the masses. Mode shapes are harmonic vibrations that are the outcome of distinct initial values. Each mode shape has a natural frequency, the lowest frequency is called the fundamental frequency. The free dynamic deflection in time is described by the following equation:

$$u(t) = \phi(A_n cos(\omega_n t) + B_n(\omega_n t)) \tag{12}$$

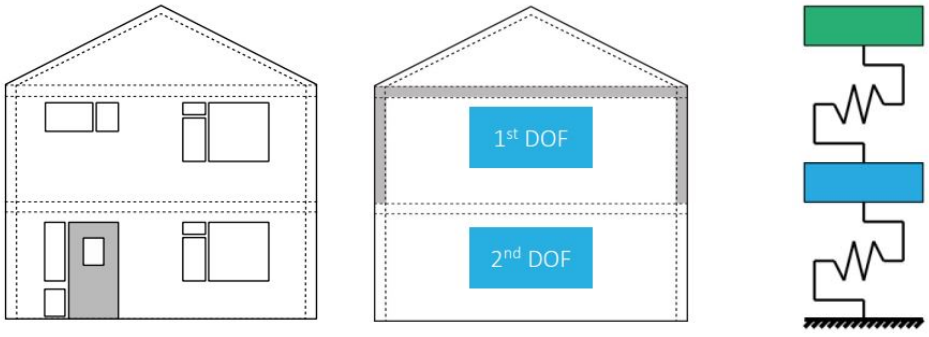

Figure 8: A:Two storey house. B: Two degree of freedom model

Where ϕ_n is the modes of vibration, ω_n the natural frequency and A_n and B_n are constants based on the initial conditions. Herein, ϕ_n and ω_n are the unknowns. Substituting the deflection equation in the equation of motion gives:

$$[\omega_n^2 M\phi_n + K\phi_n]q_n(t) = 0 \tag{13}$$

With $\bar{K}$ and $\bar{M}$ known the corresponding values ω_n and ϕ_n can be found by solving this matrix:

$$[K - \omega_n^2 M]\phi_n = 0 \tag{14}$$

In conclusion, MDOF systems have multiple natural frequencies and resonance responses can therefore be initiated by multiple base motions. From the equation of motion, it is clear that the dynamic response of a MDOF is dependent on the mass, stiffness, damping and displacement of each component.

2.2.3 Sensitvity of residents

The sensitivity of humans to vibrations is dependent on multiple factors. According to the Timber Engineering book [16], the sensitivity of humans to vibrations depends on:
1. The vibration acceleration for natural frequencies below 8 Hz
2. The vibration velocity for natural frequencies above 8 Hz
3. Vibration duration
4. Proximity and awareness of the vibration source
5. Physical activity and familiarity
6. The logarithmic characteristic of the vibration sensitivity

The human body cannot detect high-frequency vibration. The British Standards Institution (BSI) defines frequency weighting curves that can be applied so that a floor frequency can be interpreted to sensitivity, comfort and whole-body vibration. The standards distinguish three translations: fore-and-aft, lateral and vertical within a range of 0.5Hz to 80Hz[17]. Footfall analysis considers vertical vibrations. For vertical vibrations about 50 percent of the people sitting and standing can sense a vertical weighted peak acceleration of 0.015 ms-2. Figure 9 depicts the frequency weighting curve of vertical vibrations given by the BSI and the blue line depicts the peak acceleration threshold [17]. The weighting curve shows that the critical frequencies are between 3 and 25 Hz, where the weighting curve is above the blue line.

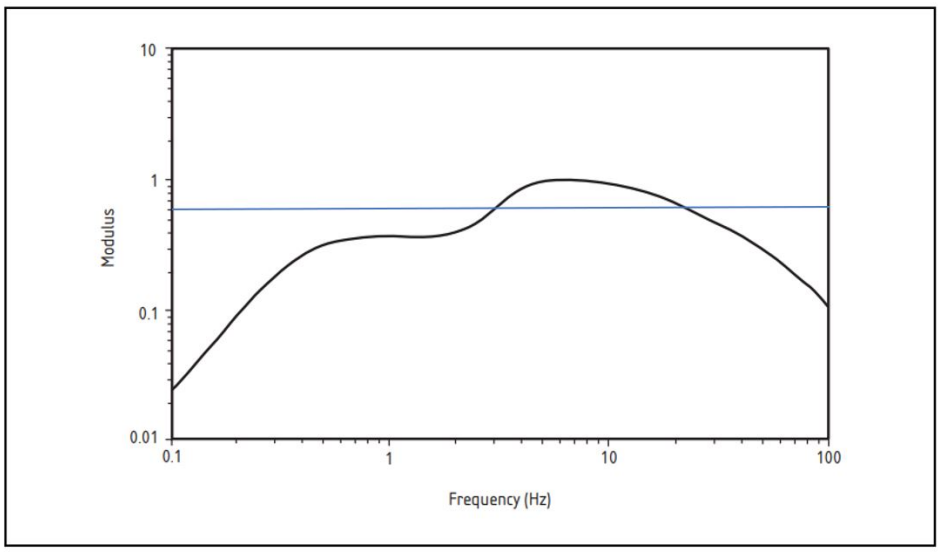

Figure 9: Weighting curve

2.3 Vibration performance calculation methods

As a result of the information presented in chapters 2 and 3, which explains footfall-induced vibrations and the impact of timber elements and connections on such vibrations, we will now examine how the vibration performance of timber floors is quantified in practical terms. In Europe, the prevailing approach for designing timber structures in buildings and other civil engineering works is provided by Eurocode 5: "Design of Timber Structures." In response to the growing popularity of timber structures, the existing Eurocode 5 is being expanded and enhanced in the preliminary Eurocode 5, scheduled for publication in 2026. With a focus on the future, this chapter outlines how the overall dynamic behavior of Cross-Laminated Timber (CLT) floors is evaluated according to the prEC5, placing particular emphasis on the consideration of architectural finishes. Furthermore, a comparison is made between the prEC5 and other currently utilized vibration calculation methods to answer question: Which parameters used in the prEC5 vibration calculations may cause inaccuracies in the vibration performance of CLT floors?

2.3.1 Eurocode 5: vibration calculations

In public contracts, the Eurocodes serve as the recommended reference for technical specifications. They are primarily intended to ensure a consistent level of safety during construction and throughout the service life of structures. Additionally, they provide a design guide that enables a more efficient and cost-effective design process. Due to market demands, advancements in products and materials, and three decades of research, the current version of Eurocode 5, published in 2004, has become outdated. The next generation of Eurocodes, expected to be published in 2026, is currently under constant revision and updating, thus referred to as the preliminary Eurocode 5 (prEC5). Especially

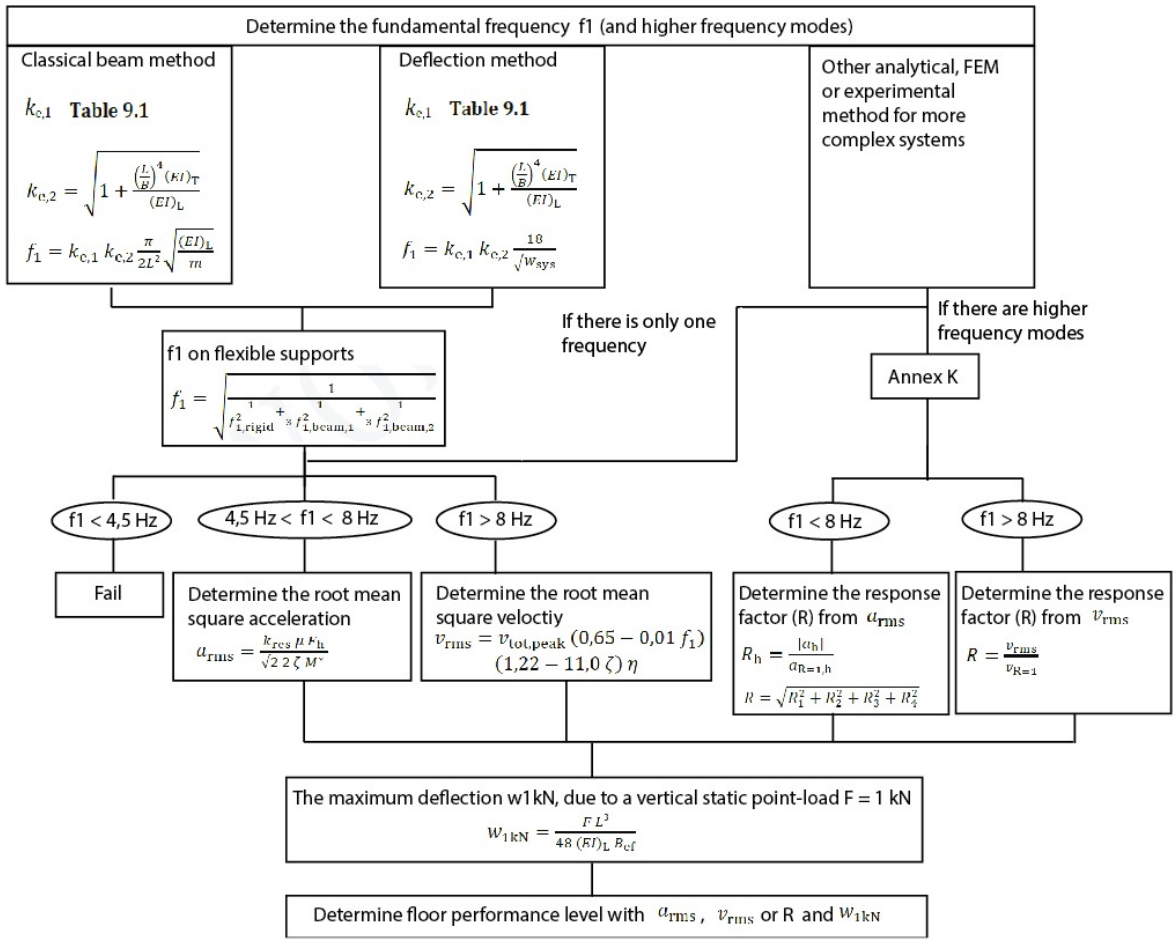

Figure 10: Flow chart of dEC5

the calculations on footfall-induced vibrations are expanded on in the prEC5.

The vibration calculation procedures outlined in the prEC5 are visually represented in a flow chart, depicted in Figure 10. The classical beam method and deflection method are employed for straightforward floor systems with only one predominant fundamental frequency acting. In cases where the floors are more complex and exhibit multiple active frequency modes, the dEC5 offers an alternative method in Annex K. Within Annex K, the frequencies and modal mass serve as inputs, which can be determined through analytical, Finite Element Method (FEM), or experimental analyses.

Classical beam theory method

The first method described in Chapter 9 of the prEC5 to determine the fundamental frequency is the classical beam theory method. This method offers a straightforward and efficient approach to

Table 9.1 — Factor $k_{e,1}$ to calculate the fundamental frequency in case of a two-span floor on rigid supports.

l_2/L [a]	1,0	0,9	0,8	0,7	0,6	0,5	0,4	0,3	0,2
$k_{e,1}$ [b]	1,00	1,09	1,16	1,21	1,25	1,28	1,32	1,36	1,41

[a] L is the longer span as used in Formulae 9.12 and 9.14, l_2 the shorter span of a two span floor in m.

[b] Intermediate values may be obtained by linear interpolation.

Figure 11: Table 9.1 in the prEC5

Table 9.2 — Floor vibration criteria according to the floor performance level.

	Floor performance levels					
Criteria	**I**	**II**	**III**	**IV**	**V**	**VI**
Response factor R	4	8	12	24	36	48
Upper defelction limit $w_{lim,max}$ mm	0,25		0,5	1,0	1,5	2,0
Stiffness criteria for all floors w_{1kN} mm ≤	w_{lim} calculated with Formula 9.30					
Frequency criteria for all floors f_1 Hz ≥	4,5					
Acceleration criteria for resonant vibration ($f_1 < f_{1,lim}$) design situations a_{rms} m/s² ≤	0,005 R					
Velocity criteria for all floors v_{rms} m/s ≤	0,0001 R					

Figure 12: Floor vibration criteria according to the prEC5

Table 9.3 (NDP) — Recommended selection of floor performance levels for use categories A (residential) and B (office).

Use category	Quality choice	Base choice	Economy choice
A (residential) – multi-family block – single family house	 levels I, II, III levels I, II, III, IV	 level IV level V	 level V level VI
B (office)	levels I, II, III	level IV	level V

Figure 13: Use categories according to the prEC5

assess the vibration performance of a floor, but its applicability is limited to simple floor systems or highly simplified representations of complex systems. The accuracy of the results decreases as the real geometry deviates further from the simplified geometry used in the analysis. In general, the classical beam theory method is constrained to the following criteria:

1. Floors with a fundamental frequency exceeding 4.5 Hz.
2. Floors with openings that do not exceed 15 percent of the total area and 40 percent of the floor dimensions.
3. Floors with at least a floor performance level of 6.
4. Discontinuous floors.
5. Simply supported floors.
6. Floors with a uniform transverse and longitudinal bending stiffness in their respective directions.

Static deflection method
The second method given in Chapter 9 is the static deflection method. In this approach, the fundamental frequency is determined by evaluating the static deflection resulting from a point load of 1 kN applied at the most unfavorable location. Essentially, all structural components that influence the dynamic response can be taken into consideration. The static deflection (wsys) can be computed using well-established manual calculation methods or by employing Finite Element Method (FEM) software. The static deflection method exhibits fewer limitations compared to the classical beam method and can be applied to slightly more complex floors, offering a more precise prediction of the fundamental frequency.

Annex K
Annex K in the prEC5 offers additional guidance for the vibration design process, specifically for more complicated floor systems. This comprehensive method can be applied to assess various types of floors, including those with irregular shapes. To utilize this method, the natural frequency of mode m, modal mass, and damping parameters must be determined through analytical, experimental, or Finite Element Method (FEM) modeling analyses. The Annex K, provides alternative formulas for the root mean square velocity, root mean square acceleration and response factor. The Annex K method follows the left side of the flow chart. For the calculation of transient responsive floors the v-rms and response factor take into account all frequencies that lie within the fundamental frequency and twice the fundamental frequency [18]. For example, if the fundamental frequency would be 10,5 Hz, all vertical modes between 10.5 and 21 Hz should be identified and used to determine v-rms and the response factor.

2.3.2 Other calculation methods

The 'prEC5: Vibrations' draws upon a wide range of guidelines, research papers, industry standards, and expert recommendations accumulated over the past 30 years. Indicated by the explanatory background documents of the prEC5, notable references include technical reports from the Steel Construction Institute (SCI), A Cement and Concrete Industry Publication (CCIP), and the Joint Research Centre (JRC) in collaboration with the European Convention for Constructional Steelworks (ECCS). The JRC published its technical report: 'Design of floor structures for human-induced vibrations' in 2009 in support of the harmonization, implementation, and further development of the Eurocodes. While these documents focus on lightweight steel and concrete floors, their principles are applicable to timber structures, making them valuable resources for reliable vibration assessment and design.

A comparison study is done of the prEC5 and background documents to assess the influence of parameters and identify parameters that may cause inaccuracies in the prEC5. The parameters that will be discussed are the: fundamental frequency limit (f_{lim}), the fundamental frequency (f_1), the damping ratio (ζ), the Modal mass (M^*) and the resulting response factor (R). Special attention is given to how the effect of architectural finishing on vibration performance is considered in the prEC5. Finally, guidelines for onsite testing are discussed according to the NEN-EN 16929: 'Beproevingmethoden' [19].

Fundamental frequency limit
The fundamental frequency limit determines whether a floor is categorized as a low-frequency floor (LFF) or a high-frequency floor (HFF). The limit is based on the first four possible harmonics of the walking frequency that can provide enough energy to cause a resonant response of the floor. Figure 18 represents the first four harmonics for a simply supported beam or floor on two sides. LFF floors have to be assessed according to the root mean square acceleration criteria (a_{rms}) due to the possibility of having a resonant response, while HFF floors should be checked according to the root mean square velocity criteria (v_{rms}). The prEC5 sets the limit at 8 Hz for most floors and 7 Hz for floors with a performance level 6. Reference design guidelines SCI, JRC, and CCIP suggest resonant responses can occur in floors with fundamental frequencies up to 9-10 Hz. As the prEC5 considers walking frequencies between 1.5 and 2.5 Hz, the 4th harmonic of 2.5 Hz is 10 Hz. Based on the walking frequency, assuming floors above 8 Hz only exhibit transient response may be to low a value. Especially for areas with big spans, walking loads with higher frequencies are expected, which may result in resonant responses in floors with fundamental frequencies of 10 Hz.

Fundamental frequency
As can be seen in the flow chart, the prEC5 gives two formulas to determine the fundamental frequency, in addition, two factors are introduced. The $k_{e,1}$ frequency factor to consider the geometry in case of a two-way spanning floor on rigid supports. The $k_{e,1}$ factor is related to width to length ratio. As can be seen from figure 14 and 15 the smaller the ratio between $l2/L$ the bigger the $k_{e,1}$ factor. Secondly, the $k_{e,2}$ frequency factor is introduced to consider the effect of the transverse floor stiffness in the case of a double span floor and is determined with equation 15. The frequency is thus dependent on the geometry, bending stiffness in both directions and the mass of the floor. The span of the floor is especially of significance on the fundamental frequency.

$$k_{e,2} = \sqrt{1 + \frac{(L/B)^2 * (EI)_T}{(EI)_L}} \tag{15}$$

$$f_1 = \frac{\pi}{2} \frac{EI_y}{\mu * l^4} \sqrt{1 + [2(\frac{b}{l})^2 + (\frac{b}{l})^4] \frac{EI_x}{EI_y}} \tag{16}$$

The background document by the JRC also gives a formula for the frequency that takes into account the ratio between the length and the width of the plate and the stiffness in orthotopic plates, formula 16. The ke,2 factor is similar to the squared part of equation 16. The JRC also gives fundamental frequency formulas that take into account different support conditions, these formulas can be employed to support the prEC5 vibration calculations.

Damping
The damping value is very hard to predict analytically therefore the prEC5 gives standardized damping values that are based on a lot of floor vibration studies done throughout Europe and worldwide. Standardized damping values are given for the four categories given in table 1. According to the background document of the prEC5 these damping ratio's are conservative in comparison with damping values measured on-site.

[3]:
The design of floors for vibrations', published by the SCI in 2009 recommends using the values given in figure 16. The SCI distinguishes between three different building stages, however, there are also

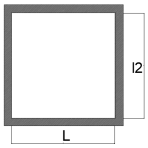

Figure 14: ke,1 = 1 for l2/L = 1

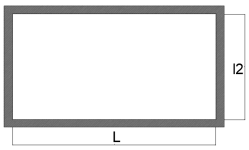

Figure 15: ke,1 = 1,28 for l2/L = 0,5

more elaborate methods. The JRC determines the damping value by adding the structural damping, damping due to furniture and damping due to finishing. Figure 17 shows the critical damping values per component given by the JRC. Notable is the high structural damping corresponding to wood of 6%, which is much higher than prescribed by the prEC5. Timber as material has a inherent relative high damping property compared to other building materials, in addition to often using mechanical connections [20]. Mechanical connections, such as bolts and fasteners can introduce added damping into systems because they allow for movement between the elements, which contributes to energy dissipation. This also explains why in the SCI [3] partitioning walls add damping to the system, because it is and added vibrating element that can dissipate energy.

Floor-type	Damping
Joisted floors	0,02
timber-concrete, rib type and slab type (e.g. CLT, LVL, GLT) floors	0,025
joisted floors with a floating floor layer	0,03
timber-concrete, rib type and slab type (e.g. CLT, LVL, GLVL, GLT) floors with a floating floor layer	0,04

Table 1: Modal damping ratio given by dEC5

ζ	**Floor finishes**
0.5%	for fully welded steel structures, e.g. staircases
1.1%	for completely bare floors or floors where only a small amount of furnishings are present.
3.0%	for fully fitted out and furnished floors in normal use.
4.5%	for a floor where the designer is confident that partitions will be appropriately located to interrupt the relevant mode(s) of vibration (i.e. the partition lines are perpendicular to the main vibrating elements of the critical mode shape).

Figure 16: Damping values according to SCI [3]

Type	**Damping (% of critical damping)**
Structural Damping D_1	
Wood	6%
Concrete	2%
Steel	1%
Composite	1%
Damping due to furniture D_2	
Traditional office for 1 to 3 persons with separation walls	2%
Paperless office	0%
Open plan office.	1%
Library	1%
Houses	1%
Schools	0%
Gymnasium	0%
Damping due to finishings D_3	
Ceiling under the floor	1%
Free floating floor	0%
Swimming screed	1%
Total Damping $D = D_1 + D_2 + D_3$	

Figure 17: Damping values according to JRC [4]

Modal mass

The dEC5 gives the following formula for the modal mass for the calculation of the acceleration root mean square value in Chapter 9:

$$M = 0.25 * m \tag{17}$$

As explained in the previous chapter the modal mass is dependent on the mass, geometry, floor supports and stiffness in longitudinal and transverse directions. The JRC [4] gives modal mass formulas for floors with different support conditions. Figure 20 and figure 21 respectively depict a floor clamped and simply supported on all four sides. Floors with clamped support conditions show a lower modal mass than simply supported floors. In addition, one-way spanning floors show a higher participating mass than two-way spanning floors, this is clear when comparing the modal masses of figure 19 with figure 21 and 20. The formula given by the prEC5 in Chapter 8 for the modal mass is equal to the modal mass formula given by the JRC for a floor hinged supported on all four sides. In the prEC5 Annex no modal mass formula is given.

R-factor

The R factor is based on currently used floor structures where experience shows acceptable performance and the logarithmic relation between acceptability and acceleration. Finally, it is also based on the JRC report [4] that recommends response factors for residential and office use between 8 and 32(class C), these values agree with the floor performance levels from table 9.3 (figure 13.

Non-structural

Figure 18: First four harmonics

Supporting Conditions	Natural Frequency	Modal Mass
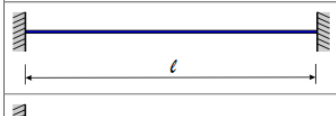	$f = \frac{4}{\pi}\sqrt{\frac{3EI}{0.37\mu l^4}}$	$M_{mod} = 0{,}41\ \mu\ l$
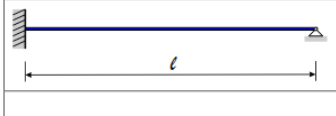	$f = \frac{2}{\pi}\sqrt{\frac{3EI}{0.2\mu l^4}}$	$M_{mod} = 0{,}45\ \mu\ l$
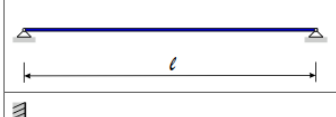	$f = \frac{2}{\pi}\sqrt{\frac{3EI}{0.49\ \mu l^4}}$	$M_{mod} = 0{,}5\ \mu\ l$
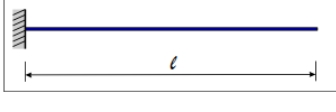	$f = \frac{1}{2\pi}\sqrt{\frac{3EI}{0.24\mu l^4}}$	$M_{mod} = 0{,}64\ \mu\ l$

Figure 19: Modal mass of one way spanning floors

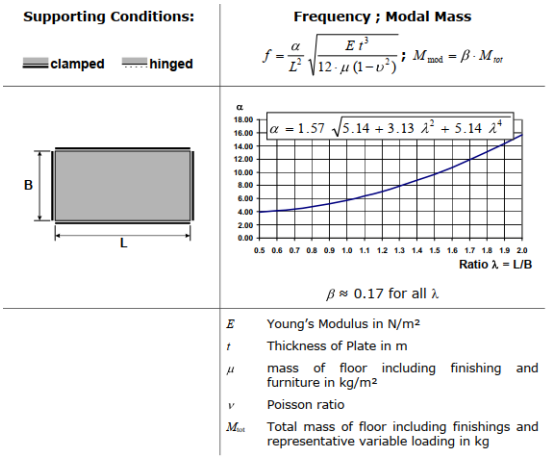

Figure 20: Frequency formula given by JRC [4]

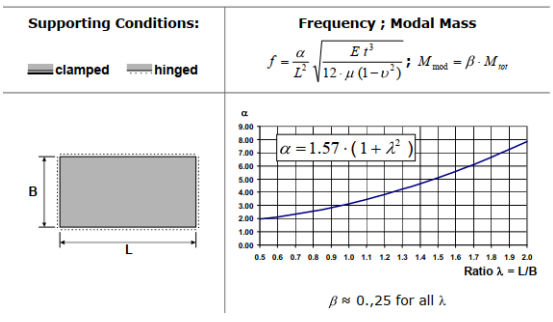

Figure 21: Modal mass of a double span simply supported floor

Additional effects as a result of the structural properties of partitions are not mentioned and generally not taken into account in the prEC5. However, background documents referenced by the dEC5 show how on-site tests revealed that partitions can restrict certain modes, leading to lower predicted frequencies and improper modal damping [4]. A study comparing on-site tests and FE models demonstrated that adding an "effective partition" improved frequency matching between the model and tested frequencies. Simplified methods that consider the span between partitions resulted in more accurate prediction of dynamic response factors than those neglecting partitions. Modeling partitions accurately is challenging due to their type and connection details. The classical beam method in the prEC5 considers only the partition mass in floor vibration assessment, disregarding structural contributions. The static deflection and Annex K methods allow for the inclusion of additional partition effects, but an appropriate method needs yet to be given. Regarding floor finishing, the prEC5 states that the stiffness of the non-structural layers should be taken into account but any composite action between the non-structural layer and load-bearing floor should not. Finally also mentioned under damping is that besides a floating screed, the type of architectural finishing used in the structure is not translated to the added damping in the prEC5.

2.3.3 Onsite testing procedure

Experimental tests are very valuable due to the complexity of the dynamic behavior and the accuracy of the experimental test results. In general, the measurements are conducted by applying excitation at specific locations and measuring the corresponding vibration responses using force transducers or accelerometers. However, to obtain reliable and comparable results a test method should be followed. This chapter follows the test method and procedure provided by the NEN-EN 16929: 'Beproevingsmethoden' [19]. In addition, reliable modal analysis methods to identify the model parameters are explained.

Determination of the frequency
To determine the frequency from on-site testing the floor must be adequately excited and a fitting acceleration measurement must be taken. From the measurements, the fundamental frequency, that is the lowest measured frequency, and the higher frequency modes must be calculated. In timber floors, these modes often lie very close to each other with a distance ranging from 0.5 Hz to 5 Hz. An adequate excitation can be enforced by using a heel drop, rubber ball drop or an impact hammer. The load must be applied at the location where the biggest deformations are expected, in addition, the accelerometer must be placed 300 mm to 500 mm from the exciter. The test should be recorded for at least 10 s with a minimum sampling rate of 500 Hz. A sufficient sampling rate (sr) must be chosen to determine accurate dynamic floor properties. A sampling rate of at least 10 times the highest estimated natural frequency of timber floors is recommended [19]. The more sr the more accurate, however, this will also increase the computational time. An sr must be chosen that provides enough accuracy but will not end in very lengthy computations.

Determination of the mode shapes
The load must be located where the highest deformations are expected, mostly in the middle of a floor span or at the end of a cantilevering floor. The response measurements must be recorded at a sufficient amount of locations over the entire floor plan to determine the full mode shape of each mode of importance.

Determination of the damping
The damping ratio is preferably measured using a mechanical exciter or stepping person. The mechanical exciter should excite the floor in resonance with the floor. After the steady-state vibration is secured the exciter is stopped and the vibration is measured. A stepping person can also be used, stepping should be done at half or one-third of the fundamental frequency of the floor to excite the floor in resonance. Again after the steady state is secured, the stepping is stopped and the vibration is measured. It is also possible to obtain damping values from an adequate single impulse. This impulse must cause a free vibration where the floor vibrates in its own fundamental frequency. Due to the different types of loading attention must be taken when comparing damping values from previous research to experimentally obtained data.

2.4 Modal analysis

Modal analysis is the process of identifying the dynamic characteristics of a system, that is its natural frequencies, damping factors, and mode shapes, to create a theoretical model that describes the system's dynamic behavior. The theoretical model relies on a physical model of the system that is described by the basic vibration theory in previous chapter. The analysis is based on the concept that the vibration response of a linear time-invariant system can be expressed as a combination of natural modes of vibration [21]. A physical model can be created from the differential equations of motion, that then with the superposition principle of a linear dynamic system can be transformed to a typical eigenvalue problem. The solution of the eigenvalue problem provides the dynamic characteristics of the system [21]. As modern structural design focuses on more efficient and lighter unique structures, understanding vibration sensitivity becomes increasingly important, thus modal analysis needs to be employed.

Modal analysis embraces a big range of theoretical and experimental methods to investigate, enhance, and optimize the dynamic properties of structures. Finite element analysis has proven valuable for engineers to examine dynamic properties. However, computer modeling alone cannot fully capture the dynamic behavior of structures due to certain factors such as damping, nonlinearity, and uncertainties in boundary conditions. To address these limitations, experimental testing is needed[21]. This chapter discusses the methods that are of importance for this thesis, in addition the limitations and applicability of the method is discussed so that it can be taken into account when discussing the results.

2.4.1 Numerical determination of dynamic characteristics

In order to analyse the dynamic behavior of structure the equilibrium of imposed loads, internal forces, inertial forces and damping needs to be found, while for static analysis only a equilibrium of the imposed loads and internal forces is needed. The inertial forces are the masses of a structure that move with acceleration during vibration. Just as in static analysis a deformation shape of the floor is determined from the equilibrium of forces, for dynamic analysis this is referred to as the mode shapes. The mode shape can be output in two forms: mass normalized and unity normalized. In mass-normalized mode shapes, the output displacements are adjusted so that the modal mass, denoted as M*, is equal to 1 kg [3]. While these mode shapes can be used in equations, they don't provide information about the contribution of each mode to the overall response. Therefore, the participating modal mass cannot be determined through this normalization method.

In unity normalized mode shapes, the maximum displacement of each mode is set to a non-dimensional value of 1 [3]. To calculate the modal mass corresponding to a unity normalized mode shape, the maximum kinetic energy in each mode shape must be determined, either through finite element software or manually. The modal mass can be obtained manually by normalizing the displacement using the following steps:

1. First the displacement at each mesh point of the first harmonic must be obtained by either a FEM dynamic analysis or a formula describing the displacement form. For a floor simply supported on two sides the displacement can be obtained as output from a FEM sofware in figure 22 or equation 18

$$d = \sin \frac{\pi x}{l} \tag{18}$$

2. Secondly the displacement at each point is normalized by dividing it by the maximum displacement

$$d_{n,i} = \frac{d_i}{d_{max}} \tag{19}$$

$d_n = the\ normalized\ displacement$
$d_1 = the\ displacement\ on\ the\ ith\ mesh\ point$
$d_{max} = the\ maximum\ displacment$

3. Then the modal mass factor can be determined with the equation:

$$c_m = \frac{\sum(d_{n,i}^2)}{n} \tag{20}$$

$n = number/of/mesh/points$

4. The modal mass is finally obtained by multiplying the total mass with the modal mass factor:

$$M^* = m * c_m \tag{21}$$

It's important to note that some finite element software may provide an output of mass participation or effective mass, which is different from the modal mass. To ensure that the software gives the modal mass as output, it is recommended to consider a model of a simply supported beam where the modal masses should theoretically be half of the total mass (integrated for a sinusoidal mode shape) [3].

Software

FEM software provides engineers with a multi-functional design tool, that can help derive the dynamic properties of a system. However, a deep understanding of the theoretical background used in the FEM is needed to assure meaningful outcomes. There are several FEM software, such as SCIA, RFEM, ABAQUS, OASYS GSA, ANSYS, etc. that contain modal analysis. SCIA determines the mode shapes based on mass normalization and therefore does not give the modal mass. It is possible to determine the modal mass manually from the displacements given by SCIA's dynamic analysis. However, this is a cumbersome and time-consuming calculation. The modal mass can also be obtained by using the specialized software CADS Footfall Analysis (CFA) in correspondence with SCIA.

During footfall analysis, the floor is loaded with a walking load, which gives the velocity in time response. CADS Footfall Analysis utilizes the modal analysis results from Dlubal RFEM or SCIA Engineer for the footfall analysis. The software incorporates the latest analysis procedures and provides the user with the option to choose between two commonly used calculation methods: the Concrete Centre Method (CCIP-016) and the Steel Construction Institute Method (SCI). Though both methods, CCIP-016 and SCI, are based on modal analysis there are some differences. First of the CCIP method determines the vrms, arms and response factor, whereas the SCI method only uses the arms and response to determine the vibration performance of a floor. Another difference is the type of footfall loading. The CCIP-016 uses a standardized design force that is based on 882 measured footfall

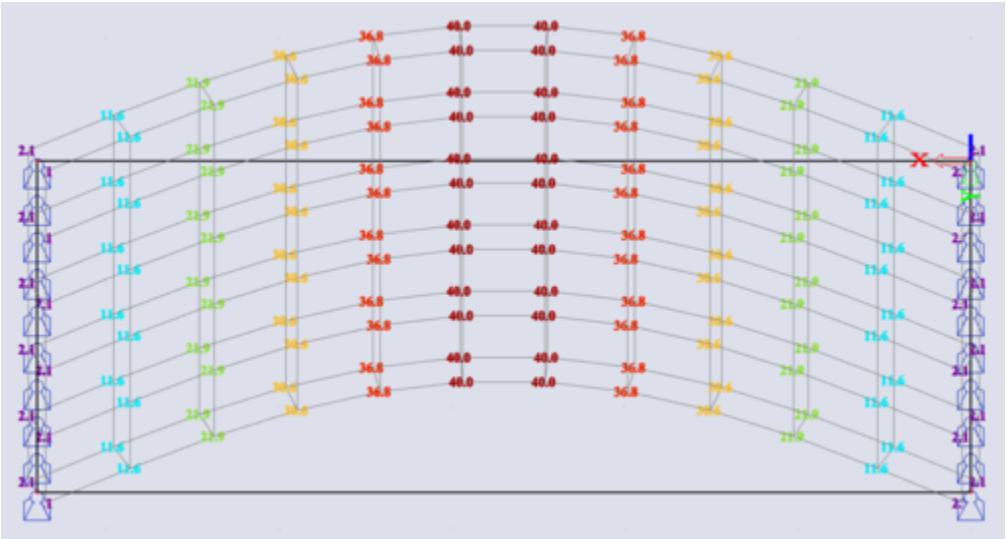

Figure 22: Displacement per mesh given by SCIA dynamic analysis

load measurements and has a 25 percent probability of exceedance [18]. The SCI gives a dynamic load function that is dependent on the static force exerted by a person. The forcing function of walking is assumed to be perfectly periodic and can therefore be described by the first four harmonic components calculated from Fourier analysis. The amplitude of the harmonic force is given by:

$$F_h = \alpha_h * Q \tag{22}$$

α_h = the Fourier coefficient of the h^{th} harmonic (taken from table 3.1)
Q = is the static force exerted by an 'average person' (normally taken as 76kg x 9,81 m/s^2 = 746N)

As a result of the high similarities of the CCIP-016 method to the prEC5 method, especially the method specified in the Annex, the CCIP-016 will be further used in this research.

2.4.2 Experimental modal testing

Experimental modal testing is the process of deriving the vibration properties from the measured velocities or acceleration. It is useful to process onsite measured data.

Time domain
In the context of floor vibration, the vibration is usually measured in velocity or acceleration. Figure 23 depicts the measured velocities of a CLT floor during a vibration test, where the floor is excited by a single force. As velocity is the first derivative of the displacement and acceleration is the second derivative, it is possible the translate the velocity-time graph to obtain the displacements and acceleration response of the floor. The motion of the displacement and acceleration is equal to the velocity in time, so can all be used to transform the data from the time domain to the frequency domain.

Frequency domain
The measured data can be transformed from the time domain to the frequency domain using the Fourier method. This is helpful in finding the fundamental frequency, modal frequencies and helps to reveal oscillations hidden in the original time data. The Fourier method is named after the French mathematician and physicist Joseph Fourier. The Fourier transform breaks down any signal into simple sine and cosine waves wherefrom the frequency, amplitude and phase can be determined. In 1965 Cooley and Tukey's created the Fast Fourier Transform (FFT), which is an algorithm that transforms the data in a much more efficient way. Using the build-in FFT function from Python, the measured data from figure 23 is transformed to the frequency domain in figure 25. The peaks depict the frequency in which the floor is oscillating. In this case, there are two frequencies excited, a fundamental frequency of around 13,5 Hz and a second frequency of 20 Hz. The width of the peak shows that it is a damped system, if it was an undamped system the frequency domain would show two vertical lines at 13,5 Hz and 20 Hz.

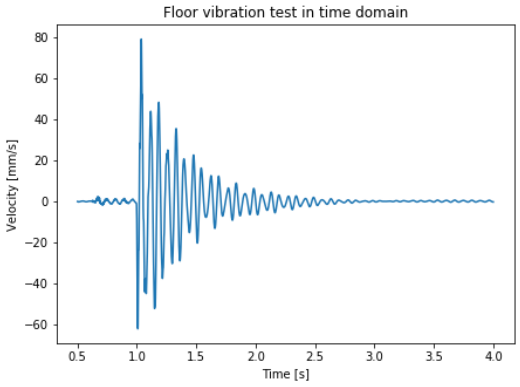

Figure 23: Time domain

Damping

There are different approaches determining the damping ratio within the time and frequency domain. A method in the time domain is the Envelope fitting method depicted in figure 24. In this method, the exponential curve is fitted through the amplitude peaks to approach the damping of a free vibration. This method is only applicable when there is a clear single fundamental frequency peak and can not well manage noise. The decay profile is given by[20]:

$$X(t) = Ae^{-\xi\omega_n t}$$

Where $A = constant$ and $\omega_n = fundamental frequency$

The damping can also be estimated in the frequency domain with the peak-picking method, using the fundamental frequency f_1 and the half power points f_a, f_b. The half power points can be found on either side of the fundamental frequency peak by finding the intersection points with the $\frac{\alpha_{max}}{\sqrt{2}}$ as shown in figure 25. The damping ratio can then be determined from the width of the frequency with equation 23. The peak-picking method is one of the simplest methods, this method is suitable for lightly damped data with well-separated modes and good frequency resolution. Due to its simplicity, it has not a very high accuracy and it can not deal well with noise. Both methods need data with a high sampling rate. The lower the rate the more inaccurate the approximation of amplitudes is[20].

$$\zeta_r = \frac{f_b - f_a}{2f_1} \tag{23}$$

2.5 Conclusion

In conclusion, the vibration performance of floors subjected to footfall loading is governed by a combination of factors explained in this chapter. The fundamental principles of footfall-induced vibrations are expressed by the footfall loading, the vibrating structure, and human sensitivity. Footfall loading, primarily from walking, is characterized by the step frequency and weight of the person. The dynamic response of the structure is determined by its stiffness, mass, and damping and can be described by its inherent natural frequency. Risk on resonance response is especially detrimental to vibration performance and occurs when the excitation frequency is close to the natural frequency. Additionally, human sensitivity to vibrations is dependent on factors such as vibration acceleration, velocity, duration, proximity to the source, physical activity, and awareness. To quantitatively assess vibration sensitivity, frequency weighting curves are employed.

The vibration performance of CLT floors is assessed using prEC5 methods and compared with industry standards. While prEC5 is comprehensive, some parameters may cause inaccuracies. Notably,

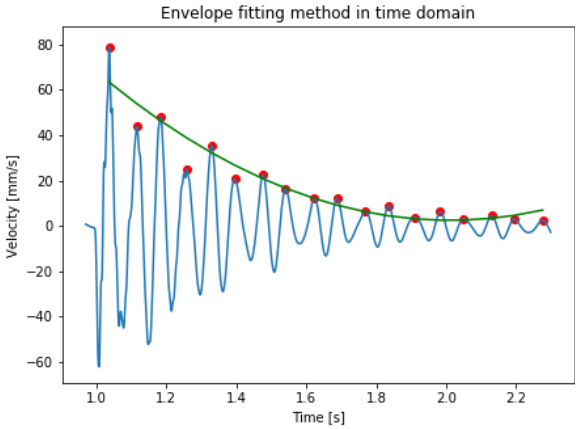

Figure 24: Envelope-fitting method

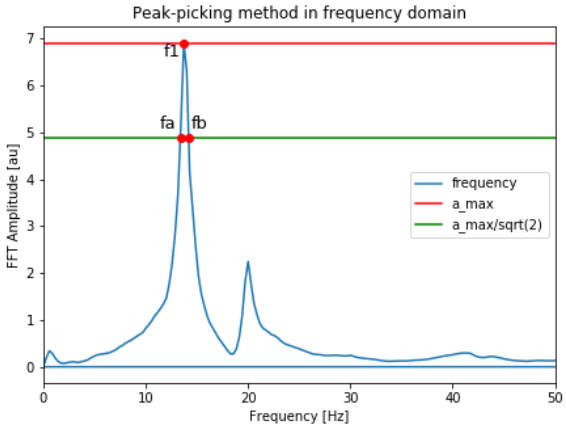

Figure 25: Peak-picking method

the fundamental frequency limit is set to 8 Hz, which might underestimate resonance risks. Fundamental frequency determination relies on geometry, span and boundary conditions. The may be employed to take into account different boundary conditions. Damping ratios from prEC5 might be conservative compared to other standards. Modal mass, vital in vibration analysis, is influenced by supports and geometry. In Chapter 9 the PrEC5 proposes the modal mass of a simply supported two-way span floor for all types of floors, which is contrasting with other standards. Non-structural elements like partitions and finishing impact vibrations, but prEC5's treatment is limited. Enhancing accuracy requires considering these factors and using alternative formulas. prEC5 refinement through research could improve CLT floor vibration assessment.

To conclude, Modal analysis involves deriving the modal model of a dynamic system using theoretical and/or experimental systems. There are typically multiple approaches to the same problem, resulting in Finite Element Method (FEM) software being based on different methods. SCIA determines mode shapes by normalizing the mass, which means that the participating masses given by SCIA cannot be used to determine the modal mass. Therefore, in this study, the CADS plug-in is utilized to determine the modal mass. Within CADS the CCIP method is utilized because it shows higher similarity to the prEC5, which is studied in this thesis, then the SCI method. In addition, the peak-picking method is found most suitable, because it is less sensitive to noise than the envelope method. However the peak-picking method is still sensitive to noise, this needs to be taken into account when discussing the estimated damping ratio's.

3 Dynamics of CLT floor systems

3.1 Introduction

In the previous chapter, a general understanding of footfall-induced vibrations is presented. Consequently, in this chapter explicitly the dynamic behavior of CLT floors in timber structures is assessed, taking into account the structural and non-structural components. Special attention is given to partitions, screed and inter-CLT panel connections, as it has been shown from previous research that these non-structural components have an effect on the overall dynamic behavior of timber structures. This chapter is the basis for the initial parameters and modal assumptions for the case study. In addition supports interpreting and validating the results from the experimental, analytical and numerical analysis. The following questions will be answered during this chapter:

- What is the current state of the art research concerning the dynamic response of CLT floors subject to footfall loading?
- How does architectural finishing influence the dynamic response of lightweight floors subject to footfall loading according to existing research?

3.2 Dynamics of stand-alone CLT floors

Cross-Laminated Timber (CLT) floor panels consist of solid wood panels stacked crosswise and bonded under pressure. This assembly enhances properties such as strength, rigidity, stability, fire resistance, and aesthetics, making CLT panels well-suited for applications in mid- and high-rise buildings [22]. CLT's mechanical properties stem from the arrangement of wood panels, which are orthotropic materials. This orientation allows CLT to exhibit varying strengths and stiffnesses in longitudinal and transverse directions. Additionally, the removal of low-quality sections, such as those containing knots, enhances overall material properties. CLT floors commonly employ strength grade 24c or 28c, comprising at least five crosswise layered wood panels. The bending stiffness of a CLT floor can be calculated using Steiner's rule, and variations may exist in bending stiffness and elastic modulus between CLT floors of similar type and thickness that utilize different wood types as raw materials [23]. Table 3 provides the material properties corresponding to grade 24c. Studies show that modal parameters are not sensitive to poison ratios [7].

CLT floors possess a high strength-to-mass ratio, rendering them relatively light compared to concrete floors. As a consequence, footfall loading induces larger vibrations in lighter CLT floors than in heavier concrete alternatives. Furthermore, the fundamental frequency of a CLT floor, often determined by thickness and support conditions, can fall below 9-10 Hz, potentially increasing the risk on resonant response. Resonance leads to amplified vibrations and can result in discomfort for occupants due to increased perceptible motion. Bending stiffness and span length play significant roles

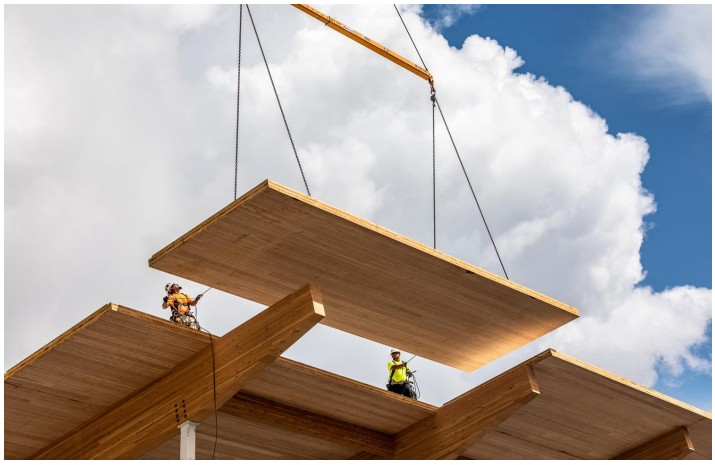

Figure 26: CLT panel

in influencing the fundamental frequency, with fixed-supported CLT floors generally exhibiting higher frequencies and lower modal masses compared to hinged-supported counterparts [4]. In CLT floors, damping mechanisms are the material damping and friction at connections. Timber has a relatively high damping, which helps reduce the vibration, enhancing occupant comfort.

3.3 Dynamics of timber-to-timber connections

In timber structures, the behavior of joints significantly influences overall system performance, as they often represent weaker points compared to the members they connect. The design of joints in mass timber construction is crucial, with semi-rigid connections playing a key role. Diverse mechanical fasteners are employed, categorized into dowel-type and surface-type connections, each transmitting forces differently. While joints aim for some level of rigidity, achieving full rigidity is hard to achieve and costly [16]. Within timber construction, the main advice kept for joint design is to use simple joints and minimize fastener types [16].

Mechanically jointed members, such as the CLT floor-to-beam connection in figure 27, comprise elements connected by mechanical fasteners. The semi-rigidity of these joints allows relative displacements due to shear forces. Methods like the y-method and shear analogy handle mechanically jointed beams and columns, with the γ-method accommodating up to three-member composite beams. The γ coefficient, influencing composite stiffness, ranges from 0 to 1, with γ=1 implying full cooperation and γ=0 indicating disconnected members.

Timber structures commonly exhibit high damping due to friction in mechanical fasteners during vibrations. About the stiffness of connections under footfall-loading, there exist divergent beliefs. On the one hand according to the prEC5, the rotational stiffness of timber floor-to-beam connections; given the low dynamic forces from footfall compared to serviceability limit state (SLS) loads, dowel-type connections are expected to remain within the initial slip region of force-displacement curves, behaving as pins. On the other hand for translation stiffness, a lab test on dowel-type connections under cyclic loading parallel to the grain demonstrated that connections behave significantly stiffer under small vibration [24]. Only thing definite is that the stiffness behavior of timber-to-timber connections is not the same under dynamic loading and static loading, but is dependent on the type of loading. This research will further investigate the behavior of connection by testing different stiffness assumptions on connections transferring moment and/or shear forces.

Inter-panel connection
Due to constraints in transportation and manufacturing, CLT panels are usually recommended to be used within certain size limits, such as being less than 3 meters wide and 20 meters long according to Dutch codes [6]. Consequently, CLT floor systems are often composed of prefabricated CLT panels that are placed adjacently on-site and interconnected using inter-panel connections. These connections, primarily fastened on-site, serve to transfer in-plane bending moments and shear forces [6]. Notably, these inter-panel connections facilitate efficient assembly, allowing for a variety of panel

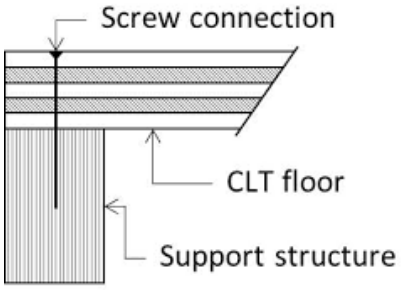

Figure 27: Simple pinned connection of CLT to beam [5]

length-to-width ratios. Several common inter-panel connections are illustrated in Figure 28, with relatively simple connections achieved using a few screws per connection point.

While inter-panel connections are typically not considered in floor dynamics calculations, however some research has considered their influence. Several numerical studies show that the rotational stiffness of the inter-panel connection has a relatively small effect on the frequency compared to the effect it has on the mode shapes, which is measured with the v_{rms}. The influence on the modal properties is especially significant when the mode shape has a nodal line in the longitudinal direction [7]. A recent numerical study on the influence of inter-panel connections on the vibration performance of CLT floors, compared compared floor slabs consisting of two panels with and without an inter-panel connection. The results showed that when a walking load is applied parallel over the inter-panel connection line, vrms were 67% higher for the floor with an inter-panel connection compared to the monolithic slab [6]. Thus concluding that these lines should not be placed on dominant walking paths or and should be considered in the vibration performance quantification. It is especially crucial to take into account the inter-panel connection to identify critical vibration areas.

Finally, the initial space clearance and the delayed hardening of timber can impact the behavior of these connections. When subjected to compression perpendicular to the grain, timber exhibits a distinct stress-strain relationship with a sigmoid (S-shaped) curve from figure 29[25]. This non-linear behavior includes a delayed hardening phase followed by continuous hardening without a stress peak, particularly for strains exceeding 10%. This delayed hardening behavior can lead to initial slip in connections involving perpendicular-to-grain timber, introducing relative movement due to this behavior. It should be noted that the bigger the mass of the floor, the higher the contact area in the inter-panel connection, thus increasing the rotational stiffness of the joint. Due to relatively small displacements related to footfall-induced vibrations, it may be expected that initial space clearance and delayed hardening play a significant role in the stiffness behavior of inter-panel connections.

3.4 Architectural finishing

Architectural finishing refers to the final steps and elements that are added to a building's interior and exterior to enhance its appearance, functionality, and overall aesthetic appeal. It encompasses a wide range of design, construction, and decorative elements that contribute to the final look and feel of a building. Some of the common components for interior finishes are: internal partitions, wall finishing, flooring, ceiling finishes and installations. For exterior finishes, there is cladding, roofing material but also windows and doors. Generally, the architectural finishing increases the damping value, as the damping of footfall-induced vibrations is dependent on the mechanical connections and the material damping of the floor and surrounding building elements. In the general practice of footfall analysis, only the weight of architectural finishing is taken into account, however, experimental research shows that under small vibrations architectural finishing also influences other vibration properties.

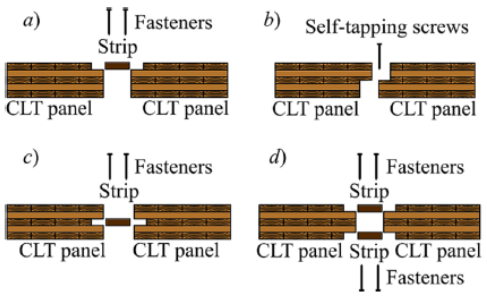

Figure 28: Four types of inter-panel joints [6]

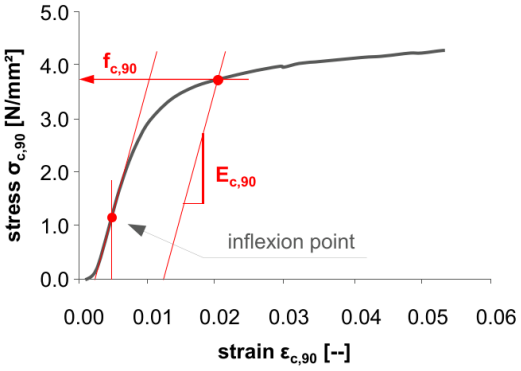

Figure 29: Stress-strain diagram of timber

3.4.1 Screed

There are three main types of screed possible, bonded, unbonded and floating screed. Bonded screed is bonded to the substrate by slurrying bonding, this type is ideal for thinner applications and heavy loading. The unbonded screed is bonded to a Damp Proof membrane (DPM) that is laid on top of the base. Floating screed is the most popular option in offices and dwellings due to the need for insulation in modern buildings. The floating screed is laid on a layer of insulation with a slip membrane, that separates the insulation for the screed. A general build-up of a floating screed floor is the base floor, a slip membrane (sheet of Polythene), insulation, another slip membrane and then screed [26]. Cement screed is often favored for CLT floors due to its weight and stiffness contribution. The addition of a screed introduces significant modifications to the floor's vibration properties.

The interplay between stiffness and mass determines whether the natural frequency increases or decreases after placing a screed layer. For lightweight floors, added mass decreases the frequency while added stiffness increases it [27]. Experimental analysis of a CLT floor with cement floating screed, depicted in figure 30, observed a frequency reduction of approximately 2 Hz, from 12.78 Hz to 10.68 Hz, accompanied by decreased damping values from 8 percent to 3.6 percent after placing a cement screed on top of a CLT floor [7]. Although a decrease of 2 Hz, according to practical engineering models the predicted frequency after placing the cement screed was determined 25% lower than the measured fundamental frequency. Thus resulting in a big underestimation of the frequency. According to Kawrza [7] this can partly be attributed to modeling the bonded fill as a mass but without a stiffness. However, the bonded fill only has a bending stiffness that is 4.5% of the bending stiffness of CLT so can only explain a very small part of the 25% discrepancy found after placing the floor finishing. Because the modeling inaccuracies have less effect on the overall mode shapes, it can be deduced that the overall bending stiffness in both directions is estimated too low for unknown reasons. According to Kawrza [7] the decrease in the damping is due to that the screed layer acts as a unifying element, closing joints and enhancing contact between components, resulting in reduced energy dissipation through friction. More studies showed that as mass increases the incremental declination of the frequency and damping will weaken [27].

Interfaces and connections between different layers, such as CLT, screed, and insulation, further contribute to the overall dynamic behavior by influencing force transmission and deformation. For example, an experimental study on timber-concrete composite (TCC) floors connected to each other with dowels depicted in figure 31, showed that the dynamic frequencies were notably higher than the static frequencies [8]. The dynamic eigenfrequencies suggest that the bending stiffness from the dynamic test is higher than that of the static test, moreover, it suggests that the bending stiffness is equal to the bending stiffness of a TCC beam where no slip is allowed between the timber and concrete. These findings emphasize the distinct behavior of connections subject to small vibrations.

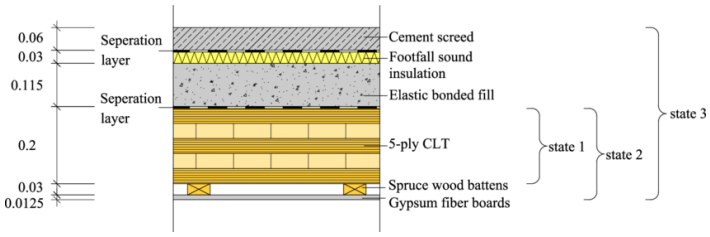

Figure 30: CLT floor with cement screed [7]

Figure 31: TCC floor during lab test [8]

3.4.2 Partitions

Partition walls, spanning from floor to ceiling, play a crucial role in shaping a building's dynamic response. However common engineering practices only consider their mass in vibration calculations. A recent study where experimental tests in different building phases resulted in an increased frequency after placement of a partitioning wall, of a mode shape with maximum displacement at the location of the partition [7]. Must be noted that in addition to the partition, also a drywall was installed. To determine the actual effect of partitions on vibrations, their behavior must consider both material properties, geometry and interactions with the surrounding structure. Initial stiffness values for various partition types, such as full-height glass partitions and double-boarded plasterboard walls, have been derived by Miskovic [28]. The partition arrangements are of significance, which substantially influences the floor natural frequencies and corresponding mode shapes [28]. Integrating partitions into analytical models is essential for accurate vibration assessments, particularly when partitions are integral to the floor layout [18]. Nonetheless, the development of guidelines to incorporate partitions effectively in whole-floor structural design are yet to be established.

3.5 Modeling

As is clear from prior research, the connections and building components may behave differently under small cyclic loading than under static loading. This means that for the numerical analyses also different modeling methods are needed to simulate the accurate response of structures subject to dynamic loading. This chapter looks at prior studies for methods to model the CLT floor, concrete screed, partitions, and connections in the case study.

Modeling CLT floor
CLT floor panels can be modeled using FEM according to equivalent single-layer (ESL) or layerwise plate theories [29]. Despite the layerwise plate theory providing more accurate results than the ESL theory, it is the ESL theory that is mostly used due to its simplicity and shorter computer simulation time[30].

FEM models of inter-panel connections are scarce. The study by M.Milojecive [6] however presents a method to model two of the most common inter-panel connections, that can be applied to different types of FE software used to determine the vibration modes of a CLT floor. This study clearly states how the rotational and shear stiffness of the connection can be determined from the real geometric. Figure 32 depicts the schematization of the half-lapped joint to determine its rotational stiffness. Must be noted that this method is based on static calculations, and its dynamic applicability remains to be established with experimental analysis. It is reasoned by M.Milojevic [6] that the four connection types in figure 28 have equivalent modal properties and dynamic responses after resulting from his study that that was, in fact, the case for single surface spline and half-lapped joints. The dynamic response properties of CLT floors are closer to real data when a group of adjacent CLT panels is modeled as a monolithic slab then not connected at all [6].

Numerical simulations that take into account the semi-rigidity of inter-panel connections show significantly different modal properties and vibration responses with simulations of stand-alone or mono-

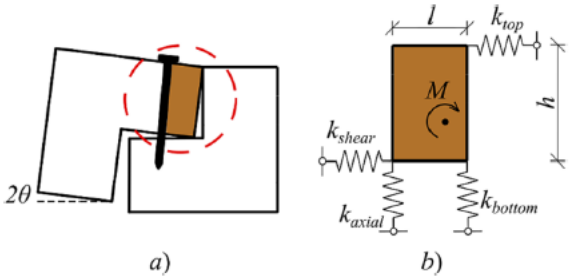

Figure 32: Schematization of inter-panel connection[6]

lithic slabs. The differences are the biggest for slabs modeled as stand-alone slabs because each panel dynamically behaves as a single floor. Between the monolithic and semi-rigid slabs, the biggest difference is in the mode shape where the connection lines move largely in relation to the rest of the floor [6].

Modeling of screed
For most CLT floors with a floating screed, only the added mass is taken to account in the FEM model. However, research shows that the screed layer also adds to the bending stiffness of the floor. A method to model the floor depicted in figure 30 is given by Kawrza [7] where the CLT slab is discretized with four-node shell elements with full nu- merical integration. The gypsum fiber boards added in state 2 are modeled as a ho- homogeneous, isotropic board with shell elements, the spruce wood battens with beam elements. In the FE model of the test object in state 3, both the elastic bonded fill and the footfall sound insulation are discretized with continuum elements, while the floating cement screed is described with shell elements.

Modeling of partitions
Assuming that the partition walls only restrict the vertical translation of a floor system, partitions can analytically be modeled as spring elements with just axial stiffness. This spring element can be modeled in different manners. One way is using a beam element with exclusively an axial stiffness of 1 m length [28]. On the other hand on, the nonstructural wall can be considered by distributing its effective mass evenly over its base dimensions [7]. Correct modeling of full-height partitions makes models a more accurate representation of reality and increases the accuracy of dynamic property prediction. This is especially true for establishing the mode shapes.

3.6 Conclusion

This chapter delved into the intricate dynamics of Cross-Laminated Timber (CLT) floors and their interactions with various components in timber structures, shredding light on both structural and non-structural elements. Due to the low density of CLT floors, they are sensitive to unwanted floor vibrations, in addition, there is the risk on resonance response. On the other hand, due to timber having a high material damping and timber structures commonly exhibit high damping due to friction in mechanical fasteners during vibrations, CLT floors have a relatively high damping ratio.

The stiffness behavior of timber-to-timber connections is dependent on the type of loading, sometimes argued as more stiff or less stiff when subject to small vibrations. The effect of inter-panel connections is relatively small on the frequency but is significant on the v_{rms} values. A numerical study showed that when a walking load is applied parallel over the inter-panel connection line, v_{rms} were 67% higher for the floor with an inter-panel connection compared to the monolithic slab [6]. Concluding that overlooking inter-panel connections will lead to an overestimation of the vibration performance. However, this has to be substantiated with experimental data.

Architectural finishing components, namely partitions, and screed, proved significant in shaping dynamic responses. Partition walls, reaching from floor to ceiling, showcased an increase in the floor's natural frequencies and mode shapes. The integration of partitions orthogonal to span into analytical models emerged as crucial for precise vibration assessments. Meanwhile, screed layers altered the vibrational properties of CLT floors, affecting natural frequency, modal mass, and damping. Experimental evidence illustrated that the reduction of the fundamental frequency upon the addition of a cement screed layer was less than determined according to common engineering practices, implying a higher increase of the bending stiffness than assumed [7]. The increase is possibly a result of friction between the interlayers, however, this hypothesis must be further explored with experimental and numerical analysis. In summary, the dynamics of CLT floors in timber structures encompass a complex interplay between various factors, including material properties, structural components, and architectural finishing. This chapter provides a foundation for subsequent experimental, numerical and analytical analyses.

4 Case study

4.1 Introduction

This chapter employs a case study approach to fulfill two purposes: first to identify and quantify the distinctive impact of CLT floor characteristics and architectural finishing on the dynamic behavior of CLT floor systems via experimental analyses. This is done by conducting onsite measurements during two building phases, specifically before and after the architectural finishing is placed. Secondly, the onsite measurements are used to evaluate the precision of common engineering practices within footfall analysis and test alternative assumptions on the behavior of CLT floor systems subject to small vibrations.

Section 4.2 presents the analysis procedure employed to obtain the needed results. Section 4.3 presents the building design and the two building phases during which onsite measurements are conducted. Section 4.4 displays the properties of the structural elements and the architectural finishing. Section 4.5 Presents the different analysis methods used in this study; experimental, analytical, and numerical. Section 4.6 describes the parameter identification of the parameters that have a significant influence on the modal properties of the floor system. Section 4.7 presents the design choices and assumptions following common engineering practices and alternative possibilities that will be tested. Finally, section 4.8 presents a validation of the analysis methods.

4.2 Analysis procedure

The analysis procedure follows the subgoals set for this thesis, an outline of the Case study is presented in figure 33. This chapter elaborates on the analysis procedure based on the three steps taken during the case study which are in line with the objectives set for this study. The research outcome discusses and analyses the results of the three parts in order to answer the main research question set for this thesis.

Part 1: Onsite measurements
The first objective is to identify and quantify from onsite measurements the effect of CLT floor characteristics and architectural finishing on the vibration performance. This is achieved by carrying out onsite measurements before and after architectural finishing is placed. From the measured velocity

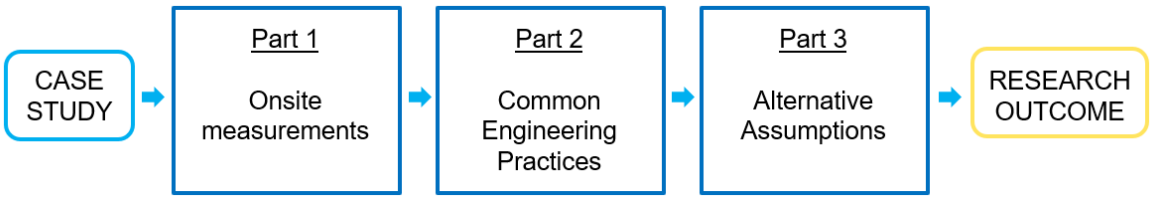

Figure 33: Outline of Case Study

Figure 34: Houtlab render [9]

Figure 35: Houtlab during construction [10]

response the frequency, damping and v_{rms} are obtained using modal analysis. The effect of CLT floor characteristics is identified and investigated by comparing the measured modal properties to each other and to empirical values given by standard guidelines. The effect of architectural finishing is determined by defining the change of the modal properties before and after architectural finishing is placed.

Part 2: Common Engineering Practices (CEP)
The second objective is to investigate design codes and common engineering design assumptions on the structural behavior of CLT floors subject to footfall-induced vibrations. This is accomplished by a comparative study where analytical and numerical prediction following CEP are compared to onsite measurements. Measured frequency values are directly comparable with analytical and numerical determined frequency. However due to that onsite test where carried out using a single force as load and numerical footfall analysis software assumes footfall loading, the v_{rms} values are not directly comparable. To assess the mode shape and v_{rms} values given by the numerical analysis, the ratio between the measured v_{rms} at the inter-panel connection and in the middle of the panel, from the numerical analysis is compared to the measured ratio. The ratio is defined as:

$$\triangle v_{rms} = \frac{v_{rms,P11} - v_{rms,P10}}{v_{rms,P10}} \tag{24}$$

Part 3: Alternative Assumptions
The last objective is to investigate other possible design assumptions on the structural behavior of CLT floors to footfall-induced vibrations. The final goal is achieved by further studying possible other behaviors of the inter-panel connections and floor finishing compared to common engineering beliefs. Numerical analysis is employed to investigate the influence of the stiffness of connections by applying different stiffness scenario's to the FEM model and comparing the resulting modal properties to onsite measurements.

Similarly, possible cooperation between the floor finishing and CLT floor is investigated by comparing analytical analysis assuming different cooperation scenario's to onsite measurements. Analytical analysis is used to investigate the cooperation due to that it is a straightforward method. For numerical analysis the orthogonal plate properties must be determined and possible incorrect methods may result in uncertainties in the results.

4.3 Building design

The building taken for the case study is a timber building called HOUTlab, which is a timber-post beam structure located in the south of Holland [9]. Figure 34 depicts a render of the finalized building. HOUTlab will function as an office and a lab for innovations in the field of sustainable construction. The building itself is a sustainable and inspiring timber building designed by the progressive engineering firm *Lüning* that specializes in timber structures[31]. The case study is focused on the first floor of the building. A distinction is made between the two building phases during which onsite measurements are conducted, Phase 1 is when the bare CLT floor is realized and Phase 2 is after the architectural finishing is realized. This subchapter describes the general structure at the moments of building phases 1 and 2, where the next chapter describes in depth the floor plan and relates measured modal properties to boundary conditions.

4.3.1 Phase 1: Bare CLT floor

The load-bearing structure of the four-story building, depicted in figure 35, is built out of GL beams, GL columns, CLT floors and CLT walls. Figure 40 depicts the floor plan, test points and location where pictures from figure 36 are taken. Figure 36 depicts the bare timber structure. Stability is achieved by a stiff core of CLT panels placed in the middle of the floor plan. Within the stiff core lies a staircase and the liftshaft. The CLT floor is placed on supporting beams and connected via self-tapping screws. The CLT floors mainly span in one direction from beam to beam with a span of 5.4 m. At some locations, the floor is also supported by a side support, as in axis E, which is part of a wind brace. The CLT floors are connected to the CLT load-bearing core with screws and to the columns with angled brackets. What is also visible is the HSB facade panel, the open area will be

filled with windows during the next building phase. Exact dimensions and material properties can be found in table 2 ,3 and 4. In addition, a schematization of the prevalent connections is given in the next chapter as part of the results.

4.3.2 Phase 2: CLT floor with architectural finishing

In phase 2 the architectural finishing and installations are placed, as depicted in figure 37. The architectural finishing consists of the partitioning walls, insulation, floor finishing, HSB facade, and windows. The floor finishing encompasses 30 mm of Rockwool insulation and 80 mm of reinforced concrete screed. Exact thicknesses and material properties can be found in table 2 and 3. During measurements in phase 2 in plane A-B there were construction materials that caused big loads on the floor. This makes the test situation not ideal to measure the dynamic behavior of the stand-alone CLT floor. There were no big loads in plane F-E, which is one of the reasons plane F-E is preferred for the comparison to analytical and numerical analysis.

(a) Picture: floor plane axis F-E where the structural timber is visible

(b) Picture: floor plane axis A-B where the structural timber is visible

Figure 36: Building phase 1

(a) Picture: floor plane axis F-E where the architectural finishing and installations are visible

(b) Picture: floor plane axis A-B where the architectural finishing and installations are visible

Figure 37: Building phase 2

4.4 Properties Structural elements

Properties	Values	Unit
Dimensions of CLT panel(L x w x h)	5400 x 2700 x 200	mm
Thickness cement screed (h)	80	mm
Thickness loadbearing insulation (t)	30	mm
Main supporting beam (w x h)	240 x 600	mm
Wind supporting beam (w x h)	240 x 340	mm
Column (w x h x L)	340 x 340 x 3900	mm

Table 2: Dimensions

Property	Symbol	Value	Unit
Density mass CLT	ρ_m	500	$kg/m3$
Density concrete screed	ρ_c	2500	$kg/m3$
Density loadbearing insulation	ρ_i	32,5	$kg/m3$
Modulus of elasticity concrete	E_c	30000	Nmm^2
Modulus of elasticity insulation	E_i	11	N/mm^2
Shear modulus of insulation	G_i	5	N/mm^2
Longitudinal bending stiffness	$EI_{CLT,L}$	$6336{\cdot}10^9$	Nmm^2
Transversal bending stiffness	$EI_{CLT,T}$	$1664{\cdot}10^9$	Nmm^2

Table 3: Material properties of 5L-200CLT according to CLT supplier en insulation according to EN13163

Property	Symbol	GL28h	C24	Unit
Bending strength	$f_{m;k}$	28	24	N/mm^2
Tension strength //	$f_{t;0;k}$	19,5	14	N/mm^2
Tension strength -—	$f_{t;90;k}$	0,45	0,4	N/mm^2
Compression strength //	$f_{c;0;k}$	26,5	21	N/mm^2
Compression strength -—	$f_{c;90;k}$	3,0	2,5	N/mm^2
Shear strength	$f_{v;k}$	3,2	4	N/mm^2
Mean Modulus of elasticity //	$E_{0;mean}$	12600	11000	Nmm^2
Modulus of elasticity //	$E_{0,05}$	10200	7400	Nmm^2
Modulus of elasticity -—	$E_{90;mean}$	420	370	Nmm^2
Shear modulus	G_{mean}	780	690	Nmm^2
Density-char	ρ_k	410	350	kg/m^3
Density mean	ρ_{mean}	490	420	kg/m^3

Table 4: Material properties GL28h and C24 according to EN338

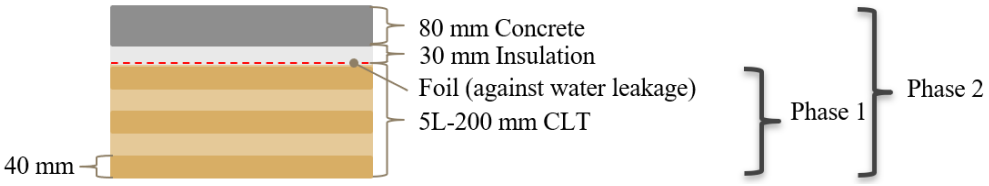

Figure 38: Cross-section case study floor

4.5 Analysis methods

Different analysis methods are employed to assess CLT floor characteristics and effects of architectural finishing on the dynamic response of CLT floor systems. Experimental analysis is used to study the real response, whereafter it is used to assess the accuracy of the analytical and numerical analysis. The analytical and numerical analysis are used to investigate assumptions on the behavior of the CLT floor system to footfall-induced vibrations.

4.5.1 Experimental

Experimental analysis is used to determine the actual modal properties of the Case Study floor. This chapter describes how the onsite measurements are conducted and how the raw data is processed to obtain the modal properties. The onsite tests are executed using a loading mechanism and a velocity sensor. Figure 39 illustrates the test setup, where the load and sensor are both placed in point 1 from figure 40. The loading mechanism uses a 10 kg weight, which was dropped from a height of 83 cm. To ensure accuracy and reliability, each test setup was repeated three times, maintaining the same test procedure. The detailed test procedure is provided in Annex B.

The chosen measurement points are depicted in Figure 40. Similar measurements were performed on floor planes A-B and F-E, to evaluate the influence of distinct boundary conditions and validate the results. Comparing similar measurements served as a validation. The measurements are labeled as P'test point' when both the loading mechanism and the sensor were positioned at the same location. If the sensor is placed on another location, the measurements are labeled as P'loading point'-S'sensor point', for instance, measurement P11-S13.

First of all measurements are conducted before and after architectural finishing is placed to investigate the real effect of the architectural finishing on the modal properties and resulting vibration performance. Second, measurements on the inter-panel connection line (P7, P8, and P11) and in the middle of the CLT panel (P1 and P10) are chosen to investigate the effect of the inter-panel connection. In addition, measurements P4 and P12 were placed on the mid-span of supporting beams to determine the vibration characteristics of the supports. The flexibility of supports is considered in the analytical and numerical prediction models, measurements P4 and P12 were used to verify the accu-

Figure 39: Test setup: Loading mechanism and velocity sensor

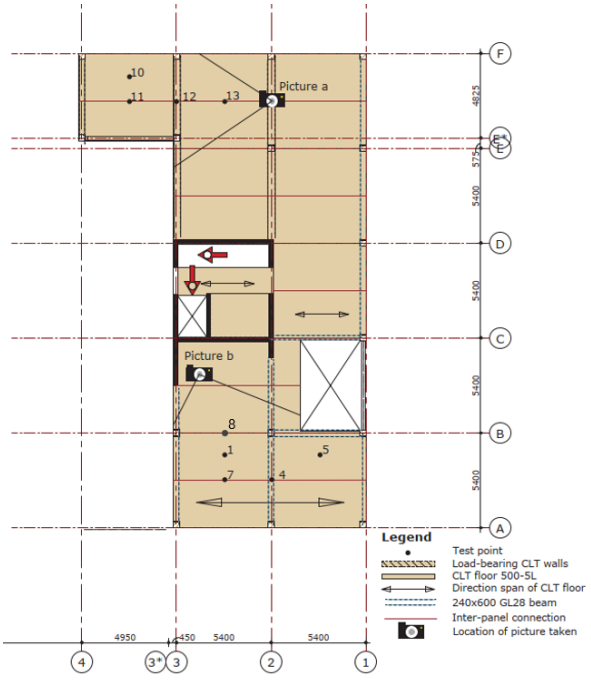

Figure 40: Location of test points and picture a and b

racy of these calculations. Finally, measurements P11-S13 and P1-S5 were conducted to analyze the transfer of vibrations to adjacent floor plans that are respectively continuous and not continuous floors.

Processing results
To determine the modal properties from the measured velocities, Modal analysis from chapter 2.4.2 is employed. The raw data is processed using the programming language Python. To minimize noise induced by the dynamic response of the floor to random impulses, a time window is chosen from 0.5 to 4 seconds. Within this time window, the dynamic response to the mechanical impulse is totally died out at all points, while minimizing noise. To determine the damping two methods are explored: the peak-picking method and the curve-fit method. As explained in chapter 2.4.2 the peak-picking method is preferred and applied to process the actual data. The curve-fit method is however used to validate the peak picking method in chapter 4.8. Each measurement is conducted three times, the dynamic response of the three measurements shows very high similarities. Especially the frequency is exactly the same up to two decimal points. An visual illustration of the dynamic response can be found in Annex figure 82 where the three measurements taken at point 11 are depicted. The final result shown in this study is the average value of the three measurements. After processing the velocity response, the active frequencies, damping and vrms are determined. The Python script can be found in Annex C.1 in figures 77 and 80.

4.5.2 Analytical

For the analytical analysis, Chapter 9 of the prEC5: 'Vibrations' is employed. This method is selected, because it is a straightforward and easy method to use as well as becoming the most widely used standard in Europe after publishment. For single or multiple span floors that are approximately rectangular in-plane and are one- or two-way spanning, the frequency may be determined using the formula 26. The method is discussed in depth in chapter 2.3 and at outline is given in figure 10.

$$f = k_{e,1} k_{e,2} \frac{\pi}{2L^2} \sqrt{\frac{(EI)_L}{m}} \tag{25}$$

This method only distinguishes between one-way spanning floors and two-way spanning floors. For the analytical analysis, the three-sided supported floor plane between axes E and F from figure 40 is considered. Because the numerical study specified in Annex F showed that the modal properties of a three-sided supported floor are closer to a two-sided supported floor than to a four-sided supported floor, the choice is made to consider the three-sided supported floor as a one-way spanning floor. A one-way span floor is schematized in figure 41, for this floor the $k_{e,1}$ and $k_{e,2}$ factor are equal to 1 and the frequency is determined with equation 26.

$$f = \frac{\pi}{2L^2} \sqrt{\frac{(EI)_L}{m}} \tag{26}$$

To make a good comparison to experimental data, the load used in the analytical and numerical calculations should be close to the load present during onsite testing. Therefore only the self-weight of the floor is taken into account, while it should be noted that according to the prEC5, an additional mass equivalent to 10% of the characteristic imposed loads should be considered to determine the vibration performance. The weight of the loading mechanism, velocity sensor, and person handling the loading mechanism are chosen to be neglected because the weight of the measuring equipment is less than 5% of the total weight of the floor. The self-weight of the CLT and concrete screed is determined using the densities specified in table 3. The bending stiffness of the CLT is according to the CLT supplier and

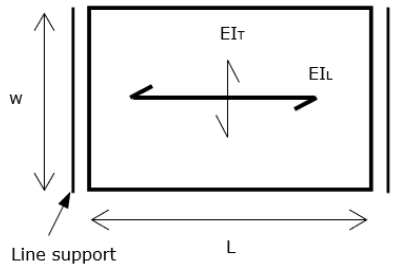

Figure 41: Schematization of floor plan for analytical analysis

that of the concrete is determined using the elastic modulus
specified in 3. With the analytical analysis, the frequency,
vrms value, and response factor are determined according to the prEC5.

4.5.3 Numerical

For the numerical analysis, the FEM software SCIA is employed. Modal analysis in SCIA provides the mode shapes and corresponding frequencies. In addition, it produces the model that is used in footfall analysis software CFA, which determines the modal mass, vrms values and response factor according to the CCIP method. The FEM model for the numerical analysis should accurately represent the structure during building phases 1 and 2, with as few parameters as possible for the applicability and optimization of the method. For the numerical analysis, the assumed floor system encompasses the floor, supporting beams, and columns, with its dimensions given in table 2. Modeling the columns aligns with standard engineering practice for floor vibrations, as it provides a representation of the surrounding structural system. The weight of the adjacent CLT panel has a negligible effect on the vibration properties and is therefore not taken into account. A demonstration of the minor effect can be found in Annex E.

The material properties of the GL28h beam and columns are according to European standards (Table 4). The bending stiffness of the 5L-200mm CLT floor is according to the CLT supplier. The proper linear elastic orthotropic material behavior of CLT is determined by implementing the orthotropic plate parameters given in figure 42. This is done by using the bending stiffness given, in figure 26 and applying them to equations the orthotropic plate parameters 27 to 35 [32].

$$D_{11} = (EI)_L \tag{27}$$

$$D_{22} = (EI)_T \tag{28}$$

$$D_i = \frac{h_{CLT} \cdot D_{i,CLT} + h_c \cdot D_{i,c}}{h_{CLT} + h_c} \tag{29}$$

for i = 33,44 and 55, with:

$$D_{33,CLT} = \frac{G_{12} \cdot h^3}{12} \tag{30}$$

$$D_{44,CLT} = G_{mean} \cdot h_x \tag{31}$$

$$D_{55,CLT} = G_{mean} \cdot h_y \tag{32}$$

$$G_c = \frac{E_c}{2 \cdot (1 - \mu)} with \mu = 0.15 \tag{33}$$

$$D_{33,c} = \frac{G_c \cdot h_c^3}{12} \tag{34}$$

$$D_{44,c} = D_{55,c} = G_c \cdot h_c \tag{35}$$

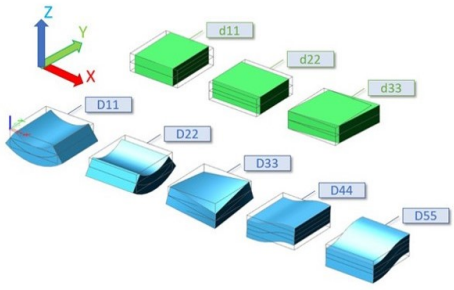

Figure 42: Orthotropic plate parameters

4.6 Parameter identification

Two sensitivity studies are carried out to quantify the influence of stiffness parameters and material parameters on the modal properties to subsequently rule out parameters that have only a minor influence. In this manner, focus can be placed on the important parameters, which will be further tested in the next subchapter 4.7. Regarding the stiffness parameters, a numerical sensitivity study is conducted using FEM software SCIA. The parameters depicted in table 5 and figure 43 are chosen because they possibly affect the vertical displacement of the floor, thus the dynamic response of the floor to footfall loading. In the base model, all connections are rigid in rotational and translational stiffness, whereupon the specified stiffnesses in table 5 are one-by-one set to free. The resulting frequency and mode shape of the models are assessed to determine if the stiffness parameter is of significant influence and should be considered in further analysis.

Regarding the material parameters, a sensitivity is conducted on the frequency and vrms value to the density of CLT. Densities given for CLT range between 470 to 500 kg/m3, therefore an analytical calculation is carried out assuming the lower and upper bound values for the density of CLT. All other material parameters are not considered to have such a big influence and are equal to the parameters specified in chapter 4.4.

4.7 Design choices and assumptions

Different design choices and assumptions have to be made regarding the structural behavior of the floor system for the determination of the modal properties using analytical and numerical methods. This subsection provides an overview of common engineering practices within vibration performance calculations and other possible assumptions, based on prior research. A summary of the three scenarios with different assumptions is given in table 6.

$K_{Rx,f-b}$	Rotational stiffness of connection between CLT floor and supporting beam is set to zero
$K_{Tx,f-b}$	Translation stiffness of connection between CLT floor and supporting beam is stiff
$K_{Rx,b-c}$	Rotational stiffness around x-axis of connection between bean and column is stiff
$K_{Ry,b-c}$	Rotational stiffness around y-axes of connection between beam and column is stiff
$K_{Rx,ip}$	Rotational stiffness of inter-panel connection is stiff

Table 5: Rotational and transversal stiffness alterations for Sensitivity Study

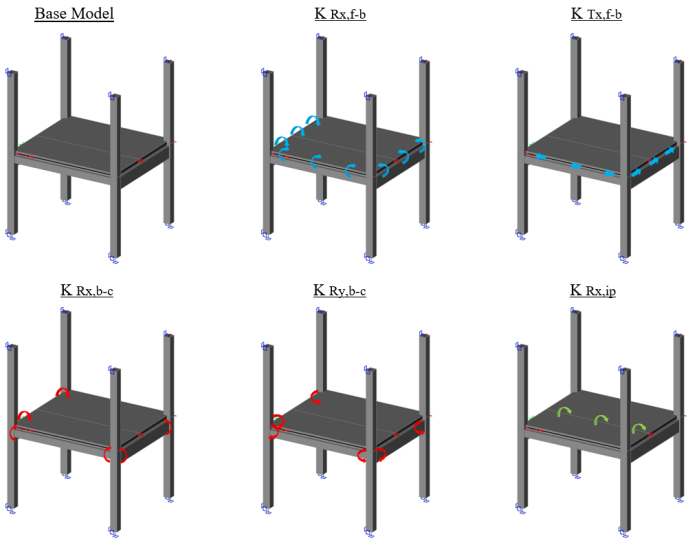

Figure 43: Description of rotational and translational stiffnesses that may influence dynamic behavior of CLT floor

	$K_{Rx,f-b}$ [MN/m/rad]	$K_{Rx,ip}$ [MN/m/rad]	γ [-]
Common engineering practices	hinge	rigid	0
First test scenario	0.36	0.39	0.11
Second test scenario	hinge	hinge	1

Table 6: Assumptions on rotational stiffness and slip

Common engineering practices

Due to the semi-rigidity of timber-to-timber connections, according to common engineering practices CLT floors are commonly assumed to be hinged connected to the supporting beams. On the other hand, it is common to not consider the inter-panel connections but to model multiple CLT panels as a monolithic slab. In other words, this means that the inter-panel connections are assumed to be totally rigid.

Regarding the bending stiffness of the floor. The bending stiffness of the CLT floor is commonly used as prescribed by the supplier or can be determined using the elastic modulus of CLT. The bending stiffness of the concrete floating concrete screed is determined using an elastic modulus of 30000 Nmm2. Due to the presence of the insulation layer, common engineering practices assume that there is slip between the CLT panel and concrete, therefore the bending stiffness is the sum of the stand-alone CLT and concrete, equation 36. The floor buildup, bending stiffness and self-weight of the floor during building phase 1 and 2 are specified in figure 44.

$$EI_{tot} = EI_{CLT} + EI_{concrete} \tag{36}$$

Alternative assumptions

Prior numerical research on the influence of the inter-panel connection on the vibration response, concludes that not taking into account the rotational stiffness of the inter-panel connections results in an underestimation of the vibration performance [6]. This is partly attributed to the mode shape not being properly determined when assuming the inter-panel connection as rigid. However, there still does

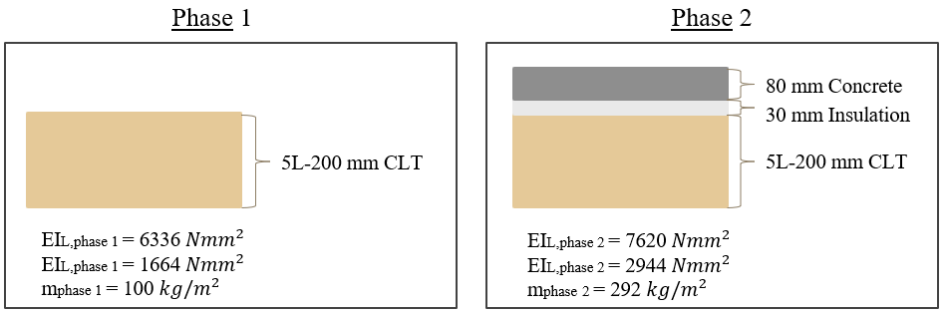

Figure 44: Cross section floors taken for analytical analysis

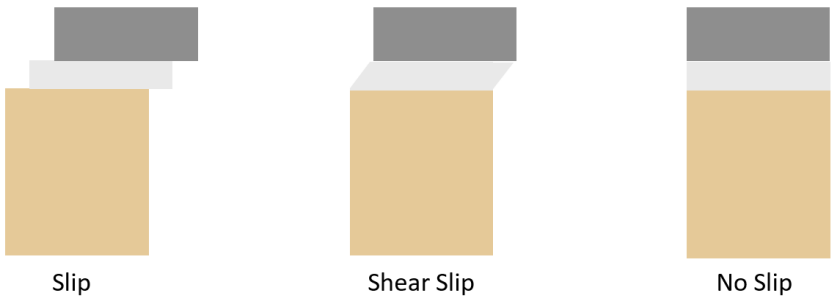

Figure 45: Different types of collaboration between interlayers

not exist a straightforward method to determine the rotational stiffness of joints subject to footfall-induced vibrations. Therefore the two scenarios specified in table 6 regarding the rotational stiffness of connections will be tested on its accuracy. The first scenario assumes both the support connections and inter-panel connection have a rotational stiffness that is based on the prEC5, see Annex G for the employed method. The calculation results in a stiffness of the support of $K_{support} = 0.36MN/m/rad$ and of the inter-panel connection of $K_{Inter-panel} = 0.39MN/m/rad$. The second scenario assumes both connections are a hinge.

Another preceding study that compared onsite measurements to numerical calculations during different construction phases found that measured frequencies after the concrete floating screed is placed are much higher compared to prior calculations, indicating that the bending stiffness of the floor increased much more than expected [7]. The bending stiffness of the overall floor increases when the floor layers work as a collaborative package. This leads to the hypothesis that the insulation layer might transfer shear forces. For this to happen there has to be friction between the concrete screed-insulation interface and insulation-CLT interface, which is not commonly assumed for static analysis. To explore the assumption that the floor layers work as a collaborative package, the analytical calculations are performed in two additional scenarios, figure 56 gives a visual representation of the assumptions. The first scenario assumes that there is shear slip originating from shear deformation of the insulation layer, while the second scenario assumes there is no slip between the layers. The bending stiffness (EI_{tot}) of the floor system in each scenario was determined as follows:

$$EI_{tot} = EI_{CLT} + EI_{concrete} + \gamma \cdot EI_{steiner} \tag{37}$$

where EI_{CLT} and $EI_{concrete}$ are the bending stiffnesses of the CLT floor and concrete screed, respectively, and $EI_{steiner}$ is the bending stiffness of the total cross-section. The parameter γ represents the degree of cooperation between the layers. Slip is no cooperation so $\gamma = 0$. If only shear slip is considered the γ-factor can be estimated with [32]:

$$\gamma = \frac{1}{1 + \frac{\pi^2 E_{screed} t_{screed}}{l^2} * \frac{t_{insulation}}{G_{insulation}}} \tag{38}$$

with $E_{screed} = 30000N/mm^2$, $t_{screed} = 80mm$, $t_{insulation} = 3mm$ and $G_{insulation} = 5N/mm2$. Finally, No slip means full cooperation so $\gamma = 1$. Cooperation is analyzed by comparing the frequency of the analytical calculations to the experimental analysis. Other modal properties can not be compared, because first of all the measured damping is a rough estimate and there exist only empirical standard values set by guidelines to compare to. Second of all the v_{rms} of the analytical calculations are not directly comparable to measured values because the v_{rms} is dependent on the type of loading and in this study, onsite measurements are carried out using a single weight drop while analytical calculations assume a walking load.

4.8 Validation

Validation of Onsite Measurements
To validate onsite measurements, the exact same measurement procedure, described in detail in Annex B is performed three times in each test set up. Resulting time and frequency spectrum are immediately checked after measurements. In the event of any inadequacies or anomalies in a measurement, an additional measurement is conducted to guarantee three dependable measurements for each test setup.

Validation of post-processing methods
The onsite measurements undergo post-processing to extract essential modal properties, including frequency, damping, and modal mass. Firstly, these measurements are validated by comparing them with expected values derived from prior experimental investigations on CLT floors and established design codes such as prEC5. Secondly, the results from the three measurements are subjected to comparative analysis to identify and exclude any outliers. The resulting values for frequency, damping, and Vrms in this study are derived from the average of reliable results obtained for each test setup.

Furthermore, the validation of the damping ratio is conducted through two distinct methods, as introduced in Section 2.4.2. The preferred peak-picking method is chosen for its slightly reduced sensitivity

to noise and its independence from the selection of specific time domains for each measurement point. However, the envelope method is used to validate the peak-picking method by comparing the results of measurement in point 11. The Python script for the peak-picking method and envelope method can be found in Annex C.

Table 7 shows that both methods result in similar damping ratio values, validating that the peak-picking method is used properly. The envelope method results in higher or lower damping values because it is very sensitive to the chosen time range. If a bigger time range is chosen the damping ratio using the envelope method will decrease, while the peak-picking method will stay relatively the same. Figures 46 to 48 depict the fitted line that is used to estimate the damping with the envelope method for measurements 11, 10 and 7 during building phase 1.

Measurement	Time range envelope method	$\zeta_{envelope}$	$\zeta_{peak-picking}$
11	1-2.2s	3.2	3.0
10	1-2.2s	2.4	3.1
7	1-3s	1.3	1.6

Table 7: Damping estimates using two methods

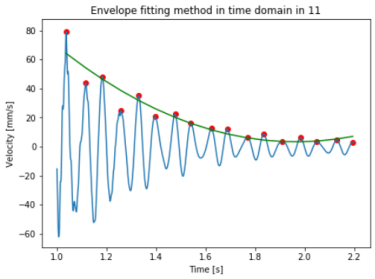

Figure 46: Fitted line

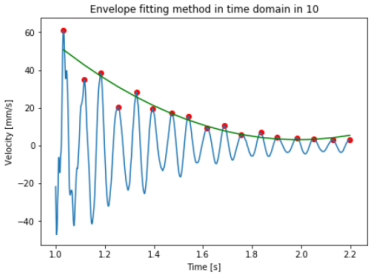

Figure 47: Fitted line

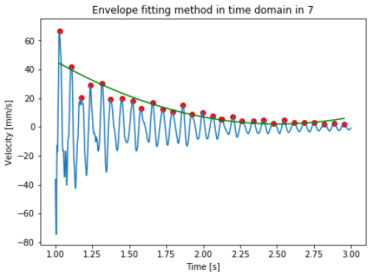

Figure 48: Fitted line

Validation of Analytical and Numerical analysis
The fundamental frequencies determined using the analytical and numerical mothods are compared, revealing highly agreeable values, as is evident from table 8. The minor differences of 3% and 1% for phases 1 and 2, indicate robustness of the two methods.

Moreover, the numerical model is subjected to two other validation checks. Firstly, the total weight of the structure is assessed through manual calculations. Secondly, the displacement of the finite element model resulting from static analysis is verified using straightforward mechanics formulas for displacements. In this manner reliability of both methods is ensured.

	Analytical	Numerical	Difference
Frequency phase 1 [Hz]	13.5	13.87	3%
Frequency phase 2 [Hz]	8.7	8.75	1%

Table 8: Validation of Analytical and Numerical determined frequency

5 Results

5.1 introduction

This chapter presents the results of the onsite measurements, analytical analysis and numerical analysis. The analytical calculations follow the prEC5 and the numerical analysis uses a 3D frame model in the software SCIA. The analysis models, method, material input parameters, connection properties and applied loads are introduced in Chapter 4.

In section 5.2 the results of the onsite measurements with and without architectural finishing are presented and discussed. Section 5.3 compares the modal properties and vibration performance according to common engineering practices to onsite measurements. Section 5.4 displays the results of the numerical sensitivity analysis on the stiffness of connections and the results of the analytical sensitivity analysis on the density of CLT. In section 5.5 the results of the numerical analysis on the subject of different connection stiffness assumptions and the results of the analytical analysis on different floor cooperation assumptions are presented. Finally, 5.6 gives a summary of the remarkable findings that will be further analyzed in the discussion.

5.2 Onsite measurements

5.2.1 Bare CLT floor

The floor plan represented in Figure 49 provides an overview of the boundary conditions and the measured vibration properties for the experimental setup during phase 1. During this phase, the timber load-bearing structure is realized and there are already facade panels placed on axis A, F and 1. In addition, there are partitions placed on axis E and 3 that divide the office and the lab. The floor plane denoted as F-E primarily spans from axis 4 to axis 1. The Cross-Laminated Timber (CLT) floor rests on GL28h beams and is connected using screws, as detailed in D1, D6 and D7 from figure 50. Additionally, there is a beam on axis E, extending from axis 4 to 3, which serves as a stabilizing wind brace and supports the floor (Detail D3). The CLT floor is not continuous over axis 3 but is continuous over axis 2, respectively details D6 and D7. The timber frame construction (TFC) facade on axis F and A is connected only to the columns and not to the beams, except for axis 1 where the facade is connected to the supporting beam, as shown in detail D5. Moving on to floor plane A-B, the floors primarily span from axis 3 to 1, from one beam to another. There is also a beam on axis B, extending from axis 1 to 2, supporting the staircase opening, and the floor is connected to this beam using screws. The red lines spanning from axis 4 to axis 1 depict the connection of CLT panels to each other via half-lapped joints, as detailed in D4.

Regarding the analysis of the vibration properties and their relation to the boundary conditions, the following discussion points emerge. It is important to underscore that the three measurements conducted at each specific point yielded precisely the same fundamental frequency, accurate to the second decimal place. For a more comprehensive evaluation of the frequency spectrum across identical measurements, a detailed examination is presented in Annex D. The damping ratio and root mean square velocity, measured within a particular test setup, display an average fluctuation of approximately $\pm$ 0.5

- Studying the v_{rms} values, which is a measure of the amplitude of the vibration an interesting observation is that the measurements resulted in a higher v_{rms} value at the inter-panel junction compared to that on the panel. P7, P8 and P11 are placed on the inter-panel junction while P10 and P1 are placed in the middle of a panel. P11 has a v_{rms} that is 36% higher than P10. P7 and P8 respectively have a v_{rms} that are 78% and 53% higher than in P1. This observation aligns with prior numerical analysis that investigated the effect of rotational stiffness in inter-panel connections [6]. The difference between P11 and P10 is relatively less than between P7 and P1, this can be attributed to the side support close to P10 in axis E. If there is no side support the v_{rms} is up to twice as big when loaded and measured on a inter-panel junction then in the middle of the panel. This is a significant difference.
- The damping is higher in plane F-E compared to A-B, which can be attributed to the presence

of the side support and facade in plane F-E. The floor is connected to the supporting beam via screws at the side support, and these connections may aid in dissipating vibration energy.

- The prEC5 recommends using a damping ratio of 2.5% for CLT floors without finishing. The damping values measured range between 1.6 and 3.1 %. The prEC5 gives a relatively good average value of the measured damping values.
- The fundamental frequency at points 11 and 10 is slightly lower than at points 1 and 7. This is not necessarily expected, as for a three-sided supported floor, higher stiffness and lower modal mass are anticipated, resulting in a higher fundamental frequency. The observed difference could be attributed to the longitudinal stiffness governing the frequencies. This could also explain the slightly higher frequency at points 1 and 7, as the CLT floor is continuous in this floor plan region, whereas at points 11 and 10, the floor is not continuous to the adjacent floor.
- P11-S13 does not have exactly the same fundamental frequency as P11 and P10. While P1-S5 does have exactly the same f_1 as P7 and P1. This is because the floor is not continuous over axis 3 but is over axis 2 (see details D6 and D7 in figure 50). As the v_{rms} of P1-S5 is 55% of the v_{rms} of P1, while the v_{rms} of P11-S13 is only 28% of the v_{rms} of P11, the continuous floor results in a higher tranfer of vibrations to the adjacent floor.

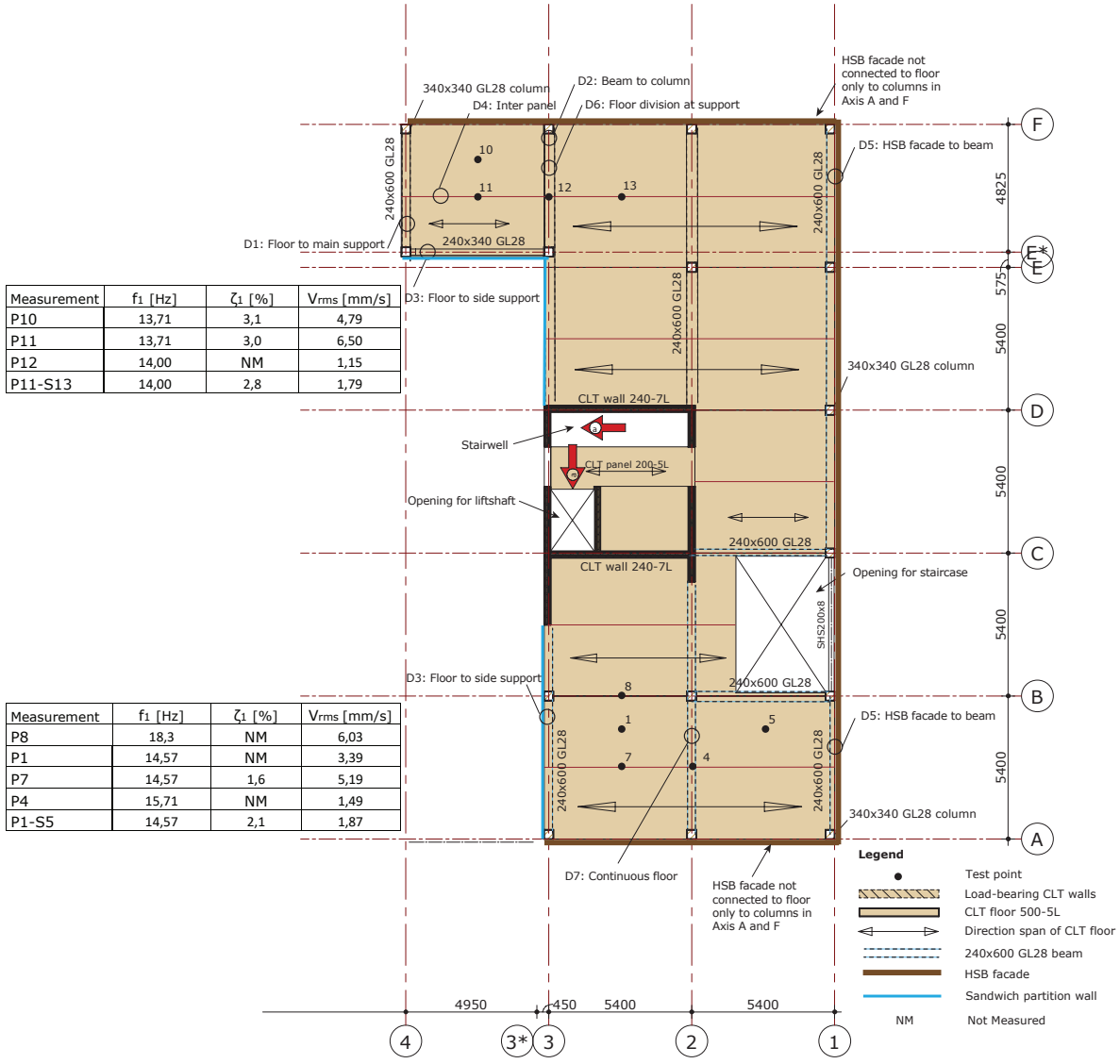

Measurement	f_1 [Hz]	ζ_1 [%]	v_{rms} [mm/s]
P10	13,71	3,1	4,79
P11	13,71	3,0	6,50
P12	14,00	NM	1,15
P11-S13	14,00	2,8	1,79

Measurement	f_1 [Hz]	ζ_1 [%]	v_{rms} [mm/s]
P8	18,3	NM	6,03
P1	14,57	NM	3,39
P7	14,57	1,6	5,19
P4	15,71	NM	1,49
P1-S5	14,57	2,1	1,87

Figure 49: Phase 1: First floor overview and vibration properties from onsite measurements

D1: Floor to main support	D3: Floor to side support
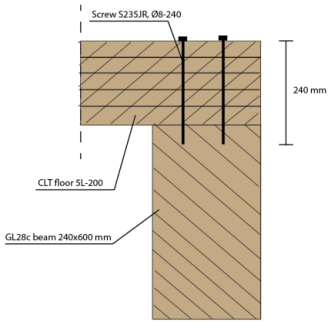	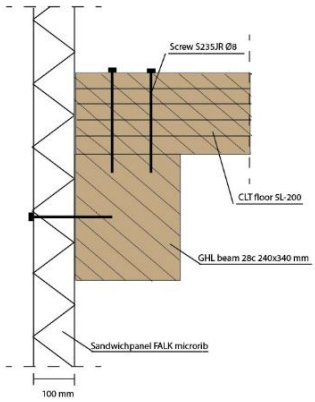
D4: Inter panel connection	**D5: HSB facade to beam**
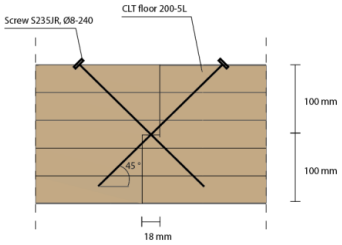	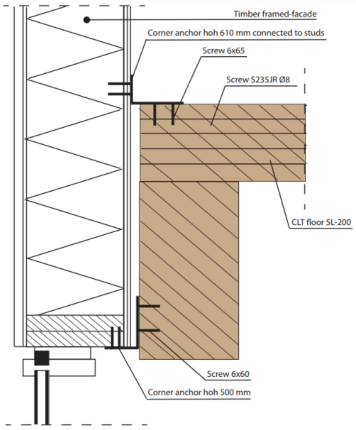
D6: Floor division at support	**D7: Continuous floor**
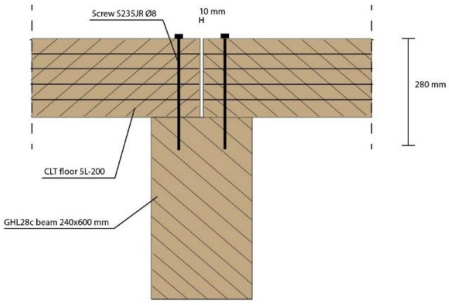	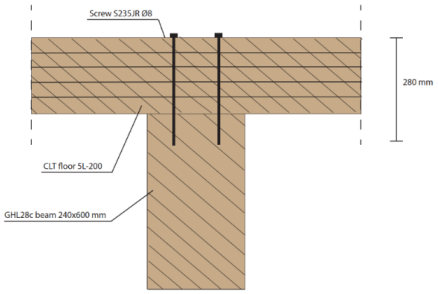

Figure 50: Detail of connections

5.2.2 CLT floor with architectural finishing

The floor plan depicted in Figure 49 provides an overview of the boundary conditions and the measured vibration properties during the second phase of the experimental setup. In this phase, the architectural finishing elements were introduced, including insulation, concrete screed, partition walls on and under the first floor, facade, and staircases. The HSB facade was added to axis 4, and windows were installed on the facades along axis A, F, 1, and 4. On top of the Cross-Laminated Timber (CLT) floor, a 30 cm insulation layer was applied, followed by an 80 cm reinforced floating concrete screed as depicted in figure 38. Metal stud partitions (MS) were placed on the concrete screed. As observed in Annex: (picture concrete floor phase 2), the concrete floor extends up to the columns, and wall panels are placed directly on the concrete screed.

Regarding the analysis of the vibration properties and their relation to the boundary conditions, the following discussion points emerge:

- The prediction calculations of the fundamental frequency prior to onsite measurements resulted in a frequency of 8 Hz. However, the measured frequencies are much higher ranging from 12.29 to 14.00 Hz. The predicting calculations may have used a to low stiffness, to high modal mass or a combination of the two that resulted in a underestimation of the fundamental frequency.

- The v_{rms} in P11 is 19% higher then in P10. The v_{rms} is bigger at point 11, however, the difference is less than in phase 1. This may imply that the concrete screed causes an increase of the inter-panel joint stiffness. This is in line with previous experimental research that showed that the rotational stiffness of the joint increases as the mass of the floor increases, due to a expanding contact area.

- In phase 1 the v_{rms} of P7 was lower than in P8. Now the v_{rms} of P7 is slightly higher than in P8. This could be attributed to partitions placed under the first floor close to P8 that increase the stiffness and damping.

- The damping value from measurement P7 remains lower than in P10 and P11, likely due to the influence of the side support, as seen in phase 1. This might also explain the slightly higher damping in measurement P1-S5 compared to P7, as point 5 is also located near a side-support on axis B.

- The concrete reinforced screed covers the entire floor. If it were placed directly on the CLT floor, it could result in making the floor continuous over axis 3. However, measurements P11-S13 exhibit a different fundamental frequency than P11, where the CLT floor is discontinuous over axis 3. While, in-plane A-B, where the CLT floor is continuous over axis 2, measurements P1-S5 exhibit again the same fundamental frequency as measured by P7. Likely due to the presence of insulation, the CLT floor is not continuous at axis 3 in this case.

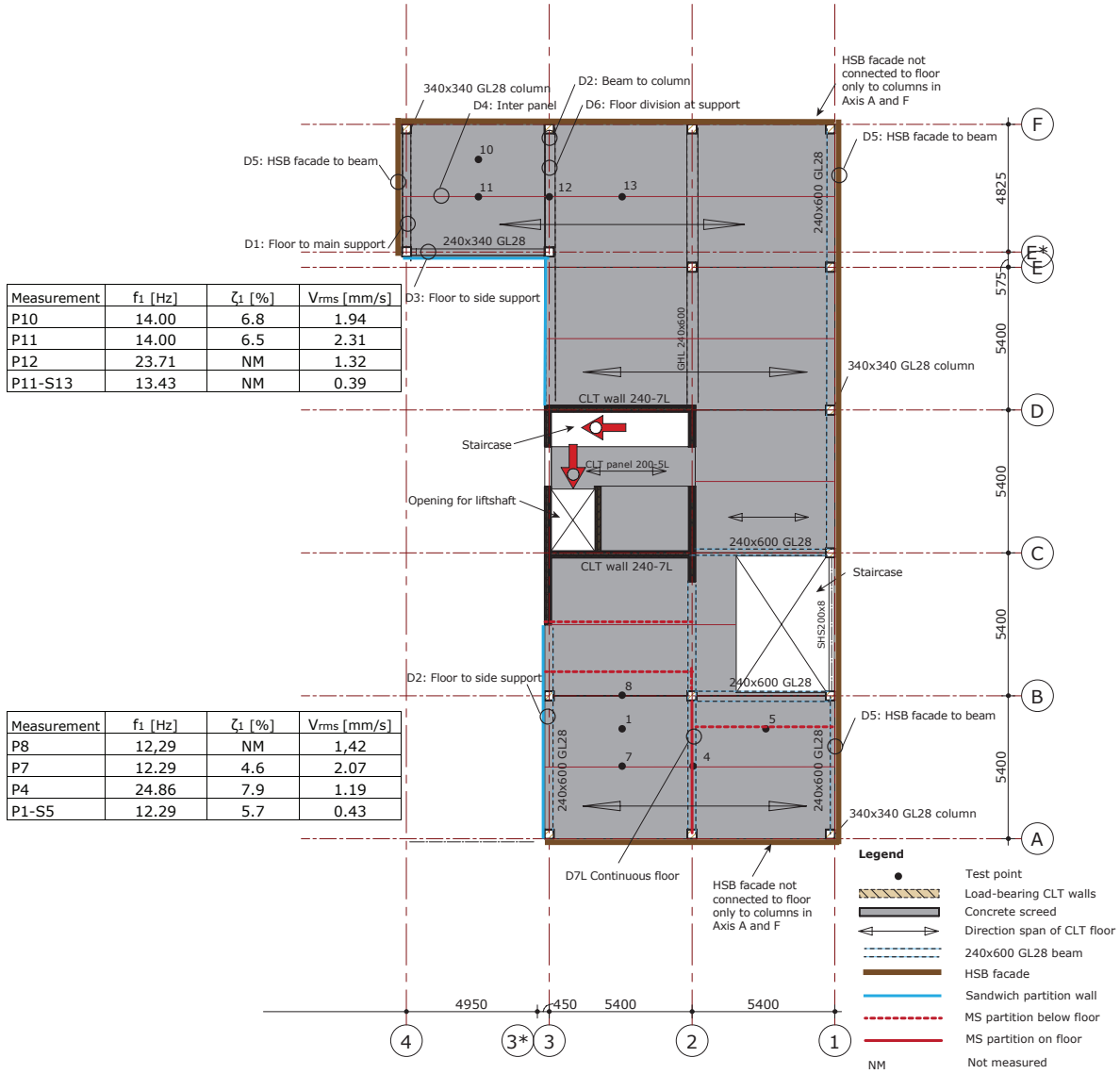

Measurement	f_1 [Hz]	ζ_1 [%]	V_{rms} [mm/s]
P10	14.00	6.8	1.94
P11	14.00	6.5	2.31
P12	23.71	NM	1.32
P11-S13	13.43	NM	0.39

Measurement	f_1 [Hz]	ζ_1 [%]	V_{rms} [mm/s]
P8	12,29	NM	1,42
P7	12.29	4.6	2.07
P4	24.86	7.9	1.19
P1-S5	12.29	5.7	0.43

Figure 51: Phase 2: First floor overview and vibration properties from onsite measurements

5.2.3 Onsite measured differences between Phase 1 and 2

Table 9 presents the variations in fundamental frequency (f), damping ratio (ζ), and root mean square velocity (v_{rms}) as measured during both phase 1 and phase 2 of the experiments. Analyzing the changes in f, it is evident that it decreases in plane A-B (measurement P7) while remaining relatively equal in planes F-E (measurements P10 and P11). A possible explanation is that the modal mass in plane A-B could have increased relatively more than in plane F-E due to the weight of the partitions along axis 2 and temporary big loads from building material.

The damping values exhibit a significant increase for measurements P7, P1-S5, P10, and P11. In plane A-B (measurements P7 and P1-S5), the damping values increase slightly more compared to plane F-E (measurements P10 and P11). This difference could be attributed to the proximity of metal stud (MS) partition walls, which are placed under and on top of the first floor between phases 1 and 2.

The introduction of the concrete screed leads to a substantial reduction in v_{rms} at critical areas, specifically the middle of the floor, with reductions of 78% and 85%. This result aligns with expectations, as the floor becomes heavier in this phase, causing smaller deformations under the same force. Thus, the concrete screed proves to be highly beneficial for enhancing vibration performance. However, it should be noted that this experiment applies a single impulse as a force load, not a footfall load. As the v_{rms} is influenced by the type of loading, the change in v_{rms} may differ for a walking load scenario.

Figure 52 depicts the response factor according to chapter 9 of the prEC5 when using the measured frequency and damping. The first observation is that in building phase 1 the response factor is similar for all the measurements. Although the frequency is higher in measurement 7 than in 11, because the damping is higher in measurement 11 than in 7, the resulting response factor is almost equal in phase 1. After the architectural finishing is placed the response factor in 10 and 11 increases slightly more than in 7. With a response factor of 0.0006 in measurement 7 the floor performance level (FPL) is 2, while in measurements 10 and 11 the FPL is 1. As mentioned in building phase 2 around measurement 7 there were big loads close to the supporting beams, however, these loads are not taken into account in the response calculations. Maybe if these loads are correctly taken into account as distributed loads the response factor in measurement 7 is lower and becomes more similar to 10 and 11. In addition in these calculations, the 10% variable loads are not taken into account (23 kg/m2). If this is done the floor performance will increase. The response factor in 7 will increase from 0.0006 to 0.0005, resulting in a floor performance level of 2. In Europe, the base recommendation for offices is an FPL of 3, so the FPL of the case study floor fulfills the base requirement for vibration performance.

Measurement	Phase 1			Phase 2			Change (%)		
	f [Hz]	ζ [%]	v_{rms} [$\frac{mm}{s}$]	f [Hz]	ζ [%]	v_{rms} [$\frac{mm}{s}$]	$\triangle f$	$\triangle \zeta$	$\triangle v_{rms}$
P8	18.3	NM	6.03	12.29	NM	1.42	−33		−76
P7	14.57	1.6	5.19	12.29	4.6	2.07	−16	+196	−60
P4	15.71	NM	1.49	24.86	7.9	1.19			−20
P1-S5	14.57	2.1	1.87	12.29	5.7	0.43	−16	+175	−77
P10	13.71	3.1	4.79	14.00	6.8	1.94	+2	+123	−59
P11	13.71	3.0	6.50	14.00	6.5	2.31	+2	+118	−64
P12	14.00	NM	1.15	23.71	NM	1.32			+15
P11-S13	14.00	NM	1.79	13.43	NM	0.39	−4	−23	−78

Table 9: Changes in vibration characteristics

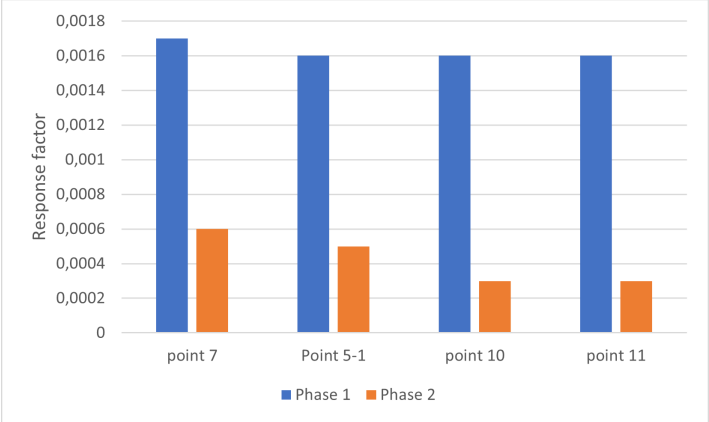

Figure 52: Response factor according to prEC5 chapter 9

The last observation is that the damping relatively increases more in measurement 7 compared to 11 with 78% (196-118) while the frequency decreases more in measurement 7 compared to 11 with 18% (-16 - (+2)). Although the increase in damping in percentage is much more than the decrease in frequency the response factor in 11 becomes better, thus it seems that the response factor is more sensitive to changes in the frequency than changes in the damping value.

5.3 Design codes and common engineering practices

Table 10 depicts the frequency of the experimental, analytical and numerical analysis from the bare CLT floor system. The first and second frequencies correspond to the first and second mode shapes depicted in figure 53 and 54. The analytical and numerical analysis both accurately predict the frequency very well.

Table 10 depicts the results of the experimental, analytical and numerical analysis after the architectural finishing is placed. In the analytical and numerical analysis, from the added architectural finishing in phase 2, only the floating concrete screed is accounted for. Other architectural finishing

Method	Phase 1				Phase 2			
	$f_1\ [Hz]$	$f_2\ [Hz]$	$\triangle f_1[\%]$	$\triangle f_2\ [\%]$	$f_1\ [Hz]$	$f_2\ [Hz]$	$\triangle f_1[\%]$	$\triangle f_2\ [\%]$
Experimental	13.71	20			14.00	26.86		
Analytical	13.5		-2		8.7		-38	
Numerical	13.87	20.69	+1	+2	8.75	15.00	-38	-44

Table 10: Initial analytical and numerical vibration prediction of building phases 1 and 2 and its discrepancy to experimental data ($\triangle f$)

Measurement	Phase 1		Phase 2	
	Experimental	Numerical	Experimental	Numerical
$v_{rms,P10}[mm/s]$	4.79	4.23	1.94	2.75
$v_{rms,P11}[mm/s]$	6.50	2.81	2.31	1.66
$\triangle v_{rms} = \frac{v_{rms,P11} - v_{rms,P10}}{v_{rms,P10}}$	+36%	-34%	+19%	-40%

Table 11: Comparison of difference in Vrms between P10 and P11

in this part of the floor consists mainly of loads of the HSB facade and adjacent floor panels on the supporting beams, which are not taken into account in the initial calculations. Opposing to Phase 1, in phase 2 the analytical and numerical analysis does not result in a good prediction of the measured frequency. In addition, the difference between the analytical and numerical determined f_1 in Phase 2 is bigger. This may be the result of the method used to account for the concrete floating screed in the FEM model. The numerical analysis results in a slightly better estimation of the fundamental frequency, however both methods are not deemed accurate predictions.

Table 11 depicts the experimental measured v_{rms} compared to the v_{rms} obtained from numerical analysis. The numerical obtained v_{rms} values are determined using footfall analysis software CADS, where the experiment is simulated by also loading and measuring in points 10 and 11. It must be noted that it is not possible to simulate the exact force from onsite testing, therefore the v_{rms} values of the experimental and numerical analysis are not comparable. However what is comparable is the difference between P10 and P11 of the experimental and numerical analysis. Experimental analysis during phase 1 showed that point 11 is the critical loading point of the two points, with a v_{rms} of 36% higher than in point 10. However, numerical analysis resulted in point 11 having a v_{rms} of 34% lower than determined in point 10. This means that the numerical model does not accurately predict the critical loading point and thus probably does not determine the mode shape accurately. In phase 2, after the placing of the floating concrete screed, the same problem remains. It should be noted that the difference between the experimental determined v_{rms} become closer to each other, while the numerical determined v_{rms} become further from each other.

To conclude, the analytical and numerical analysis predicts the frequency accurately of the bare CLT floor. However, after the architectural finishing is placed, both methods do not accurately estimate the frequencies anymore. In addition, the numerical analysis does not determine the critical loading point accurately during building phases 1 and 2. This is attributed to not considering the rotational stiffness of the inter-panel connection, but assuming the two panels as one monolithic slab. Further research is needed on the dynamic properties of the building elements and connections to accurately predict the frequencies and critical loading points.

5.4 Sensitivity analysis

Connection stiffness

Regarding the stiffness parameters, the parameters depicted in table 5 and figure 43 are specified because they possibly affect the vertical displacement of the floor, thus the dynamic response of the floor to footfall loading. A sensitivity analysis is carried out to quantify the influence of every stiffness parameter on the modal properties and subsequently to rule out parameters in the model optimization

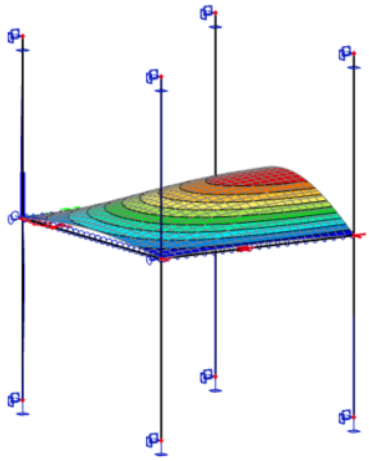

Figure 53: First harmonic mode shape

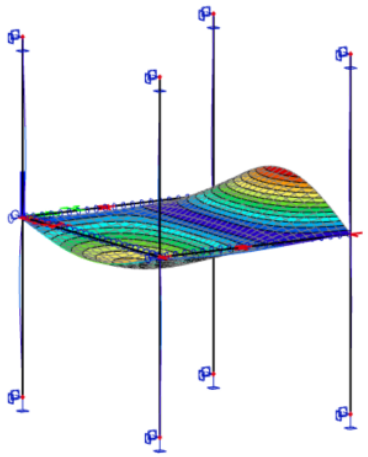

Figure 54: Second harmonic mode shape

Method	f_1 Hz	f_2 Hz	M_1^* %	M_2^* %	v_{rms} m/s	$\triangle f_1$ %	$\triangle f_2$ %	$\triangle M_1^*$ %	$\triangle M_2^*$ %	$\triangle v_{rms}$ %
Base Model	15.6	23.8	19.7	6.1	3.23					
$K_{Rx,f-b}$	13.5	20.3	12.7	8.0	3.00	-14	-15	-36	+31	-7
$K_{Tx,f-b}$	14.5	21.6	21.0	7.0	3.45	-7	-9	-6	+15	+7
$K_{Rx,b-c}$	15.4	23.7	19.9	6.2	3.23	-1	0	+1	+2	0
$K_{Ry,b-c}$	15.6	23.7	19.9	6.2	3.23	0	0	+1	+2	0
$K_{Rx,ip}$	15.0	21.3	15.7	5.6	4.31	-4	-10	-20	-8	+33

Table 12: Results of Sensitivity study with left the Vibration properties and right the relative change compared to the Base Model

process, which have only a minor influence on the outcome of the numerical computations.

Figure 55 depicts the mode shapes of the dynamic analysis of the base model and the altered numerical models with the corresponding fundamental frequency. The base model is a model where all connections are rigid in rotational and translation stiffness. Compared to the base mode, changing the rotational stiffness of the floor-to-beam connection and inter-panel connection, respectively $K_{Rx,f-b}$ and $K_{Rx,ip}$ have the biggest influence on the mode shape. The other changes cause a slightly bigger deformation but do not change the form of the mode shape. Making $K_{Rx,f-b}$ free in rotation causes the critical deformation point to move to the side, while making $K_{Rx,ip}$ free in rotation causes the critical point to move to the middle.

Now we look at the frequencies in table 12 the biggest change occurs when the rotational stiffness of the floor-to-beam connection $K_{Rx,f-b}$ is set to zero, hereafter changing $K_{Tx,f-b}$ and $K_{Rx,ip}$ also

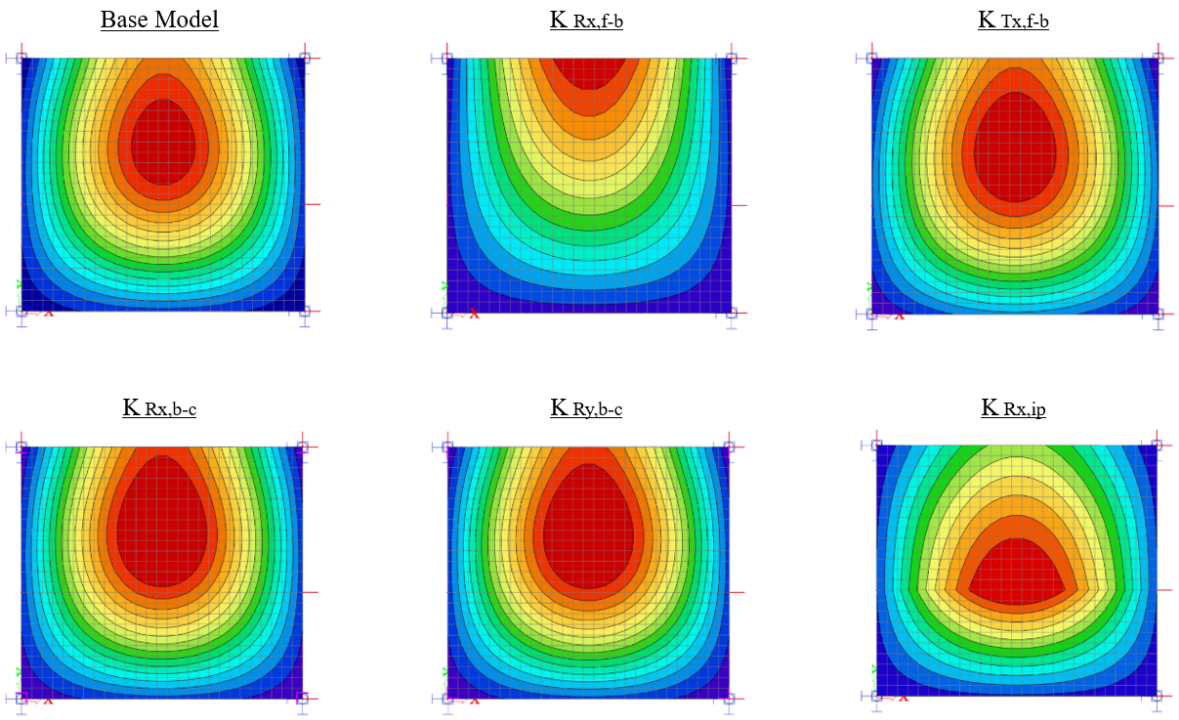

Figure 55: Top view of mode shape from Base Model and sensitivity study models

significantly alters the vibration properties. Changing $K_{Rx,b-c}$ and $K_{Ry,b-c}$ has almost no influence on the vibration properties and can therefore be assumed either rigid or hinged in the numerical model. So to conclude the rotational stiffness at the floor supports and inter-panel connection have the most influence on the dynamic behavior of the floor. Where making the floor hinged supported instead of rigid, causes the critical point to shift to the free side. While making the inter-panel connection a hinge shifts the critical point to the middle, specifically the inter-panel line.

Density of CLT

The prEC5 predicts the frequency of the bare floor structure with a small discrepancy of 2%. The values for the bending stiffness, density and span according to the manufacturer therefore are already a good starting point for the analytical calculations. However, a density for CLT of 500 kg/m3 is used, which is a relatively high value, as the density of CLT is given to be between 470 and 500 kg/m3. Table 13 depicts the frequency, damping and root mean square velocity (v_{rms}) when using the lower and upper bound density values in the prEC5 calculations, and the experimental data. Looking at the resulting frequencies in table 13, notable is that the measured frequency lies in between the lower and upper bound prEC5 calculations. The density range has a notable influence of 0.5 Hz but it is not a very significant one. In addition, table 13 shows that the different densities do not affect the v_{rms}. This is because a higher mass, causes the v_{rms} to increase due to a lower fundamental frequency. While simultaneously causing the v_{rms} to decrease, as is visible from the v_{rms} formulas of the prEC5:

$$v_{1,peak} = k_{red}\frac{I_M}{M^* + 70kg} \tag{39}$$

with:

$$I_m = \frac{42 f_w^{1.42}}{f_1^{1.3}} \tag{40}$$

To conclude, a better estimation of the frequency is reached by using an average density of CLT of 485kg/m3 and for the v_{rms} both lower and upper bound density result in the same value. Therefore in this research, the upper bound is used over all analysis to maintain continuity of results.

Method	ρ_{CLT} [kg/m3]	f_1 [Hz]	ζ [%]	v_{rms} [m/s]
prEC5 CB method	470	14.00	0.025	0.0017
prEC5 CB method	500	13.50	0.025	0.0017
Experimental analysis	470 - 500	13.71	0.031	0.0015

Table 13: CLT density sensitivity analysis

5.5 Alternative assumptions

5.5.1 Connection stiffness

Table 14 depicts the first and second frequency measured onsite and the ratio between the vrms calculated in points 10 and 11. The positive $\triangle v_{rms}$ shows that higher v_{rms} values are measured onsite

	$f_1[Hz]$	$f_2[Hz]$	$M_1^*[\%]$	$M_2^*[\%]$	$\triangle v_{rms}[\%]$
Experimental	13.71	20			+36
Common engineering practices	13.87	20.69	13.87	7.7	-34
Test scenario 1: Static stiffness	13.33	17.91			-1
Test scenario 2: Hinged	12.73	16.00	17.04	7.48	+35

Table 14: Frequencies and vrms in point 10 to point 11 ratio

in point 11. The results of the numerical analysis are given for the three scenarios. The initial FEM model accurately predicts the frequencies but not the critical loading point, because $\triangle v_{rms}$ is negative which indicates a higher v_{rms} is now found in point 10. Then it can be observed that assuming static stiffness the v_{rms} found in p10 and p11 is almost the same, which is not comparable with onsite measurements. Finally assuming the floor support and inter-panel connections as hinges, results in a similar $\triangle v_{rms}$ value to onsite measurements, however, the estimated frequencies become less accurate. Regarding the modal mass, the modal mass corresponding to the first frequency is higher when $K_{Rx,ip}$ is assumed to be a hinged compared to assuming a rigid connection.

To conclude there is not one assumption for the stiffness of the floor supports and inter-panel connections that simultaneously increases the accuracy of predicting the critical loading point while sustaining an accurate prediction of the frequencies. Altering $K_{Rx,f-b}$ shifted the critical point to the side, while changing $K_{Rx,ip}$ moved the critical point toward the middle. The interplay between stiffness properties in the connections significantly affects the dynamic behavior of the floor.

5.5.2 Effective bending stiffness

Table 15 presents the resulting frequencies for the scenarios and the discrepancy with the measured data. The analysis with no slip assumptions resulted in a discrepancy of approximately −38%. Assuming shear slip decreased the discrepancy, but not significantly. The analysis with full bonding assumptions led to the smallest discrepancy of +9%. In this case, assuming no slip gives the best of the three estimations of the real frequency. However, none of the tested assumptions results in an accurate prediction of the frequency, implying the floor has a distinct behavior when subject to small vibrations. The presence of the insulation layer appears to enable some shear force transfer, resulting in an effective bending stiffness that is higher than under static loading conditions.

5.6 Summary of results

Onsite measurements show higher v_{rms} at the inter-panel connection than in the middle of the panel. After the concrete floating screed is placed the difference becomes less prevalent, however still the inter-panel connection seems to be the critical loading point. Modal properties after the architectural finishing is placed changed; the frequency stayed relatively equal, the damping increased significantly and the v_{rms} decreased. For the three-sided supported floor the resulting response factor decreased from 16 to 3 according to the prEC5 using the measured modal properties. Thus the vibration performance is significantly improved.

method	γ	EI [Nmm2]	f[Hz]	$\triangle f$ [%]
Common engineering practices: Slip	0	$7616{\cdot}10^9$	8.7	−38
Test scenario 1: Shear slip	0.11	$8628{\cdot}10^9$	9.3	−32
Test scenario 2: No slip	1	$24308{\cdot}10^9$	15.3	+9

Table 15: Bending stiffness and resulting frequencies using prEC5

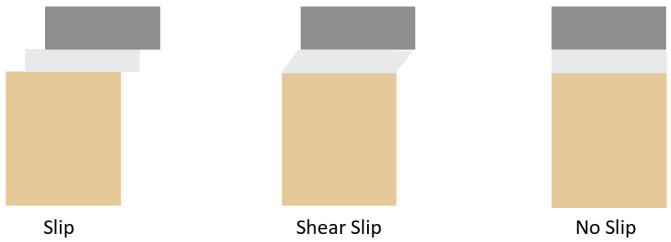

Figure 56: Different types of collaboration between interlayers

Common engineering practices accurately predicted the frequency before architectural finishing is placed, implying good initial assumptions on the structural behavior and material properties. However after architectural finishing is realized, mainly the placement of the concrete floating screed, the frequency is hugely underestimated. Suggesting the bending stiffness assumed is much lower than the actual bending stiffness of the floor, which may be the result of cooperation between the floor layers. The location of the highest measured v_{rms} value does not compare to that of the FEM model, implying the mode shape determined by the initial FEM model is not correct and possibly underestimates the vibration performance The sensitivity study showed that the inter-panel and floor support connection have the biggest influence on the frequency and mode shape, while other connections have a very small influence.

The numerical study on different connection stiffness assumptions showed that assuming hinge connections accurately predicted the ratio between the measured v_{rms} measured at the inter-panel connection and in the middle of the panel, however, compromised frequency estimates. The lower frequency does not directly mean that assuming both connections as hinged is a bad assumption, as the frequency is also dependent on other design and material assumptions. Finally, assuming full cooperation between the floor layers resulted in a better estimation of the frequency than assuming slip. However, none of the tested assumptions resulted in an accurate prediction of the frequency implying distinct behavior of the floor subject to small vibrations.

The discussion will seek to explain the findings including the distinct structural behavior to footfall-induced vibrations and what this means for the vibration performance calculations.

6 Discussion

Throughout the research, several assumptions and choices were made that influenced the results. This chapter discusses the assumptions and choices in depth that might be significant for the reliability of the results. Where after this chapter discusses on the results of the Case Study and observations made in literature research.

6.1 Experimental analysis

In the FEM software, simulating the onsite measurements conducted was not feasible. Although the excitation and measurement points could be chosen, replicating the same loading as the onsite tests was not possible. This limitation arises from the specific capabilities of CADS software, designed for footfall analysis. Onsite measurements involved a single dropping weight that induced larger forces than typical walking loads. This difference in loading conditions could impact the results and should be considered in the analysis.

Measuring procedure
During my MSc thesis on footfal-induced vibration in CLT floors, I opted for a non-conventional measuring procedure involving a single impulse, excited by a 10 kg weight falling from a height of 83 cm. This choice has both advantages and disadvantages that impact the determination of the vibration characteristics compared to exactly following the prescribed guidelines by the EN 16929: 'Beproevingsmethoden' [19]. The primary reasons for selecting this procedure is its practicality and simplicity. Conventional guidelines often involve complex and time-consuming processes. The guidelines recommend using a stepping person or mechanical exciter to load the floor in the same or multiple of the fundamental frequency of the floor. During the second test day this method was tested, however due to the high frequency of the floor it was impossible to do it by stepping and there was no access to a mechanical exciter. By using a single impulse load, the floor could effectively be excited to vibrate in its own fundamental frequency. In addition, the loading is consistent over each measurement.

The fundamental frequency is not so much affected by the type of loading as the damping and the root mean square velocity is. The root mean square velocity is highly dependent on the type of loading, measurements within this experiment can be compared to each other, but it is not possible to directly compare it with analytical results and other experimental studies. The damping is dependent on the decreasing process of the vibration amplitude, in principle, this is measurable from the velocity response of a single impulse. However, the size of the initial amplitude and multiple frequencies acting simultaneously affect this process.

To give a perspective into the difference between a walking load and the single force used, one walking load test is conducted before and after architectural finishing is placed. The comparison of the measured v_{max}, frequency and resulting maximum displacement (u_{max}) are depicted in table 16. The maximum displacement is determined with the following formula:

$$u_{max} = \frac{v_{max}}{8 \cdot f} \tag{41}$$

. It is evident that the force induces almost a ten-fold bigger response than a walking load does, but that the frequencies are very similar. In conclusion, measuring procedure offers practical advantages in terms of efficiency and consistency. However, it is essential to acknowledge the limitations concerning

	Force load phase 1	Force load phase 2	Walking load phase 1	Walking load phase 2
$v_{max}[mm/s]$	75.58	4.47	6.98	0.23
$f[Hz]$	13.71	13.43	14.28	12.89
$u_{max}[mm]$	0.6891	0.0416	0.0611	0.0022

Table 16: Modal properties resulting from force load of measurement 11 and walking load

potential data gaps As some vibration characteristics depend on the type of loading, some results should be carefully assessed when interpreting the final results.

Frequencies

Frequencies are deduced by identifying peaks from the frequency spectrum. The prEC5 states that all frequencies that are in the range of the fundamental frequency and twice the fundamental frequency should be considered in the quantification of the vibration performance, however does not state anything about the participation of a specific frequency. Numerical analysis can predict the frequency and corresponding amplitude, but does not predict the participation of the frequency. For example in figure 57 the participation of the second frequency is significantly smaller than the fundamental frequency, thus only a small influence on the overall response of the floor. This could cause an overestimation or underestimation in the quantification of the vibration performance. In addition, if we look at phase 2 in figure 58, the response of the measurements P11 and P10 differ, whereas in phase 1 they were very similar. This shows that the location of the load can determine if a mode shape is excited. In this thesis, the highest peak is taken as the fundamental frequency, because it is considered the most important frequency.

Damping ratio

In my thesis, I employed the peak-picking method to determine the damping ratio from the measured velocity response. This approach was chosen due to its simplicity and effectiveness in capturing the damping characteristics of the system. It provides a time-efficient and straightforward method to identify and extract the dominating frequencies and corresponding peak amplitudes to calculate the damping ratio. Whereas more complex methods directly increase the complexity of the calculation significantly.

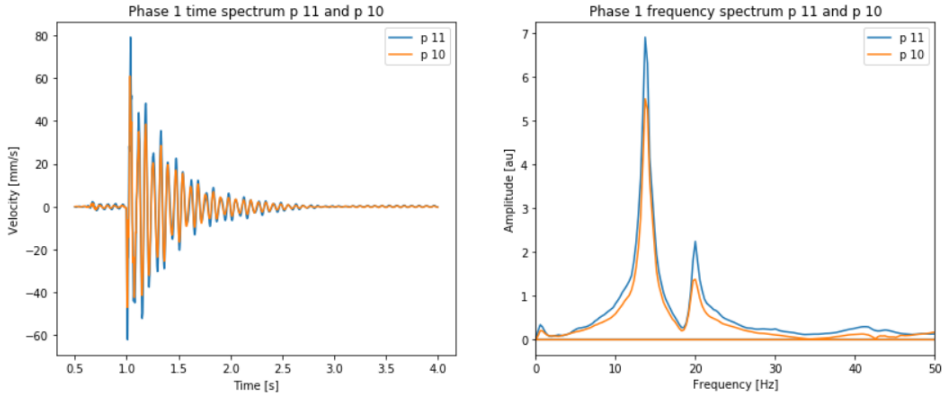

Figure 57: Velocity and frequency spectrum in phase 1 of p10 and p11

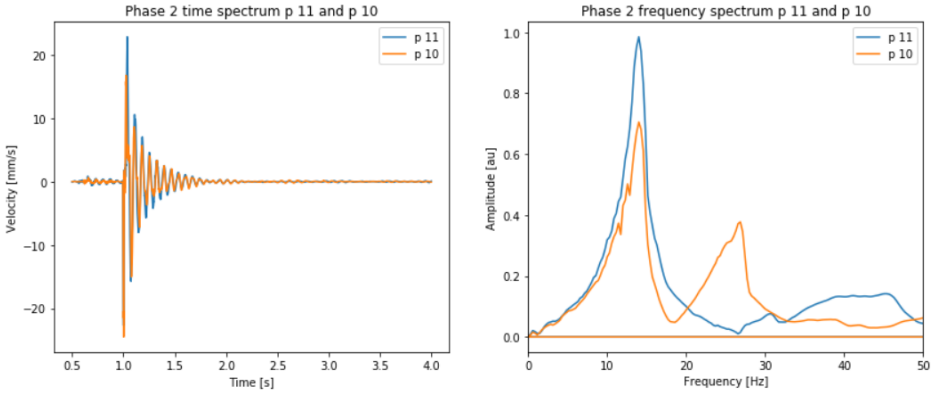

Figure 58: Velocity and frequency spectrum in phase 2 of p10 and p11

However, it is essential to acknowledge the disadvantages associated with the peak-picking method. The accuracy and reliability of the resulting damping ratio heavily depend on the quality of the velocity response data. Any noise or measurement errors can lead to inaccurate peak identification, affecting the accuracy of the damping ratio estimation. Additionally, this method is not ideal for complex vibration responses with multiple closely spaced peaks. The measurements done in this thesis were mostly complex vibration responses, especially measurements taken on the beam and on adjacent floor plans led to multiple active frequencies. The damping values in this thesis should therefore be seen as rough estimations. In addition, the damping ratio could not be determined for measurements P12 and P4 due to the presence of multiple active frequencies. These additional peaks are caused by the frequency corresponding to the beam frequency.

In conclusion, the peak-picking method is a practical choice for assessing damping ratios in CLT floor vibrations due to its simplicity and efficiency. Nevertheless, careful attention should be given to the quality of the velocity response data to ensure the accuracy and reliability of the resulting damping ratio.

6.2 Vibration prediction methods

Measurement Points for comparison
In selecting the measurement points, I prioritized minimizing external interference during onsite testing to ensure a clearer representation of the floor's inherent dynamic behavior. By choosing floor plane E-F of the case study floor with less interference, it allowed me to better isolate the impact of additional structural elements and boundary conditions have on the dynamic response of the floor.

However, the downside of this approach, is that critical areas that are especially susceptible to vibrations might be disregarded. In addition, when designing a floor, the lowest acting vibration performance determines the performance of the overall floor. In conclusion, my choice to focus on the data points with the least interference gives a clearer representation of the floor's complex dynamic behavior, while potentially overlooking localized vibration issues.

CLT floor density
The variation in CLT densities provided by manufacturers and guidelines presented a challenge in the analytical analysis. On the one hand a higher mass causes the frequency to decrease which decreases the vibration performance, on the other hand a higher mass decreases the root mean square velocity which increases the vibration performance. For this reason, the analytical calculations in phase 1 using a density of 470 and 500 kg/m3 for the CLT floor, resulted in the same vibration performance (same root mean square velocity value). Based on this finding the choice went out to using a density of 500 kg/m3 because this was the density mainly recommended by the manufacturer who supplied the CLT floors in the case study.

However using different densities in the prEC5 method can have a notable influence on the vibration characteristic, as the ratio in increase and decrease of the vibration performance with increasing density is not a linear gradient. Thus, my selection of the upper bound density value might lead to conservative estimations of natural frequencies. An exact estimation of the density of CLT can ensure a more accurate prediction of the vibration performance.

prEC5
The modal mass given by the prEC5 in chapter 9 for the analytical calculation of the v_{rms} is questionable. The method prescribes using a modal mass that is 25% of the floor mass for floors that are one-way span and two-way span. While the modal mass is dependent on the boundary conditions, for instance, the modal mass for one-way spanning floors that are simply supported is equal to 50% of the floor mass. The R-value determined using the chapter 9 method for this case study of the bare CLT floor results in a floor performance level that is equal to the base level for offices. On my own judgment, however, I would not find the floor vibration performance appropriate for an office, which is the function of the building. Insinuating that the vibration performance calculated with chapter 9 is an overestimation. In this case study I chose to use the simple classical beam method of the prEC5, however the prEC5 prescribes another method given in the Annex for more complex floors, as

Measurements	Phase 1: Bare CLT floor				Phase 2: with architectural finishing			
	$f_1[Hz]$	f_2 $[Hz]$	$R_{Ch.9}$	R_{AnnexG}	$f_1[Hz]$	$f_2[Hz]$	$R_{Ch.9}$	R_{AnnexG}
P10	13.71	20.00	13.9	15.5	14.00	26.86	4.6	4.5
P11	13.71	20.00	13.9	15.5	14.00	-	4.6	4.3
P11-13	14.00	-	13.5	13.2	13.43	-	4.9	4.6

Table 17: Comparison of R-value determined according to chapter 9: classical beam method and Annex G/K of prEC5

is specified in figure 2.3. However, when is a floor assigned to complex for the methods in chapter 9 and what consequence does using either the chapter 9 method or annex method have on the vibration performance of a CLT floor? To answer this question, the vibration performance is determined using the experimentally found frequency for the classical beam method and the Annex method. This is done for measurements P10, P11, and P11-13 and P13 during phase 1 and phase 2. These points are chosen due to their similarity to each other, distinct differences between vibration performances can then be more easily attributed to a single difference.

Python is used to calculate the R values and can be found in Annex C. The input values for both applied methods are exactly the same, except if there is a second mode shape active. In this case, the Annex takes into account the second active mode shape, while the classical beam method only takes into account the fundamental frequency. Because now we want to determine the actual vibration performance, the mass is taken according to the prEC5 which is the self-weight of the floor plus 10% of the imposed loads. Another difference is the modal mass, the modal mass in the Ch.9 calculations follows the formula prescribed formula:

$$M^*_{Ch.9} = \frac{mLB}{4} \tag{42}$$

. However the modal mass for the annex calculations follows the modal mass normally specified for a one way spanning floor:

$$M^*_{Annex} = \frac{mLB}{2} \tag{43}$$

. For the walking frequency, a standard walking frequency of 2 Hz is taken and the damping value is taken according to the prEC5. The input values for the calculations in phase 1 are then: $m_1 = 123kg/m^2$, $\zeta_1 = 0.025$, $EI_L = 6336Nmm^2$, $EI_T = 1664Nmm2$, $B = 4.825m$, $L = 5.4m$, $\mu_e = 1$ and $\mu_r = 1$. After placing the concrete screed in phase 2 and incorporating the effective bending stiffness determined in the previous chapter, the input values for phase 2 calculations become: $m_2 = 315kg/m^2$, $\zeta_2 = 0.04$, $EI_L = 19723Nmm^2$, $EI_T = 9639Nmm^2$, $B = 4.825m$, $L = 5.4m$, $\mu_e = 1$ and $\mu_r = 1$.

Table 17 depicts the resulting R-values of the classical beam method and Annex G/K, using the frequencies determined from experimental analysis. In the first phase so when there is only the bare floor, using Chapter 9 gives a better lower R-value, thus a better vibration performance. This is due to the active second mode which can only be taken into account in the method specified in the Annex, because when we look at measurement P11-13 in phase 1, the R-values are much more similar. Then looking at phase 2, it is notable that the R-values are similar to each other. Next notable is that the difference between P10 and P11 R-value determined with the Annex method is not very different from each other, this is most likely due to the relatively high second frequency. Also notable is that the Annex results in a slightly lower R-value when only a single fundamental frequency is active. This is visible from measurements P11-13 in phase 1; and measurements P11 and P11-13 in phase 2.

To conclude, if there is only one active frequency then both methods can be used. If there is a higher frequency also active, chapter 9 could give an underestimation of the R-value, resulting in a higher vibration performance than in reality. However when the second frequency is relatively high the influence on the R-value decreases and the method in chapter 9 also suffices. Finally, important is to note that different modal mass equations are used for the distinct methods.

6.3 Discussion of Results

6.3.1 Inter-panel connection

Evaluation onsite measurements

Onsite measurements were conducted to assess the dynamic response of a Cross-Laminated Timber (CLT) floor subjected to a single point load generated by a 10 kg mass dropped from a height of 83 cm. Both force and velocity sensors were strategically positioned at the same location. The study focused on investigating the impact of inter-panel connections by conducting measurements at two distinct locations: (1) along the inter-panel connection line at the mid-span of the floor and (2) at the exact center of the CLT panel. The obtained results, as detailed in Chapter 5, demonstrated a notable disparity in the root-mean-square velocity (v_{rms}) values between measurements at the inter-panel connection line and those obtained at the mid-section of the panel when subjected to a load applied at its center, denoted as $\triangle v_{rms}$:

$$\triangle v_{rms} = \frac{v_{rms,P11} - v_{rms,P10}}{v_{rms,P10}} \tag{44}$$

Figure 59 depicts the results prior to the installation of architectural finishing, on the floor supported on two sides, $\triangle v_{rms}$ readings recorded were 58% and 78%, respectively. For the floor supported on three sides, $\triangle v_{rms}$ was determined as 35% due to the presence of a side support. Notably, in the absence of side support, Vrms values at the inter-panel connection line exceeded vrms values in the middle of the panel by more than double.

Numerical Assessment of Inter-Panel Connection

A numerical study on the influence of the inter-panel connection, compared floor slabs consisting of two panels with and without an inter-panel connection. When a walking load is applied over the middle of the floor parallel to the inter-panel connection, v_{rms} were 67% higher for the floor with an inter-panel connection compared to the monolithic slab [6]. It can be argued that the FEA of the monolithic slab is comparable with measurements conducted during this study in the middle of the CLT panel, while the FEA of the floor with an inter-panel connection is comparable with measurements conducted on the inter-panel connection line. This would indicate that experimental research supports the FEM model of Kawrza that modeled the inter-panel joint as an elastic strip with an elastic modulus based on static load experiments by Macpherson [33].

In addition, a numerical study is done on the three-sided supported floor. In the first FEM model, common engineering practices are followed, where the floor is supported by hinges and the inter-panel connection is not considered, so treating the floor as a monolithic slab. The prEC5 guidelines suggest that support connections behave like a hinge due to limited deformations but do not state anything about the inter-panel connection. While the first model provided accurate estimates for the first and second natural frequencies, it did not accurately predict the location with the highest root mean square velocity (v_{rms}). Onsite measurements revealed a 35% higher v_{rms} value at the inter-panel connection

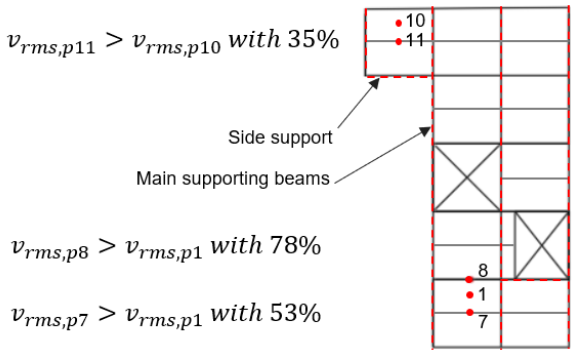

Figure 59: $\triangle v_{rms}$

line in the middle of the floor plane, whereas the FEM model predicted a 36% higher v_{rms} value at the middle of the floor plane. As a result, a second FEM model is introduced that incorporates the inter-panel connection as a hinge, which resulted in a 34% higher v_{rms} value at the inter-panel connection, thus similar to onsite measurements. This modification led to a deviation of the predicted frequencies from the measured values, however, this could also be a result of other wrongly assumed starting values. For instance, it is possible that the bending stiffness of the standalone CLT floor is higher, as an optimization study prior to this study argued that the bending stiffness of a CLT floor subject to small vibrations acts 24% stiffer [7].

Understanding the Behavior of Inter-Panel Connections
Considering the comparison of onsite measurements to numerical studies and the fact that the inter-panel connection has a similar rotational stiffness as the support connection, it can be concluded that the inter-panel connection has a very low stiffness when subject to small vibrations. This can be clarified by initial space clearance within the connection according to the prEC5. The initial slip phase can be observed in all types of timber semi-rigid connections, even for pedrilled ones, where it is possible to expect an initial slip of 0.5 - 1 mm depending on the fastener diameter or timber drying [34]. Deformations due to footfall-induced vibration of the floor are in the range of 0.1-0.2 mm, thus the deformation within the connections will be even smaller and will mostly take place in the initial space clearance area.

On the other hand, a study focused on timber-concrete composite (TCC) floors joined by dowels, unveiled that measured eigenfrequencies from vibration test were higher than eigenfrequencies determined using the bending stiffness as results of a four-point bending test [8]. The bending stiffness from dynamic testing approaches the value exhibited by a TCC beam with no slip between timber and concrete. Furthermore, studies on dowel-type fasteners highlighted that the stiffness of such connections under parallel-to-grain cyclic loading could be up to four times higher than calculated according to the slip modulus of EC5 [24].These studies suggest that connections transferring shear loads, where interface friction is present, tend to become stiffer under footfall-induced vibrations. Conversely, connections transferring moments may behave less stiff. Figure 60 depicts how the stiffness of connections can hypothetical be determined when subjected to footfall-analyis, where interface friction may be used in connections to enhance the stiffness.

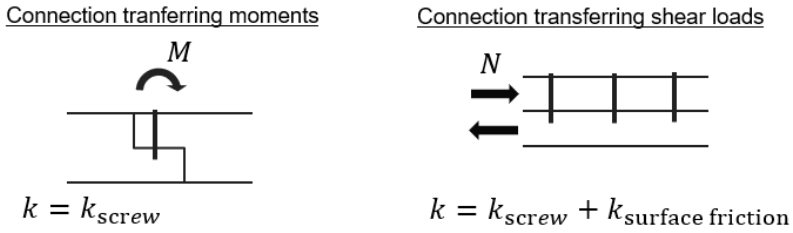

Figure 60: Stiffness of connections transferring moment and shear forces

Implications for Vibration Performance and Design
With the inter-panel connection behaving more like a hinge the mode shape of the three sides supported will be similar to the left depicted mode shapes in 61, where the main bending is in the inter-panel connection and not in the plate. The transversal stiffness of the floor is not the transversal stiffness of the CLT plate but is also dependent on the rotational stiffness of the inter-panel connections. Figure 62 illustrates $\triangle v_{rms}$ values from the FEM model assuming both rigid and hinged inter-panel connections. Notably, point 11 showed a significant increase in v_{rms} value when the inter-panel connection is changed from rigid to a hinge, while point 10 exhibited relatively similar values. Resulting in a reduction of the vibration performance of the floor. In figure 57, the big peak at 14 Hz in the measured frequency spectrum highlights the dominance of the first mode shape and frequency.

The vibration performance is a result of the v_{rms}, the v_{rms} according to the prEC5 is dependent on the span, frequency, damping, bending stiffness and modal mass of the floor. Onsite measurements showed that the frequency is exactly the same for the measurements at the inter-panel connection and

in the middle of the panel and that damping ratio values are also very similar as is clear from the time spectrum and frequency spectrum in figure 57. As the span is fixed, the higher v_{rms} found at the inter-panel connection must be attributed to a different bending stiffness or modal mass. Figure 63 depicts the expected mode shape, of a one-way span floor consisting of 4 adjacent panels connected by hinged inter-panel connections, to a load at the inter-panel connection line and mid point of the panel. As revealed by the numerical study on different floor system (Annex F) the more centralized the maximum deflection area, the lower the modal mass, which consequently results in the hypothesis that the modal mass is dependent on the location of loading for CLT floors. If the modal mass is twice as small, the corresponding v_{rms} will become twice as big, this phenomena could explain the high v_{rms} values measured onsite when loaded at the inter-panel connection line. However, as mentioned before the effect of the inter-panel connection on either the transversal stiffness and/or modal mass is not taken into account in the prEC5.

The prEC5 does consider the influence of the transversal stiffness in the k_{imp} factor, which is a factor accounting for higher modes in transient response. The lower the transversal stiffness compared to the longitudinal stiffness the higher the k_{imp} factor, thus a reduction of the vibration performance. However, the k_{imp} factor is only applied to two-way span floors and not to one-way spanning floors the

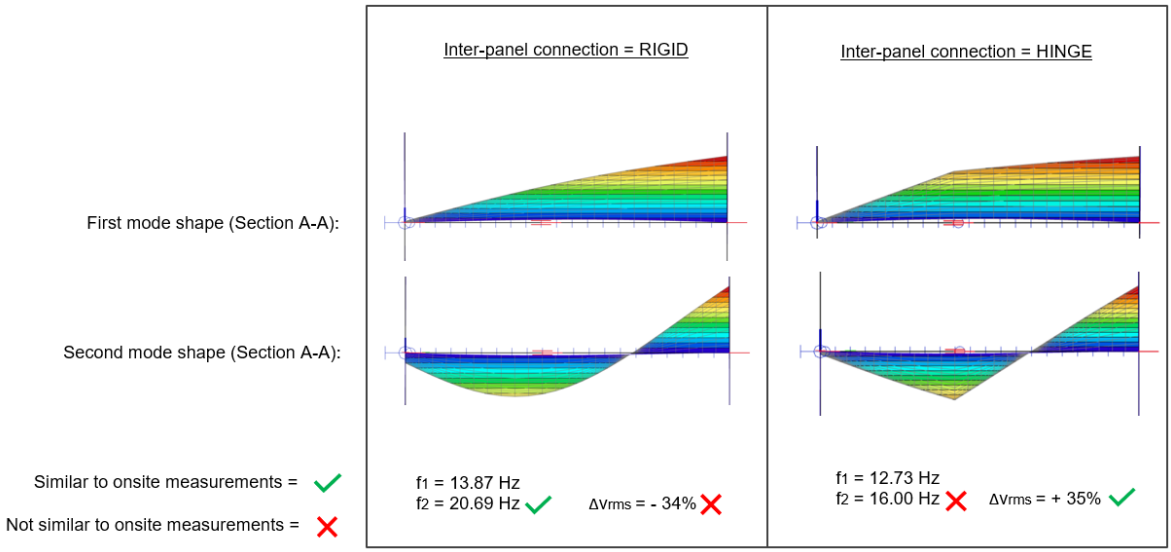

Figure 61: Mode shape at section A-A given by the FEM model

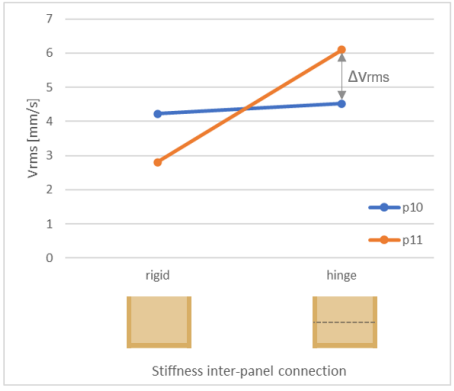

(a) The Vrms of measurements P10 and P11 assuming the inter-panel as a rigid connection and hinge

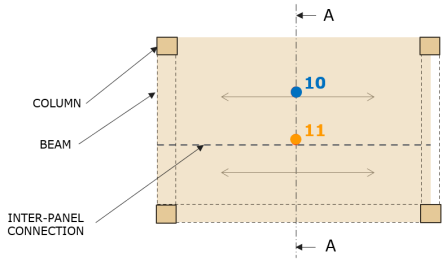

(b) Floor layout and measuring points P10 and P11

Figure 62: Effect of Inter-panel connection in FEM model

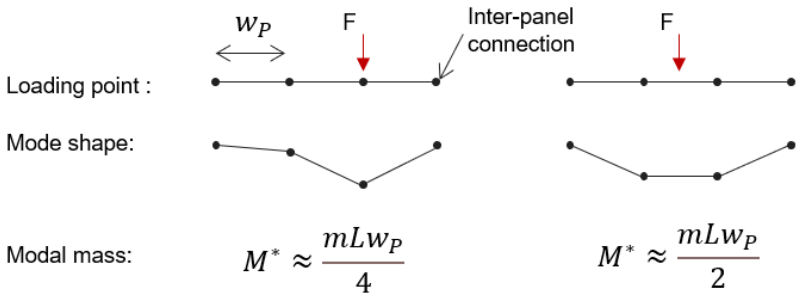

Figure 63: Hypothesis on relation between loading point and modal mass of CLT floors

k_{imp} is always 1. The k_{imp}factor is dependent on the width as is clear from figure 64, which results in irregular v_{rms} values as is visible from figure 65. However in general, the bigger the width the bigger the influence of higher modes according to the factor. This is not necessarily true for the effect of the inter-panel connection, which may be well independent of the floor width, as onsite measurements on a floor with a width of 10.8 m, found similar discrepancies to the numerical analysis that studied a floor with a width of around 6 m. In addition based on onsite measurements in this study, it is found that one-way spanning floors also experience the influence of the inter-panel connection. For these two reasons, it is recommended to use a separate factor that takes into account the reduced transversal stiffness of one-way and two-way CLT floors, to avoid overestimating the vibration performance. Especially, more research is needed on the effect of inter-panel connections in relation to the width of the floor.

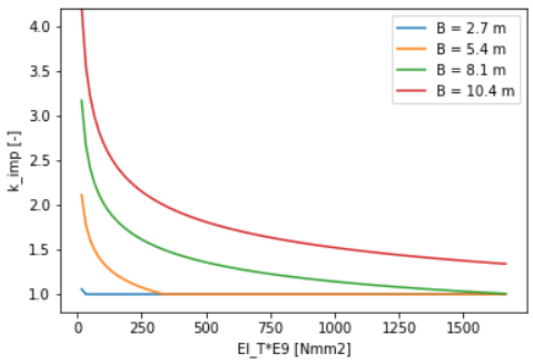

Figure 64: k_{imp} versus EI_T for different widths

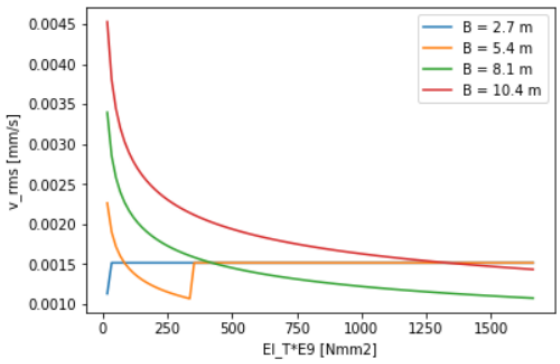

Figure 65: V_{rms} versus EI_T for different widths

6.3.2 Concrete floating screed

Impact of Architectural Finishing on Floor Vibration Performance
This study encompassed on-site measurements conducted both before and after the installation of architectural finishing to assess its influence on the vibration performance of CLT floor systems. From the installed architectural finishing the placing of the concrete floating screed is considered to have the biggest influence by far on the modal properties of the floor. The vibration performance is dependent on the modal properties of the floor. The modal properties, frequency, damping and vrms values are obtained through onsite measurements and modal analysis. After the floor finishing was placed the frequency stayed relatively stable, the damping increased, and the root mean square velocity significantly decreased. This led to the increase of the response factor according to the prEC5 from ranging between 16-17 to 3-6, indicating substantial improvements in vibration performance.

Analytical and numerical calculations in this study following common engineering practices, accurately predicted the frequency before architectural finishing is realized, but significantly underestimated it by 39% afterward. The frequency of the floor is linked to the mass, span, bending stiffness and support conditions. As the span and support conditions hardly changed between the measurement stages; and the variability in mass has shown to only have a minor influence; it is argued that the bending stiffness assumed after architectural finishing is placed is too low a value.

Influence of Bending Stiffness Assumptions
Conventional engineering practices traditionally rely on supplier-provided values for the bending stiffness of CLT. Additionally, the bending stiffness of the reinforced concrete floating screed is derived from the elastic modulus of uncracked concrete, representing an upper bound value. Given the presence of an insulation layer, the CLT and concrete components can be considered decoupled. Consequently, the bending stiffness after the screed is installed is assumed to be the sum of the individual standalone CLT and concrete floor layers.

A previous optimization study, based on on-site measurements, suggested that the bending stiffness of spruce CLT floors could increase by as much as 24% when subjected to small vibrations [7]. Moreover, our study, as discussed in relation to inter-panel connections, noted that if we assume the connections in the Finite Element Model (FEM) behave as hinges, a behavior which seems contingent with the response under footfall loading, the frequency decreases. This decline in frequency implies that the bending stiffness of the CLT floor may indeed exhibit a higher stiffness, thereby forming more accurate predictions of frequency and mode shape using the FEM model. Consequently, it is conceivable that the bending stiffness of the standalone CLT and concrete layers behaves stiffer under conditions of low-intensity vibrations. However even though the bending stiffness of CLT floor may be higher, the frequency initially is well predicted of the bare CLT floor with the analytical analysis. This means that the discrepancy of 39% is arguably only caused by an underestimation of the concrete bending stiffness and possibly cooperation between the interlayers.

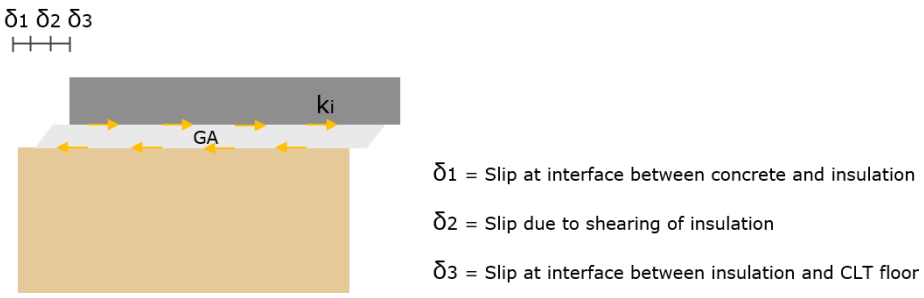

Figure 66: slip

Cooperation Among Interlayers

Cooperation among interlayers occurs when these layers are coupled, leading to an increase in bending stiffness. This increase can be calculated using Steiner's Rule, where the cooperation factor (γ) plays a pivotal role. The cooperation factor hinges on the extent of slip between the layers, which can arise from either interface slip or slip due to shear deformation of the insulation (figure 66). Interface slip depends on the interplay between friction and shear stresses resulting from floor deformation. When shear stresses exceed friction, slip occurs, while greater friction prevails when friction surpasses shear stresses. Importantly, during footfall vibrations, the deformations are approximately only 10% of those experienced during static loading, leading to significantly lower shear stresses between the floor layers. This indicates a higher likelihood that friction outweighs shear stresses.

Shear slip is further influenced by shearing deformation, a notable example being the deformation of a 30 mm Rockwool insulation layer. The cooperation factor can be quantified using a specific equation, with the shear modulus (G) being thickness-dependent, allowing for higher G modulus values in thinner layers, as per existing research. In conclusion, the degree of cooperation among floor layers is dependent on factors such as floor layer surface roughness, screed weight, shear stresses generated at interlayers due to footfall-induced vibrations, insulation thickness, and the shear modulus of the insulation material.

Analytical Assessment on the Cooperation Assumptions

In our research, we conducted an analytical analysis that involved comparing various cooperation assumptions with on-site measurements, as depicted in Figure... The initial assumption posited no interface slip but considered shear slip within the insulation layer, $\gamma = 0.11$, resulting in a considerable underestimation of the frequency. Conversely, assuming no slip at all, $\gamma = 1$, led to an overestimation. Our measurements revealed frequencies of 14 Hz in plane F-E, corresponding to a cooperation factor $\gamma - factor$ of 0.72, and 12.39 Hz in plane A-B, indicating a cooperation factor of 0.45. It's worth noting that in-plane A-B, substantial masses were present during measurements, potentially impacting the frequency. It is conceivable that in the absence of these masses, the measured frequency and corresponding cooperation factor would have been higher. These observations highlight the distinct behavior of floors under footfall-induced vibrations, characterized by the interplay between interface friction and an elevated shear modulus of the insulation.

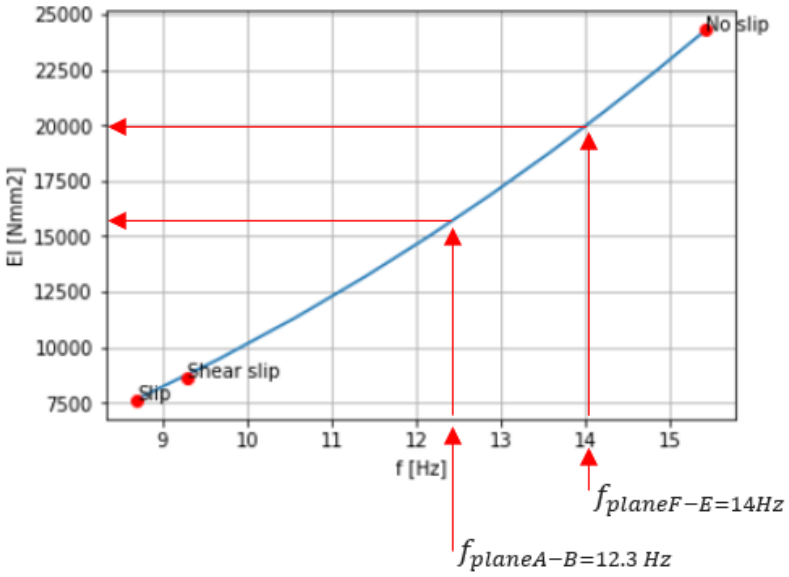

Figure 67: Frequency and bending stiffness relation for different cooperation assumptions according to the prEN5 for a one-way span floor

Implications for Vibration Performance and Design

The initial predicted response factor of the CLT floor with a concrete floating screed, following the prEC5, significantly underestimated the actual performance. Its vibration performance can therefore not correctly be valued and decreases its competitivity compared to other less sustainable floors. If well quantified, there may be room for reducing the height of CLT and reinforced concrete layers, thereby reducing costs and environmental impact while maintaining acceptable vibration performance. This underscores the need to reevaluate the prEC5, especially the guidelines set to estimate the bending stiffness of timber floors with floor finishing. This study focused on CLT floors with floating concrete screeds, revealing a 39% underestimation in frequency according to conventional engineering practices. Another study, as represented in Figure 30, examined a CLT floor with a floating cement screed, revealing a 25% underestimation of frequency compared to previous calculations [7]. These findings suggest that floors with floating screeds tend to exhibit greater rigidity under footfall-induced vibrations and therefore emphasizing the need of more experimental research on the behavior of CLT floors with different compositions of floor finishing. It is recommended to define an amplification factor for the bending stiffness of CLT floors with floor finishing in the prEC5 vibration calculations, be that using the cooperation factor (γ) or another factor.

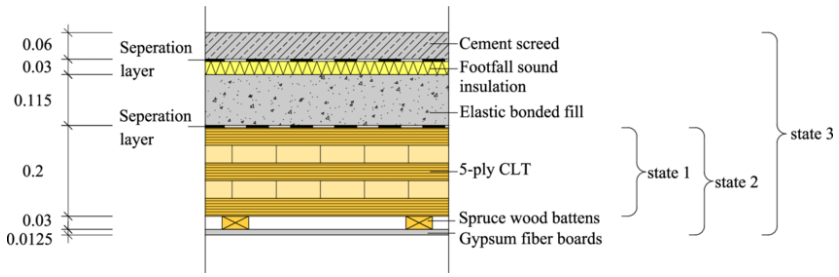

Figure 68: CLT floor with cement floating screed

7 Conclusion and recommendations

This study embarked on an exploration of CLT floor systems, with a primary focus on understanding how these systems can be accurately modeled to predict their vibration performance, particularly when considering the influence of architectural finishing. Through extensive on-site measurements during different construction phases and analytical, and numerical investigations, we have gained valuable insights into the complex dynamics of CLT floors. Based on the results of this research, the main research question is answered:

How can CLT floor systems be modeled in order to accurately predict the vibration performance when taking into account architectural finishing?

Conclusion and recommendations are presented below.

7.1 Conclusion

CLT floors

- Onsite measurements, revealed that the three-sided supported floor had a higher damping ratio than the two-sided supported floor. From this, it can be concluded that the presence of an extra support with screwed connections increases the damping of the floor system.
- The onsite measurements, where the floor was loaded and the response was measured at the same location, revealed that for both before and after the installation of the concrete floating screed, root-mean-square velocity (v_{rms}) values at the line of the inter-panel connection where higher compared to at mid-point of the CLT panels. These differences were more pronounced for the one-way span floor than for the three-sided supported floor. For the one-way span floors before floor finishing is placed, v_{rms} values at the inter-panel connection line exceeded v_{rms} values in the middle of the panel by more than double.
- The comparative analysis between onsite measurements and the FEA supports the suggestion that inter-panel connections have a low stiffness when subjected to small vibrations. In various timber semi-rigid connections, an initial space clearance of 0.5 - 1 mm is expected [34]. Within the initial space clearance connections have very little to no stiffness. The low stiffness can therefore be explained to that footfall-induced vibrations of the floor are very small (around 0.1 mm) which results in initial space clearance becoming more significant.
- This study highlights how connections transferring moments may behave less stiff, while connections that transfer shear loads may behave stiffer due to the role of interface friction during footfall-induced vibrations.
- The prEC5 standard lacks explicit consideration of the impact of inter-panel connections within CLT floors, potentially resulting in an overestimation of their vibration performance. It is important to emphasize that the connection's influence on the floor's frequency is minimal compared to its impact on the v_{rms} value. Therefore, an amplification factor for the v_{rms} value within the prEC5 is needed to account for the diminished bending stiffness in the transverse direction of CLT floors. This adjustment is essential for both one-way and two-way spanning floors to ensure accurate vibration performance estimation.
- The role of inter-panel connections must also be incorporated into the modal mass formula prescribed by the prEC5 for CLT floors. This consideration necessitates a differentiation between one-way and two-way span floors. As bending in the transverse direction of CLT floors predominantly occurs at the inter-panel connection line, it can be concluded that the modal mass is linked to the total CLT floor width and panel width.
- In the case of one-way span floors, the onsite measurements conducted in this study support the FEA model method proposed by Milojecvic [6] for modeling CLT floors. Milojecvic's FEA model, featuring CLT panels connected by inter-panel connections with rotational stiffness derived from static calculations, has demonstrated a 67% increase in v_{rms} values for one-way span floors

compared to a model assuming a completely rigid connection. In conclusion, assuming a rigid connection will result in an overestimation of the vibration performance, Milojecvic's method appears to be a good numerical approach to predicting the vibration performance of CLT floors.

- Through a comparative study of onsite measurements and FEA modeling of the Case Study, it is evident that the mode shape prediction is more accurate when the inter-panel connection is assumed to behave as a hinge rather than as entirely rigid. From this finding, it can be concluded that FEA models that assume inter-panel connections as rigid result in misleading mode shapes, and a better prediction of the mode shape is found when assuming these connections as hinges.

- The introduction of floor finishing enhances the bending stiffness of CLT floors in the transverse direction, thereby influencing the rotational stiffness at the inter-panel connection line. The mass of the floor finishing can increase the contact area within the inter-panel connection joint, further increasing the rotational stiffness. Consequently, floor finishing exerts an improvement in the vibration performance of CLT floors, particularly at critical locations. To account for this effect in FEA models, the rotational stiffness at the inter-panel connection line should be increased and the potential amplification factor for the prEC5 calculations should be decreased.

Architectural finishing

- Onsite measurements revealed the changes in modal properties of architectural finishing, specifically the placement of the concrete floating screed, which emerged as the predominant factor influencing the modal properties and subsequent vibration performance. After placement of the screed, the frequency stayed relatively stable around 13 Hz, the damping increased from ranging from 1.6-3.1 % to 4.6-6.8 %, and the vrms decreased from ranging from 3.39-6.50 mm/s^2 to 2.07-2.31 mm/s^2. Hence the installation of the architectural finishing led to a significant enhancement in the vibration performance.

- The comparative study of prEC5 standards and FEA based on common engineering practices revealed a discrepancy in the estimated frequency. Prior to finishing installation, both methods accurately predicted frequency, but subsequently, they notably underestimated it by 39%. This discrepancy suggests that the assumed bending stiffness values in both approaches do not align with the observed vibrational behavior of these floors.

- This research suggests the discrepancy of the frequency estimation is due to an underestimation of the bending stiffness, which may be attributed to the hypothesis that the bending stiffness of the standalone CLT and concrete layers exhibit higher stiffness and that there is cooperation between the layers under the condition of small vibrations.

- When full cooperation between the CLT floor and concrete screed is presumed in accordance with the prEC5 method, the frequency is overestimated by 9%. This implies that while there is probably some degree of cooperation, the floors are definitely not entirely bonded. Consequently, modeling the floating screed layers as partially coupled to CLT floors is recommended, this can be accomplished by employing the cooperation factor (γ) for mechanical joints as specified in the prEC5.

- The research has identified that the degree of coupling is dependent upon factors such as surface friction at the interfaces, shear stresses arising from floor deformation, insulation thickness, and the shear modulus of the insulation material. This underscores the significance of comprehending the intricate interplay between structural and non-structural components to facilitate precise predictions of vibration performance.

- For FEA models, the application of a similar cooperation factor as employed in analytical calculations is recommended. Furthermore, equations 27 to 35 can be utilized to estimate corresponding orthotropic plate properties. These properties have a notable influence on the frequency and v_{rms} of the FEA model, emphasizing the need for their accurate incorporation into the model.

- The findings of this study, mainly the underestimation of the vibration performance in common engineering practices highlight the need to reevaluate the assessment of CLT floor performance prediction. This not only ensures that CLT floors are valued for their true potential but also

provides opportunities for optimizing their design, potentially by reducing the height of CLT and concrete layers while maintaining acceptable vibration performance.

- FEA revealed that loads at the supports have minimal influence on the resulting frequency and mode shape, concluding that these loads may be neglected in the FEA used to predict the vibration performance of CLT floors.

In conclusion, this study contributes valuable insights into the modeling and evaluation of CLT floor systems, shedding light on the intricate dynamics affected by architectural finishing. Our findings provide a foundation for more accurate and reliable predictive models, ultimately advancing the design and assessment of CLT floors, with potential benefits for sustainability and cost-efficiency in construction practices.

7.2 Recommendation

Based on the research of this thesis, several recommendations are formulated:

- **Validation of vibration calculation method:** The analytical analysis in this study employed the prEC5 vibration calculation method. However, it's essential to note that this method is still in its developmental stage, resulting in uncertainties regarding its formulas and empirical values. Consequently, it is advisable to conduct comparisons with alternative quantification techniques and experimental data to enhance and establish the reliability of this method. Particular attention should be devoted to the "k_{red}" factor and modal mass formula, as the "k_{red}" factor yielded inconsistent vibration responses dependent on the chosen floor width, and the appropriate value for modal mass remains uncertain.

- **Modal Mass Quantification:** The modal mass has been demonstrated to be significant in the determination of the vibration performance of a floor, yet the quantification of modal mass has proven to be a challenging task for CLT floors. If inter-panel connections genuinely exhibit hinge-like behavior, as argued in this thesis, the vibration's mode shape may resemble the illustration in Figure 55. The mode shape of a three-sided supported floor in the presence of inter-panel connections appears to exhibit a division into two sections, with one-half of the floor behaving akin to a three-sided supported floor and the other half resembling a two-sided supported floor. Suggesting that CLT floor mode shape is characterized by bending in a transversal direction at the inter-panel connection, it would be interesting to further research how the modal mass of CLT floors correlates to panel width and total floor width. Accurate modal mass determination is instrumental in assessing vibration performance in accordance with prEC5 or alternative design codes.

- **Influence of Inter-Panel Connection Rotational Stiffness:** This research highlights that the relatively low rotational stiffness of inter-panel connections diminishes the transverse stiffness of CLT floors. However, it remains unclear how floor width, in conjunction with inter-panel connections, impacts transverse stiffness. In addition, this research showed that the inter-panel connections influence the vibration performance of both two-way and one-way spanning floors. Neglecting this aspect leads to an overestimation of vibration performance. Therefore, it is recommended, based on experimental data, to determine reliable rotational stiffness values for these connections and/or establish an amplification factor for the response factor that accounts for reduced transverse bending stiffness. Furthermore, the inclusion of floor finishes has been observed to mitigate these pronounced responses. Hence, further experimental investigations are necessary for CLT floors with diverse floor finishes to explore how finishing treatments can enhance transverse bending stiffness and subsequently improve vibration performance.

- **Shear Stiffness of CLT Floor to Supporting Beams:** Sensitivity analysis indicated that the shear stiffness of CLT floor-to-supporting beam connections moderately influences frequency. However hereafter, this study assumed the connection to be rigid, based on prior research demonstrating the significance of friction in such connections during footfall analysis, given the minimal vibrations and shear stresses involved. Nevertheless, this assumption lacks experimental substantiation specifically for connections between CLT floors and supporting beams. Consequently, it

is advisable to undertaken further research to prove the structural behavior of these connections, leading to reduced uncertainties in vibration performance calculations and thereby enhancing accuracy.

- **Significance of Surface friction:** Surface friction seems to increase the stiffness of connections in footfall analysis. It is therefore recommended to look into a inter-panel connection design that transfers not only moment forces but also shear forces; so that surface friction can be used to its advantage. This could possibly improve the vibration performance of CLT floors.

- **Impact of Partitioning Walls:** Within this thesis, the influence of partitioning walls on the overall dynamic behavior of floors is recognized. However, the case study measurements were not ideally suited for an in-depth analysis of partitioning walls. Measurements at a location close to underlying partitions showed a much lower v_{rms} value then measurements that were further away from underlying partitions. However, it can not confidently be attributed to the presence of partitions. Therefore, it is strongly advised to undertake a comprehensive study involving numerical analysis in conjunction with experimental measurements to understand the potential advantages introduced by the inclusion of partitioning walls. This approach will facilitate a more robust understanding of their impact on the dynamic behavior of floors.

- **Complex Dynamics of CLT floors with floor finishing:** This thesis assumed the bending stiffness of CLT and the concrete screed to be constants when determining the cooperation factor. However, the standalone dynamic behavior of these floor layers remains uncertain. Consequently, it is strongly recommended to conduct experimental research focused on standalone CLT floors. Together with experimental investigations on the dynamic behavior of CLT floors with different types and thicknesses of floor finishing layers. This approach will enhance the understanding of the dynamic behavior of CLT floors in real-world scenarios.

References

[1] European Commission, Directorate-General for Research, Innovation, M Feldmann, C Heinemeyer, and M Lukić. Background document for floor vibrations. In *Human-induced vibration of steel structures (Hivoss)*. Publications Office, 2010.

[2] Andrei Metrikine. Structural dynamics - part 1, 2022.

[3] A.L. Smith, S.J. Hicks, and P.J. Devine. Design of Floors for Vibration: A New Approach. Technical report, The Steel Construction Insitute, Berkshire, 2 2009.

[4] M Feldmann, C Heinemeyer, Chr Butz, and E Caetano. Design of floor structures for human induced vibrations. Technical report, JRC, 2009.

[5] Kirsten Lewis, Bella Basaglia, Rijun Shrestha, and Keith Crews. The use of cross laminated timber for Long span flooring in commercial buildings. In *WCTE 2016 - World Conference on Timber Engineering*, 2016.

[6] Marija Milojević, Vitomir Racic, Miroslav Marjanović, and Marija Nefovska-Danilović. Influence of inter-panel connections on vibration response of CLT floors due to pedestrian-induced loading. *Engineering Structures*, 277:115432, 2 2023.

[7] Michael Kawrza, Thomas Furtmüller, and Christoph Adam. Experimental and numerical modal analysis of a cross laminated timber floor system in different construction states. *Construction and Building Materials*, 344:128032, 8 2022.

[8] M.H. Roks. *The dynamic behaviour of timber-concrete composites*. PhD thesis, Eindhoven University of Technology, Eindhoven, 2 2017.

[9] Houtlab. Houtlab.nl.

[10] Redactie Houtwereld. Woody Buildings Concepts bouwt eigen houten huisvesting, 10 2022.

[11] T. A. Bui, P. Lardeur, M. Oudjene, and J. Park. Numerical modelling of the variability of the vibration frequencies of multi-layered timber structures using the modal stability procedure. *Composite Structures*, 285, 2022.

[12] Haoyu Huang, Xiaoqi Lin, Junhui Zhang, Zhendong Wu, Chang Wang, and Brad Jianhe Wang. Performance of the hollow-core cross-laminated timber (HC-CLT) floor under human-induced vibration. *Structures*, 32, 2021.

[13] Andrei Metrikine. Structural dynamics - part 2, 2022.

[14] Juan Negreira. Vibrations in lightweight buildings-perception and prediction. 2013.

[15] Luca Marino and Alice Cicirello. Dynamic response of multi-degree-of-freedom systems with a Coulomb friction contact under harmonic excitation. *Nonlinear Dynamics*, 106(3), 2021.

[16] Hans Joachim Blas and Carmen Sandhaas. *Timber engineering - principle for design*. Karlsruher Institut fur Technologie (KIT), Karlsruhe, 2017.

[17] British Standards Institution (BSI). Guide to evaluation of human exposure to vibration in buildings – Part 1: vibration sources other than blasting. In *British Standards BS*. BSI, Londen, UK, 2008.

[18] M R Willford and P Young. A Design Guide for Footfall Induced Vibration of Structures. *CCIP 016*, 2006.

[19] Normcommissie 351001 'Technische Grondslagen voor Bouwconstructies'. NEN-EN 16929: Beproevingmethode, 2018.

[20] Nathalie Labonnote. *Damping in Timber Structures*. PhD thesis, 10 2012.

[21] Jimin He and Zhi-Fang Fu. *Modal Analysis*. Butterworth-Heineman, Oxford, 2001.

[22] Radovan Cvetkovic, Dragoslav Stojic, Sonja Krasic, and Nemanja Markovic. Innovative structural CLT system in projecting and building of student houses. *Facta universitatis - series: Architecture and Civil Engineering*, 13(1), 2015.

[23] Nikolaos Georgios Vardaxis, Delphine Bard Hagberg, and Jessica Dahlström. Evaluating Laboratory Measurements for Sound Insulation of Cross-Laminated Timber (CLT) Floors: Configurations in Lightweight Buildings. *Applied Sciences (Switzerland)*, 12(15), 2022.

[24] Thomas Reynolds, Richard Harris, and Wen Shao Chang. Stiffness of dowel-type timber connections under pre-yield oscillating loads. *Engineering Structures*, 65, 2014.

[25] Reinhard Brandner and Gerhard Schickhofer. Properties of Cross Laminated Timber (CLT) in Compression Perpendicular to Grain. *International Network on Timber Engineering Research (INTER)*, (September), 2014.

[26] ARDEX. Types of screed, 2023.

[27] Jan Weckendorf, Binsheng Zhang, Abdy Kermani, David Reid, and Palle Andersen. Damping characteristics of timber flooring systems with respect to low-frequency vibration modes. In *10th World Conference on Timber Engineering 2008*, volume 4, 2008.

[28] Z. Miskovic, A. Pavic, and P. Reynolds. Effects of full-height nonstructural partitions on modal properties of two nominally identical building floors. *Canadian Journal of Civil Engineering*, 36(7), 2009.

[29] Junuthula Narasimha Reddy. *Mechanics of laminated composite plates and shells: theory and analysis*. CRC press, 2003.

[30] Junuthula Narasimha Reddy. A plate bending element based on a generalized laminate plate theory. *International Journal for Numerical Methods in Engineering*, 28, 1989.

[31] Luning Ingenieurs in houtconstructies. luning.nl.

[32] Swedish Wood. The CLT Handbook. *Swedish Wood*, 2019.

[33] Ewan Macpherson, Panayiotis Papastavrou, Tristan Wallwork, Simon Smith, and Allan McRobie. The rotational stiffness of cross-laminated timber half-lap joints. In *WCTE 2018 - World Conference on Timber Engineering*, 2018.

[34] Marek Johanides, Antonin Lokaj, Pavel Dobes, and David Mikolasek. Numerical and Experimental Analysis of the Rotational Stiffness of a Timber Semi-Rigid Dowel-Type Connection. *Materials*, 15(16), 2022.

A Pictures taken during onsite testing

A.1 Phase 1: more figures

Figure 69: Side column in phase 1

Figure 70: Corner column in phase 1

Figure 71: CLT floor connection to core and opening in phase 1

Figure 72: CLT floor connection to stair opening in phase 1

A.2 Phase 2: more figures

Figure 73: Corner column in phase 2

Figure 74: Wind brace in phase 2

Figure 75: Connection column to partition in phase 2

Figure 76: Stairs in phase 2

B Test procedure

Houtlab test plan

Lilly Klappe – 8/2/2023

Needed supplies:

- Laptop
- Dropping weight
- Speedometer
- Safety shoes
- Safety helmet

Preparation:

- Reserve dropping weight, speedometer, safety shoes and helmet via ABT service desk
- Download dropping weight app
- Download SYScom app
- Agree on test date with people incharge

Test step-by-step plan:

1. Link SYScom to laptop
2. Link dropping weight to app
3. Place dropping weight and speedometer in test situation
4. Note test situation in excell
5. Setup dropping weight in starting position
6. Start measuring with speedometer
7. Drop the fall weight and catch it immediately after 1 fall
8. Hold still for 5 sec
9. Return fall weight to starting position
10. Wait for the orange patch on Syscom to go out
11. Perform steps 4 until 11, two more times (a total of 3 same measurements per test situation)
12. Stop measurement
13. Save measurement data
14. Write down the measurement data number for the corresponding test situation in Excel
15. Take pictures of all measured floors

C Python script

C.1 Determining fundamental frequency and damping

In [ ]:

```
# import data first test
#t, v_z = np.loadtxt('22311018.csv', delimiter = ' ', dtype='float',
#comments = '#', usecols=(0,3), unpack = True)
#t, v_z = t[500:4000], v_z[500:4000]
#fs = 1000

#import data second test
t, v_z = np.loadtxt('23058044.txt', delimiter = ' ', dtype='float',
                    comments = '#', usecols=(0,3), unpack = True)
t, v_z = t[1000:8000], v_z[1000:8000]
fs = 2000                           # sampling rate = number of samples/1sec

# number of datapoints
size = t.size

# transfer from time domain to frequency domain
z_fft = fft(v_z)

#determine amplitude
z_ampl = 2*np.abs(z_fft/size)           # normalized arbitrary unit

# create fft bins
fftfreq = np.fft.fftfreq(size, t[1]-t[0])

# Determining the first eigen frequency of the original signal
original_eigenfreq = fftfreq[np.argmax(z_ampl[0:int(z_ampl.size/2)])] #in Hz

# plot amplitude on frequency domain
plt.figure()
plt.xlim(0, 60)
plt.plot(fftfreq,z_ampl)
plt.xlabel('frequency')
plt.ylabel('Amplitude')
plt.title('frequency spectrum', fontsize=12)

# determine amplitudes for damping calculation
ampl_max = max(z_ampl)
ampl_damp = ampl_max / np.sqrt(2)
plt.axhline(ampl_max, color='r',  label='a_max');
plt.axhline(ampl_damp, color='g' , label= 'a_max/sqrt(2)');
plt.legend()

# create array of damping values
ampl_damp = np.array([ampl_damp]*len(t))

# determine the damping according to peak-picking method
line_1 = LineString(np.column_stack((z_ampl, fftfreq)))
line_2 = LineString(np.column_stack((ampl_damp, fftfreq)))
intersection = line_1.intersection(line_2)

first_point = np.array(intersection[0])
x1 = first_point[0]
y1 = first_point[1]
second_point = np.array(intersection[2])
x2 = second_point[0]
y2 = second_point[1]

damping = np.abs((y2 - y1) / (2*original_eigenfreq))
```

Figure 77: Python script for determining fundamental frequency and damping

```
VRMS = np.sqrt(np.sum((v_z)**2)/size)
print(VRMS)
```

Figure 78: Python script used to determine v_{rms} from experimental data

In [30]:
```
# determine root mean square velocity and root mean square acceleration according to dEC5
f_w = 2.0
mu_e = 1
mu_r = 1
m = 123
L = 5.4
B = 4.825
M_m = 0.25*m*L*B
EI_L = 6336
EI_T = 1664
damping = 0.025
f_1 = 14
k_red = 0.7

I_ef = (42*f_w**1.43) / (f_1**1.3)
k_imp = 1
#k_imp = 0.48*(EI_L/EI_T)**0.25
n = 1.35 - 0.4*k_imp

# determine v_rms
v_peak = k_red*I_ef/(M_m+70)
v_tot = k_imp*v_peak
v_rms = v_tot * (0.65-0.01*f_1)*(1.22-11*damping)*n

print('v_rms is', v_rms)
```

Figure 79: Python script used to determine v_{rms} according to prEC5: chapter 9

In [32]:
```
# DETERMINE ROOT MEAN SQUARE VELOCITY with Annex
import math
from math import *
from scipy.integrate import quad

f_w = 2.0
mu_e = 1
mu_r = 1
m = 123
L = 5.4
B = 4.825
M_m = 0.5*m*L*B
damping = 0.025
T = 0.5

# # # 1; determine effective footfall impulse
f_1 = 14.0
I_ef1 = (54*f_w**1.43) / (f_1**1.3)

# determine peak velocity
v_peak1 = mu_e*mu_r*I_ef1/M_m

# determine velocity response, I = integer and err = error
def v1(t):
    return (v_peak1*math.exp(-2*np.pi*damping*f_1*t)*np.sin(2*np.pi*f_1*t))**2
I1, err1 = quad(v1, 0, 0.5)

# # # 2
f_2 = 20
I_ef2 = (54*f_w**1.43) / (f_2**1.3)
v_peak2 = mu_e*mu_r*I_ef2/M_m
def v2(t):
    return (v_peak2*math.exp(-2*np.pi*damping*f_2*t)*np.sin(2*np.pi*f_2*t))**2
I2, err2 = quad(v2, 0, 0.5)

# determine root mean square velocity
v_rms = np.sqrt((1/T)*(I1+I2))

# corresponding response factor
v_r1 = 1*10**-4                 # when f1 >= 8 Hz
R_v = v_rms/v_r1

print('v_rms =', v_rms, 'and the corresponding R-value is', R_v)
print('Errors 1, 2 and 3 are respectively:', err1, err2)
```

Figure 80: Python script used to determine v_{rms} according to prEC5: Annex

```python
# Determine damping based on fitted curve
import plotly.graph_objects as go
import numpy as np
import pandas as pd
from scipy.signal import find_peaks

# Determine time range for damping determination
td, v_zd = t[980:2200],v_z[980:2200]

# find positive peaks
indices = find_peaks(v_zd)[0]
x = np.array(td[indices])
y = np.array(v_zd[indices])

pos_peaks = []
pos_indices = []
for i in range(len(y)):
    if y[i] > 0:
        pos_peaks.append(y[i])
        pos_indices.append(i)

pos_x = x[pos_indices]
pos_x = list(pos_x)

pos_x = np.array(pos_x)
pos_y = y[pos_indices]
pos_y = list(pos_y)

# delete outliers
pos_x = np.delete(pos_x, [0,2,5])
pos_y = np.delete(pos_y, [0,2,5])

# determine envelope line
model2 = np.poly1d(np.polyfit(pos_x, pos_y,2)) # third order polynomial fits best
curve_fitting = np.poly1d(np.polyfit(pos_x, pos_y,2))

# plot velocity response and fit line
plt.figure()
fig = plt.figure(figsize=(7,5),)
plt.plot(td,v_zd)
plt.plot(pos_x, model2(pos_x), color='green',label='fitted line')
plt.scatter(pos_x, pos_y, color='r')
plt.title('Envelope fitting method in time domain', fontsize=12)
plt.xlabel('Time [s]')
plt.ylabel('Velocity [mm/s]')
fig.savefig(r"C:\Users\l.klappe\OneDrive - Oosterhoff Group\Pictures/envelope.png")

# estimate damping
damping = np.exp(curve_fitting[0]) * np.exp(curve_fitting[2]) * pos_x
dampingratio = curve_fitting[0]/ (2*np.pi*original_eigenfreq)
print('dampingratio', dampingratio)
```

```
dampingratio 3.1935540186570277
```

Figure 81: Python script used to determine the damping value according to envelope method

D Velocity and frequency spectrum of onsite measurements

D.1 All three measurements of p11

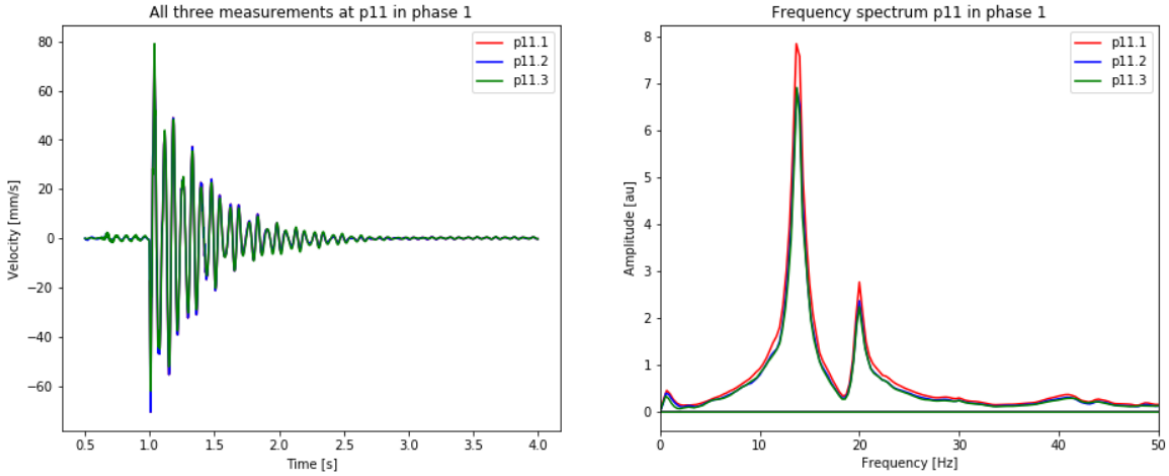

Figure 82: Results of all three measurements at point 11

D.2 Comparison of onsite measurements p11 and p7

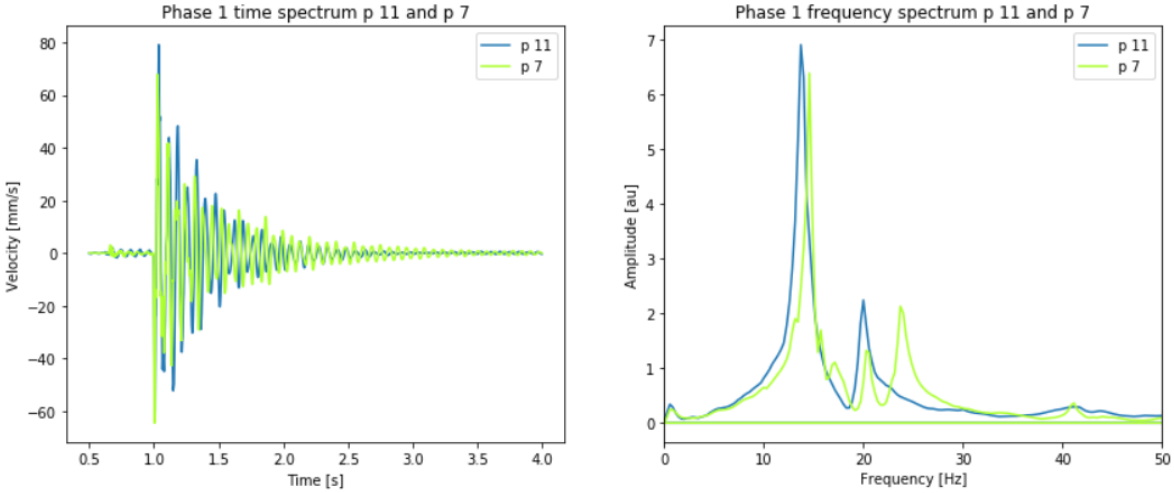

Figure 83: Results of points p11 and p7 during phase 1

Points p11 and p7 are both points in the middle of a plane, p11 between axes E-F and p7 between A-B. The damping is a bit higher in p11 in both phase 1 and phase 2. This could be due to that p11 is connected with mechanical fasteners, that dissipate energy through friction, to the CLT wall while p7 is connected to the adjacent CLT plane.

Another remarkable phenomena is that the frequency does not really decrease after placing the cement screed in all measured points. This could incline that the floating screed adds more stiffness to the floor than is initially expected.

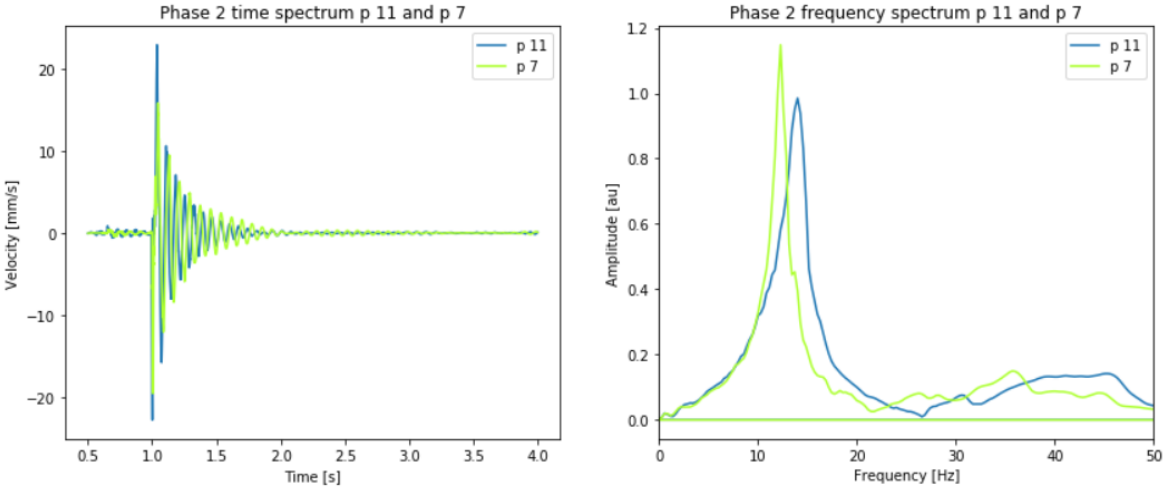

Figure 84: Results of points p11 and p7 during phase 2

E Load of adjacent panel

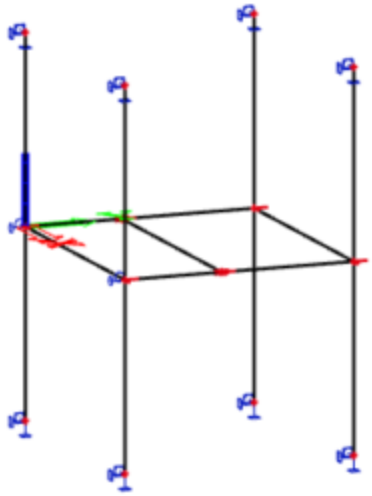

Figure 85: PHASE 1: Assumed floor system for the numerical analysis in SCIA with all rigid connections

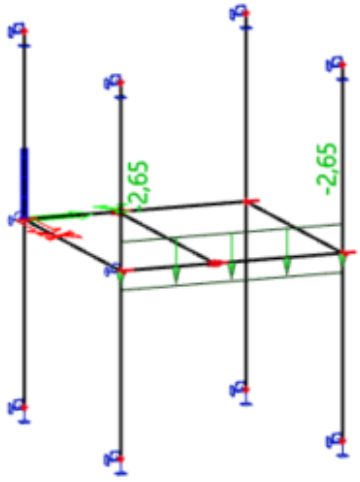

Figure 86: PHASE 1: Assumed floor system for the numerical analysis taking into account the weight of the adjacent floor panel

Method	f_1 [Hz]	f_2 [Hz]
FEM assuming all rigid connections (figure 85)	15.58	23,76
FEM assuming all rigid connection and load adjacent panel (figure 86)	15.53	23,71

Table 18: Building phase 1

F Numerical study on boundary conditions and inter-panel joint

F.1 Introduction

During literature research, there is no specific knowledge found on the dynamic response of three-sided supported floors, only for clean-cut one-way and two-way spanning floors. The goal of this numerical study is to understand the dynamic vibration characteristics of a three-sided supported floor compared to a one-way and two-way spanning floor. In addition, the effect of an inter-panel connection with very low stiffness and flexible supports is studied. Flexible supports designate the supporting beams. This study is used as support for explaining differences between experimental data and explaining discrepancies between analytical, numerical, and experimental analysis.

This is done by determining the vibration characteristics with FEM SCIA of three sets of floors. As depicted in figure 87, the first set is supported on hinged line supports, the second on beams and the third is a floor supported on hinged line supports with a hinged inter-panel connection. Each set contains a floor supported on 2, 3 and 4 sides as depicted in figure 88.

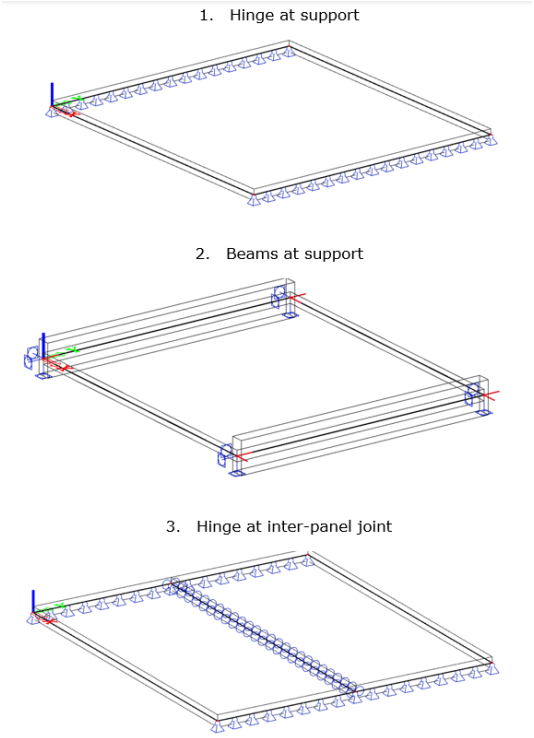

Figure 87: Numerical model set up in SCIA

As starting point only the self-weight of the floor is taken into account, so that it can be compared to experimental data. The self-weight of the floor is taken as the thickness of the CLT floor (h_{CLT}) times the density of $\rho_{CLT} = 480$ kg/m3. For the density, the mean density of CLT is taken as it should represent the real weight of the floor. This is also done for the concrete screed layer and supporting beams with densities of $\rho_{screed} = 2400$ kg/m3 and $\rho_{GL28,beam} = 460$ kg/m3. The dimensions of the CLT panel, screed and supporting beam follow that of the case study and are specified in table 2.

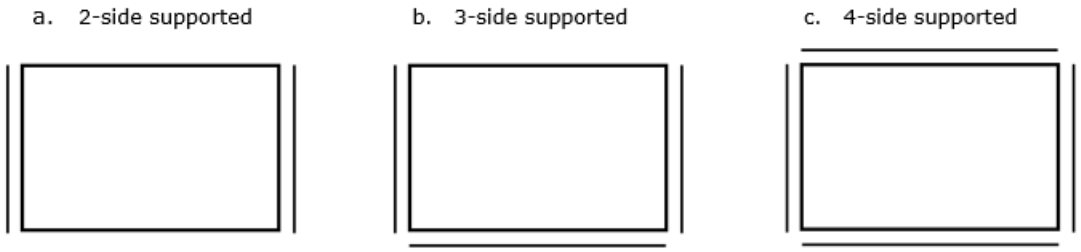

Figure 88: Assessed line supports

F.2 Results

1. Hinged support (very high vertical stiffness)

a. 2-sided hinged supported | b. 3-sided hinged supported | c. 4-sided hinged supported

Mode 1

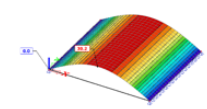

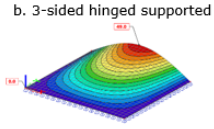

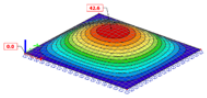

Mode 2

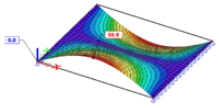

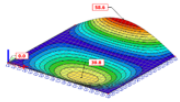

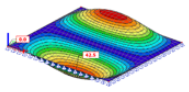

$f_{1,a}$ =13,9 Hz	$f_{2,a}$ =15,5 Hz	$f_{1,b}$ = 14,3 Hz	$f_{2,b}$ = 22,1 Hz	$f_{1,c}$ = 17,7 Hz	$f_{2,c}$ = 37,4 Hz
$M_{1,a}$ =52,1%	$M_{2,a}$ =18,3%	$M_{1,b}$ = 20,2%	$M_{2,b}$ = 14,1%	$M_{1,c}$ = 27,3%	$M_{2,c}$ = n.p.
$M_{1,a}$=1,14E3 kg	$M_{2,a}$ =0,40E3 kg	$M_{1,b}$ = 0,44E3 kg	$M_{2,b}$ = 0,31E3 kg	$M_{1,c}$ = 0,60E3 kg	$M_{2,c}$ = n.p.

2. Beam supports (low vertical stiffness)

a. 2-sided flexible supported | b. 3-sided flexible supported | c. 4-sided flexible supported

Mode 1

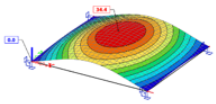

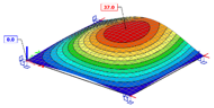

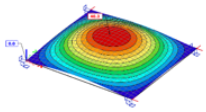

Mode 2

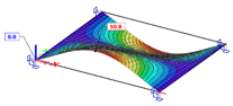

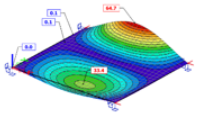

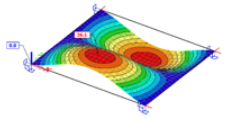

$f_{1,a}$ =15,8 Hz	$f_{2,a}$ =20,9 Hz	$f_{1,b}$ = 16,5 Hz	$f_{2,b}$ = 24,6 Hz	$f_{1,c}$ = 17,9 Hz	$f_{2,c}$ = 31,2 Hz
$M_{1,a}$ =29,7%	$M_{2,a}$ =13,6%	$M_{1,b}$ = 24,0%	$M_{2,b}$ = 14,1%	$M_{1,c}$ = 18,9%	$M_{2,c}$ = 23,6%
$M_{1,a}$ =0,85E3 kg	$M_{2,a}$ =0,39E3 kg	$M_{1,b}$ = 0,74E3 kg	$M_{2,b}$ = 0,24E3 kg	$M_{1,c}$ = 0,63E3 kg	$M_{2,c}$ = 0,78E3 kg

3. Hinged support with hinged panel division

a. 2-sided hinged supported | b. 3-sided hinged supported | c. 4-sided hinged supported

Mode 1

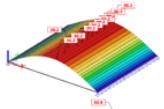

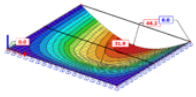

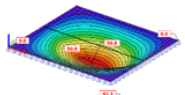

Mode 2

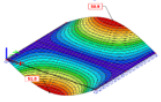

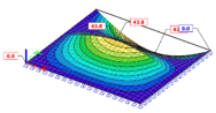

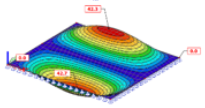

$f_{1,a}$ =13,9 Hz	$f_{2,a}$ =15,5 Hz	$f_{1,b}$ = 14,3 Hz	$f_{2,b}$ = 17,6 Hz	$f_{1,c}$ = 17,65 Hz	$f_{2,c}$ = 37,4 Hz
$M_{1,a}$ =52,1%	$M_{2,a}$ =18,3%	$M_{1,b}$ = 24,8%	$M_{2,b}$ = 12,3%	$M_{1,c}$ = 19,2%	$M_{2,c}$ = n.p.
$M_{1,a}$=1,14E3 kg	$M_{2,a}$ =0,40E3 kg	$M_{1,b}$ = 0,54E3 kg	$M_{2,b}$ = 0,27E3 kg	$M_{1,c}$ = 0,42E3 kg	$M_{2,c}$ = n.p.

F.3 Discussion

How do the vibration characteristics of a three-sided floor compare to those of a clear-cut one-way and two-way span floor?

- Fundamental and second frequency increase with the amount of line supports.
- The fundamental and second frequency of the three-sided floor in all cases closer to one-way spanning floor. This is likely due to the higher bending stiffness in the longitudinal direction, than in transversal direction, which is a general characteristic of CLT floors.
- Modal mass of three sided floor for floor on line-supports, results in lowest modal mass. However in real life the floor will most likely be supported on beams. In that case the modal mass is in between the the modal mass of a one-way and two-way span floor.
- The modal mass of a floor supported on beams is much lower than that of a floor supported on line supports. In this study the beams in SCIA are placed in the same line as the floor, thus the bending stiffness is the bending stiffness of the floor and the beam. While most likely there is cooperation between the beam and the floor, resulting in a much higher stiffness at the supports. If this is so the modal mass of a floor supported on beams will be higher.
- Placing a hinge in the middle of the floor has limited affect on the frequency and modal mass. Need to determine v_{rms} to see influence of hinge at interpanel connection.

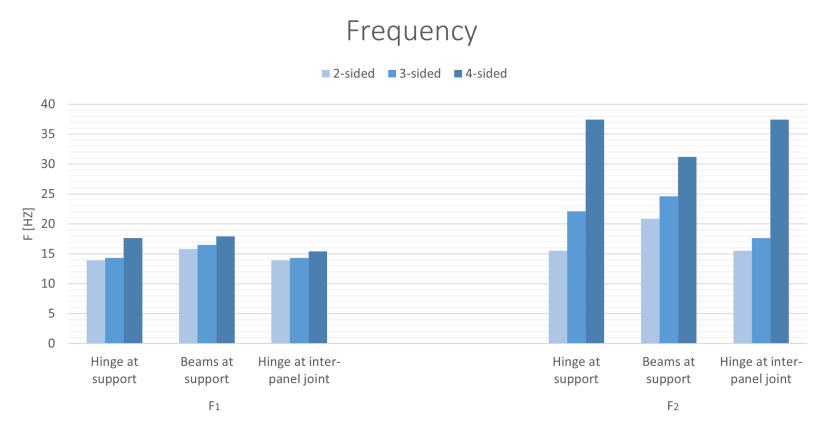

Figure 89: The first and second frequency of the numerical study floors

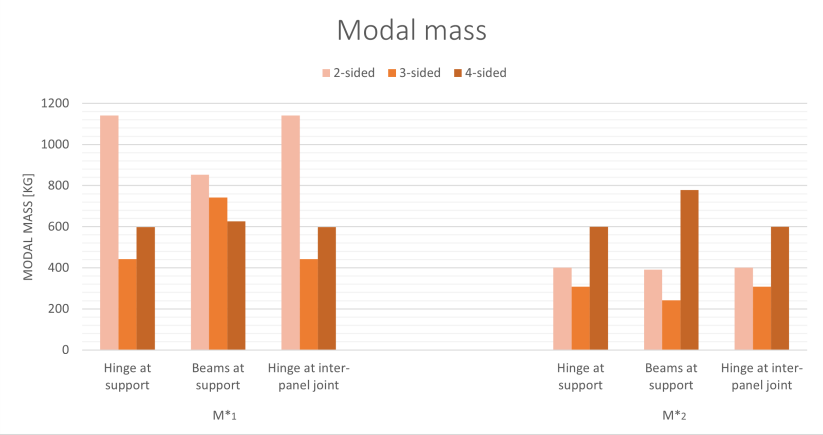

Figure 90: The first and second modal mass of the numerical study floors

G Stiffness calculations

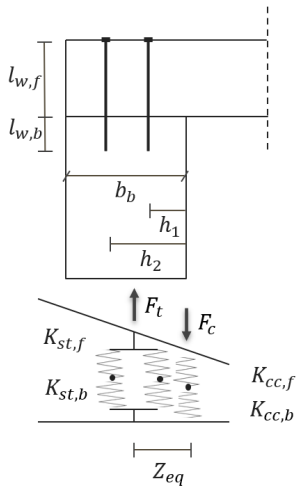

Figure 91: Support connection

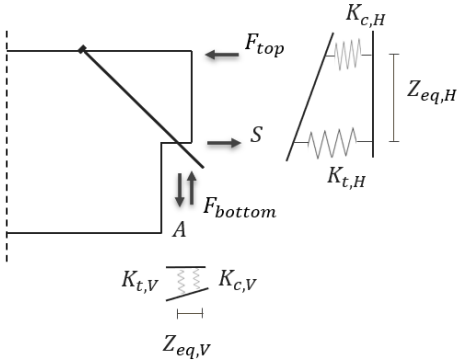

Figure 92: Inter-panel connection

To calculate the rotational stiffness of the support and inter-panel connection the prEC5 is employed. The pull-out stiffness of the screw is calculated using the axial slip modulus:

$$k_{st} = 2d^{0.6} l_w^{0.6} \rho_{mean}^{0.9} \tag{45}$$

with
d= screw diameter$[mm]$
l_w = anchoring length$[mm]$
ρ_{mean}= mean density timber $[kg/m3]$

The indent stiffness of the timber is determined with:

$$k_c = \frac{2 \cdot E_{90,mean}}{h_{ef} \cdot (\frac{1}{l_c b_c} + \frac{1}{l_{ef} b_{ef}})} \tag{46}$$

Support connection

In the support the screw is embedded in the CLT floor and supporting beam, the corresponding stiffnesses can be translated to one stiffness with:

$$k_{eff} = \frac{1}{\frac{1}{k_{st,f}} + \frac{1}{k_{st,b}}} \tag{47}$$

Then the effective distance between the line of compression and the line of tension is determined with:

$$Z_{eq} = \frac{\sum k_{eff,i} h_i^2}{\sum k_{eff,i} h_i} \tag{48}$$

Using the effective distance the effective tension stiffness of the screwed connection is determined with:

$$k_t = \frac{\sum k_{eff,i} h_i}{Z_{eq}} \tag{49}$$

Finally the stiffness of the support connection can be calculated:

$$K_{support} = \frac{Z_{eq}^2}{\frac{1}{k_t} + \frac{1}{k_c}} \tag{50}$$

Inter-panel connection

In the Inter-panel connection the screw also transfers shear forces, therefore the shear stiffness of the screw is determined with the lateral slip modulus:

$$K_{sls,V,mean} = \rho^{1.5} \frac{d}{23} \tag{51}$$

Because the screws are under and inclination the shear stiffness (S) and the axial stiffness (A) of the screw becomes:

$$S = K_{t,H} = K_{sls,V,mean} \sin(\epsilon)^2 + \frac{1}{2} K_{sls,ax,mean} \cos(\epsilon)^2 \tag{52}$$

$$A = \frac{1}{2} K_{sls,ax,mean} \cos(\epsilon)^2 \tag{53}$$

Subsequently, the stiffness of the inter-panel connection is determined:

$$K_{inter-panel} = \frac{Z_{eq,v}^2}{\frac{1}{k_{t,V}} \frac{1}{k_{c,V}} + \frac{1}{k_{t,H}} \frac{1}{k_{c,H}}} \tag{54}$$